

SCALABLE CELL CULTURE FOR PRODUCTION OF SMALL EXTRACELLULAR VESICLES FOR REGENERATIVE MEDICINE APPLICATIONS

Megan Florence Boseley
Doctor of Philosophy

Aston University



December 2023

© Megan Florence Boseley, 2023

Megan Florence Boseley asserts their moral right to be identified as the author of this thesis. This copy of the thesis has been supplied on condition that anyone who consults it is understood to recognise that its copyright belongs to its author and that no quotation from the thesis and no information derived from it may be published without appropriate permission or acknowledgement.

Thesis Abstract - Scalable Cell Culture For Production Of Small Extracellular Vesicles For Regenerative Medicine Applications

Mesenchymal stromal cells (MSCs) have evidenced to be a promising option for cellular therapy but often fail to be accepted at the clinical trial phase. Fortunately, there has been ongoing interest into MSC secreted small EVs (sEVs) due to their ability to transport cargo around the body, whilst evading the immune system and permeating hard to breach barriers. The generation of abundant small EVs for analysis is most commonly achieved by growing cells in multiple planar flasks in static culture, which can be both resource and time consuming, with relatively low yield of EVs. Alternatively, bioreactor based culture platforms have been proven to increase MSC and EV yields and hence provide a solution for scaling up. However this needs to be more thoroughly investigated in relation to the effects agitated suspension culture has on sEV profile.

The aim of this project was therefore to investigate the effects of bioprocess parameters on small EV production by MSCs, both in terms of their characterisation and functional capacity. In order to do so, bone marrow Mesenchymal Stem Cells (bmMSCs) were expanded on microcarriers (MCs) in stirred spinner flasks (SFs) for 10 days. bmMSCs were then harvested, characterised for multipotency and EVs then collected, concentrated using Tangential Flow Filtration (TFF) and isolated using Size Exclusion Chromatography (SEC). MSC-EVs populations were characterised using a number of classic and novel methodologies and cargos revealed using mass spectrometry. Potency was demonstrated through changes in T cell immunosuppression and *in vitro* proliferation and wound healing assays.

Optimising culture parameters led to changes in MSC metabolism and expansion, whilst cell stemness and differentiation potential were maintained. Bioreactor cultures produced greater quantities of EVs in comparison to standard planar cultures, and SEC isolated MSC-sEVs demonstrated immunoprivilege and regenerative potential in culture. Importantly, we demonstrate consistent, reproducible harvesting of MSC-sEVs from multiple batches from the same donor.

Therefore, this research describes a new, consistent and reliable bioprocessing pipeline for the manufacture of therapeutically functional MSC-EVs at scale. This study is the first to investigate the number, potency and cargos of MSC-EVs from multiple time points during cell expansion in the small scale stirred tank bioreactor as well as the consistency of MSC-sEV product from multiple batches and donors.

Acknowledgements

Academic

I would primarily like to acknowledge my final supervising team, Dr Ewan Ross, who dedicated unwavering time and effort into the project and myself, after adopting us in the final 2 years. His consistent support and encouragement, especially during stressful periods was much appreciated, as well as his hands on approach to assisting me with both phenotyping and flow cytometry assays. He gave me the flexibility and final push to pull as much data as possible out of the final year of my PhD, which has since increased my confidence in the project and myself. In addition, my external supervisor Dr Sophie Cox provided me with valuable connections to her research group (Mathieu Brunet) and was always present at meetings to check in and provide important feedback. I would also like to acknowledge my year 1 and 2 supervising team who laid the foundations for the project to be performed (Professor Ivan Wall and Dr Petra Hanga). Professor Ivan Wall designed a fantastic project, with novelty and value in the field of Extracellular Vesicles. He encouraged me to work to my full potential and provided an upstream bioprocessing platform for me to adapt and optimise. I would finally like to acknowledge my final year secondary supervisor, Dr Ivana Milic, for leading the mass spectrometry analysis.

Colleagues who have closely supported me throughout my PhD include staff from LabMB343 and MB344 who initially provided me with training and later became good friends (Dr David Jenkins and Dr Rachel Caves). More recently, members within and connected to the Ross research group, have been equalling as welcoming and supportive as Dr Ewan Ross himself, especially with use of their analytical software (Rachel Butler – NanoFCM).

As a collective, it is imperative that i draw attention to the unwavering support and opportunities provided for me by the 4 year LifeTime CDT programme, led by Professor Matt Dalby, who I have great respect and appreciation for. The programme itself was a fantastic opportunity to build a strong skillset and make meaningful connections. In addition the memories I have made with the team and a close group of CDT friends, will be something I will forever remember. Especially that built with Paige Walczak, a fellow CDT student at Aston University, whose friendship throughout the entire process I will always appreciate.

Collaborator Acknowledgements

Collaborators at LGC, including Dr Dorota Bartczak, Jonathan Campbell and Dr Aneta Sikora, are mentioned here for offering their facilities and expertise at LGC to me across the project, and also for acquiring additional financial funding for the project.

This work was supported by Engineering and Physical Sciences Research Council (EP/S02347X/1) and so we acknowledge them for their financial contribution to this project, which without it it wouldn't be possible.

Personal Acknowledgements

Without the strong support system I have had at home over the 4 year project this would not have been possible. Firstly I would like to thank my parents who have made a comfortable and encouraging environment for me to travel back to each evening after work. My mum who drove me to the station every morning and dad who made sure there was tea on the table for me to come home to. Our family dog, Douglas, for often sharing my lap with the laptop when I was writing up the thesis. I would like to thank Ash for being patient and positive and always there. He has been an emotional rock for me through this process and always encouraged me to keep my head up. Thank you also to all the rest of my close family and friends for always being interested in the research and motivating/encouraging me to be my best.

Table of Contents

LIST OF FIGURES	9
LIST OF TABLES	14
LIST OF ABBREVIATIONS	15
CHAPTER 1: GENERAL INTRODUCTION	17
1.1 Basis of stem cell research	17
1.2 Stem Cells	17
1.2.1 Mesenchymal Stem Cells	19
1.2.1.1 Defining MSC	21
1.2.1.2 MSCs as therapeutics	21
1.2.1.3 MSCs + EVs as immune-therapeutics	22
1.2.2 Cell culture of MSCs	22
1.3 Scale Up and Scalable systems	23
1.4 Stirred flasks culture.....	26
1.4.1 Stirred flasks	26
1.4.2 Microcarriers and Scaffolds for suspension culture	26
1.4.3 Stirred culture biophysics	28
1.5 Extracellular Vesicles	29
1.5.1 Historic timeline of EVs	29
1.5.2 EV definition	30
1.5.3 Subtypes	31
1.5.3.1 Apoptotic Bodies	31
1.5.3.2 Microvesicles	32
1.5.3.3 small EVs/Exosomes	33
1.5.4 Extracellular Vesicles Therapeutic potential	34
1.6 EV production	36
1.6.1 EVs from scalable culture	36
1.6.2 EV isolation and purification	37
1.6.3 EV storage	42
1.6.4 EV characterisation	42
1.7 Conclusions and Gaps in Knowledge	43
CHAPTER 2: AIMS AND OBJECTIVES	44
CHAPTER 3: MATERIALS AND METHODS	46
3.1 Materials and Reagents	46

3.2 Methods	53
3.2.1 Basic Cell Culture.....	53
3.2.1.1 Thawing Cells.....	53
3.2.1.2 Cell counting.....	53
3.2.1.3 Cell Passage	53
3.2.1.4 Cell Freezing	54
3.2.1.5 Cell Fixation	54
3.2.2 Microcarrier Screening	54
3.2.2.1 Coating 96 well plates for low attachment pupose.....	54
3.2.2.2 Microcarrier aggregation screening experiment.....	54
3.2.2.3 CCK-8 Cell Viability Assay.....	55
3.2.3 Spinner Flask studies	55
3.2.3.1 Siliconising Spinner Flasks	55
3.2.3.2 Spinner Flask protocol	56
3.2.3.2.1 Seeding and expansion of MSCs in Spinner Flasks	56
3.2.3.2.2 Spinner Flask Cell measurements.....	57
3.2.3.2.3 Spinner Flask harvest.....	57
3.2.4 Mesenchymal Stem Cell Characterisation	58
3.2.4.1 Colony Forming Unit (CFU) Assay.....	58
3.2.4.2 Trilineage Differentiation	58
3.2.4.2.1 Osteogenesis staining.....	59
3.2.4.2.2 Chondrogenesis stain	59
3.2.4.2.3 Adipogenic staining	59
3.2.4.3 Flow Cytometry	60
3.2.4.4 MSC-PBMC Assay	60
3.2.5 Extracellular Vesicle Preparation	61
3.2.5.1 EV Concentration and Isolation.....	61
3.2.5.2 EV storage	61
3.2.6 Extracellular Vesicle Analysis	62
3.2.6.1 Nanoparticle Tracking Analysis (NTA)	62
3.2.6.2 Dynamic Light Scattering (DLS).....	62
3.2.6.3 NanoFlowCytometry (NanoFCM)	63
3.2.6.4 Bicinchoninic Acid (BCA) protein assay	63
3.2.6.5 Enzyme-linked immunosorbent Assay (ELISA)	63
3.2.6.6 ExoView	64
3.2.6.7 Transmission electron microscopy (TEM).....	64

3.2.6.8 Proteomics and Mass Spectroscopy	64
3.3 Statistics	66
CHAPTER 4: BIOPROCESSING OF MSCS AND MSC-EVS FROM SPINNER FLASKS	67
4.1 Introduction.....	67
4.1.1 Upstream Bioprocessing	67
4.1.2 Bioprocessing factors	68
4.1.2.1 Microcarriers	68
4.1.2.2 Agitation	69
4.1.2.3 Media composition.....	70
4.1.2.4 Feeding regimes	71
4.1.3 Characterisation post Bioprocessing	72
4.1.4 Downstream bioprocessing	73
4.1.4.1 EV concentration, isolation and purification	73
4.2 Aims.....	74
4.3 Results	74
4.4 Discussion	88
CHAPTER 5: ANALYSIS OF MSC-EVS FROM OPTIMISED SF BIOPROCESS	92
5.1 Introduction.....	92
5.1.1 sEV isolation.....	92
5.1.2 EV characterisation.....	92
5.1.2.1 MISEV characterisation guidelines	92
5.1.2.2 Classical and Novel Characterisation Techniques.....	96
5.2 Aims.....	99
5.3 Results	100
5.4 Discussion	117
CHAPTER 6: THERAPEUTIC AND REGENERATIVE POTENTIAL OF MSC-EVS	123
6.1 Introduction.....	123
6.3 Functional Methods	124
6.3.1 EV dosage preparation	124
6.3.2 Fibroblast Proliferation Assay	124
6.3.3 Scratch Wound Assay	125
6.3.4 EV-PBMC Assay	125
6.4 Results	126
6.5 Discussion	132
CHAPTER 7: GENERAL DISCUSSION	135
7.1 General summary.....	135

7.1.1 MSC and MSC-EV downstream bioprocessing in SFs	135
7.1.2 MSC-EV upstream bioprocessing in SFs	136
7.1.3 sEV characterisation	137
CHAPTER 8: FINAL CONCLUSIONS	139
8.1 Novelty	139
8.2 Future work	139
CHAPTER 9: LIST OF REFERENCES	142
APPENDICES	158

List of Figures

Figure 1: Stem cell hierarchy in regards to potency, with specific examples of MSC differentiation.

Figure 2: The minimum criteria used to define a human MSC as produced by the International Society of Cell and Gene Therapy (ISCT) and their clinical applications *in vivo* [1, 2].

Figure 3: Schematic illustrating the potential bioreactor platforms and techniques to scale up MSCs and likewise EVs. These include: stirred (A), hollow fibre (B), rotary (C), wave bed (D) and vertical wheel (E) bioreactors. The full schematic was modified from a collection of figures [3-6].

Figure 4: Comparison of common microcarriers with structural, topology and chemical differences. The image is adapted from that created by Koh et al [7].

Figure 5: The biogenesis of all three main extracellular vesicle subgroups. The diagram illustrates how discharge of apoptotic bodies from apoptotic cells is comparable to the membrane blebbing observed in microvesicle formation. Exosome/small EV biogenesis involves internal MVB fusion to the plasma membrane, with no blebbing. Primarily specialised molecular signalling mechanisms facilitate late endosome/MVB internal budding and sorting of ILV contents. Following this, enzyme Rab GTPase mediates the transportation of MVBs to the plasma membrane, whereby after incorporation the ILVs are expelled as Exosomes/small EVs.

Figure 6: Upstream and Downstream Bioprocessing of MSCs in Spinner Flasks. Scalable Upstream bioprocessing to enhance MSC yield relies upon the adaptation of culture parameters, which are pinpointed with a star. These include; Microcarrier type, hold period, agitation speeds and MSC expansion media. Surrounding these is an upscale procedure consisting of steps which need to be completely controlled in order to ensure batch repeatability.

Figure 7: MC screening in 2D planar culture. Quantification of MC-MSc aggregation (A) and a selection of AM2 images from which aggregation was quantified (B). Monolayer MC dispersions were incubated with AM2, AM4 and 144 bmMSCs in 96 well plates at 5000cells/cm² for 7 days and snapshots were taken at 4x objective across this time course. The Incucyte snapshots were then quantified by background (%) unoccupied by aggregates, which indirectly reflects MC aggregation. On day 7, CCK-8 measurements were also made of cell viability post incubation and are outlined in C. Graph A and C means were plotted with SEM (A) and SD (C) from 3 technical repeats and 3 biological repeats for 3 cell lines (n=3).

Figure 8: Optimising the bioprocess parameters to increase MSC expansion and yield from Spinner Flasks. Graph A shows the effect of reducing the initial media volume (%) on AM4 MSC cell count over the course of the cell culture timeline. Graph B shows the effect of different hold period lengths in 2 cell lines on MSC expansion. Of these protocols, the most effective was employed with both plastic and plastic plus microcarriers. Each of these conditions were repeated on three separate occasions atleast with different batches of MSCs. A selection of 20x objective microscopic images are presented in D to illustrate the difference in MSC-MC bridging and aggregation across different protocols. Additionally E shows this

aggregation quantitatively using a standardised procedure/equation/method and F highlights the MSC viability post harvest from each bioprocessing protocol, all measured using the nucleocounter software. Finally graph G acknowledges the harvest (%) of 3 batches of 263 24hr hold plastic bioreactor runs. Graphs A, B, C and F mean and SEM values were plotted from 3 technical repeats of 3 independent spinner flask runs (n=3). Whilst graph E mean values with SEM was plotted from 1 technical repeat of 4 days combined calculations from 3 independent spinner flask runs (n=3).

Figure 9: MSC expansion in SFs under three different conditions used for EV collection. Graphic A describes the growth medias as; complete 10% FBS media (a), UC depleted FBS media (b) and TFF depleted FBS media (c), all with a switch to Rooster collect (RC) collection media at day 7. Graphs B both assess the effects of growth media protocols a, b and c on MSC line 263 and 271 expansion. Whilst MSC line 263 Glucose and lactate measurements across the culture timeline for all conditions are illustrated in graphs C. Graphs mean values and SEM in B were plotted from 3 technical repeats of 3 independent spinner flask runs (n=3). Whereas graph C (a,b and c) display 3 technical repeats and SEM of glucose and lactate measurements from 1 independent spinner flask run (n=1).

Figure 10: RC, UC depleted and TFF depleted nanoparticle compositions as assessed by NanoFCM. At least 2 batches of each media were sampled and analysed for concentration (A) and median size (B) and both mean and SEM values plotted (n=2). 3 batches of UC FBS were sampled and Memglow 488 lipid stained particles size distribution measured, with mean values plotted in (C) (n=3).

Figure 11: Images of 263 MSCs bridging across MCs and forming MC aggregates across the culture timeline. EVOS Light microscopy images of bioreactor samples of 3 media compositions, as well as Live stained (Calcein AM) samples on harvest day 10 from 3 cell lines run using method (b).

Figure 12: Full characterisation of bmMSCs from harvested Spinner Flasks. Histograms illustrate Flow Cytometry staining for 4 positive bmMSC markers (CD105, CD44, CD73 and CD90) (C) as well as negative markers (CD45, CD34, and HLA-DR) (B). To determine expression against the isotype control, donors 263, 267 and 271 were gated as shown in A.

Figure 13: PBMC assay of MSCs post Spinner Flask. MSCs and lymphocytes were cultured for 5 days and proliferation index quantified using cell divisions, annotated in (D) from gated lymphocytes (A). This was applied to MSC cell lines 263, 267 and 271 (B), following their harvest from agitated culture. Graph C represents the mean and SEM values for 263, 267 and 271 results combined (n=3).

Figure 14: Post harvest 263, 267 and 271 MSCs colony forming units stained with Crystal Violet. Three cell lines cultures using media protocol (b) were seeded for colony forming unit assays post Spinner Flask run and stained with crystal violet as shown macroscopically in A and microscopically in B.

Figure 15: Trilineage differentiation potential of MSC cell lines 263, 267 and 271 from the optimal SF EV collection protocol (b). 10x, 4x and 10x objective images show respectfully how once harvested, MSCs were able to be differentiated down three lineages: Adipogenic, Chondrogenic and Osteogenic.

Figure 16: EV concentration and purification from SF media via Tangential Flow Filtration (TFF). Graphic A describes the initial protocol used to isolate EVs (retentate >100kDa) from the other media components (filtrate <100kDa). The difference in the size distribution (DLS measurement) and particle concentration (NanoFCM measurement) of the filtrate and retentate is shown in graphs B and C respectively. Images E depicts the difference in filtrate and retentate samples visually by ExoView spot CD63 binding and Graph D shows the difference in protein concentration assessed using a BCA assay. Graph D is plotted mean and SEM data from 3 independent batch repeats (n=3).

Figure 17: The principle and technologies used by advanced commercial EV characterisation techniques. Images of NanoFCM single particle detection mechanism as well as the instrument (A) and ExoView fluorescent co-localisation method on the chip surface (B).

Figure 18: Cell counts and particle concentration across the culture timeline from an optimised spinner flask protocol. Three batch repeats (independent SFs) of three rooster cell lines were expanded in Spinner Flasks over 7 days in UC media and then RC media for the final 3 days. Graph A shows cell counts of both independent and MSC line repeats (n=3), where graph C illustrates the variability between three batch repeats (independent SFs) for cell line 271 (n=1). Thus, SEM bars in graph C represent three individual cell counts from 3 samples of 1 SF (technical replicates). Particles from these SFs were extracted and TFF purified for NanoFCM measurements at day 3, 5, 7 and 10. Graph B represents the particle concentrations from 1 independent SF from 3 cell lines (n=1) and 3 independent SFs/batches from 1 cell line, 271 (n=1).

Figure 19: MemGlow 488 stained particle concentration across the Spinner Flask culture timeline. TFF purified particles from the three 271 Spinner Flask batches time points were stained with Memglow 488 and their concentration measured on the NanoFCM (A) (n=1). Day 3 and day 10 scatter plots (B) demonstrate the change in ratio of stained Vesicle to unstained Particle.

Figure 20: Median size of particles across the Spinner Flask bioprocess timeline as measured using NanoFCM. Graph A demonstrates three MSC cell lines particle sizes (n=1) whilst B demonstrates the mean and SEM of three combined MSC-particle batches of the same cell line (271) (n=3).

Figure 21: Method comparison for analysis of 271 TFF purified particles harvested from Day 10 of each individual Spinner Flask batch runs. Graph A depicts the difference in concentration between 3 batches of particles measured by NTA and NanoFCM (n=3), whilst B illustrates the particle size distribution plots for these batches. The average median (D50) size values from these 3 batches were also compared using NTA, NanoFCM and ExoView systems (C) (n=3).

Figure 22: TEM images of 271 TFF secretome purified from Spinner Flasks on day 3, 5, 7 and 10. Arrows point to vesicle like structures which are representative of the size of small EVs or Exosomes.

Figure 23: Extracellular Vesicle tetraspanin markers assessed across the 271 bioprocess timeline (Day 3, 5, 7 and 10). CD9, CD63 and CD81 expression was calculated using an ELISA assay (C), measuring tetraspanin positivity against standards (A); and also using the ExoView software (D), applying an IgG negative control (B). Graph B shows cut-offs, which were consistent across all experiments to control against non-specific binding to IgG. ELISAs

were performed and both mean and SEM values plotted using 3 technical replicates (n=1), whilst ExoView mean and SEM data were derived from 3 independent grafting spots (n=3).

Figure 24: Assessment of TFF purified EVs tetraspanins, measured by ExoView software. Graph A depicts particle count across batches of 263 day 10 EVs and graph B differences between cell lines 263 and 271 EVs. Data and SEM from each batch was plotted from 3 independent grafting spot measurements (n=3), whilst cell line results (B) were obtained from both 3 spot replicates and 2 independent batch chip measurements (n=3).

Figure 25: Mass Spectrometry data depicting gene % within each protein category (A) as well as highlighted (bold) specific genes associated with sEVs and MSCs (B). Data were retrieved from three batches of 271 TFF+SEC isolated sEVs (n=3).

Figure 26: Mass Spectrometry data depicting gene fold value change between culture time points 5-7 and 7-10 within each protein category compiled from 3 batches of 271 TFF+SEC isolated sEVs (n=3). Graph A outlines protein fold change levels from cellular components which are sEV specific. Graph C illustrates fold change in categories associated with molecular function, whilst D illustrates greatest fold change for biological process'.

Figure 27: Characterisation summaries of TFF purified EVs produced from 3D and 2D culture conditions. Diagram A summarises both media collection protocols from Spinner Flasks (3D) and Planar flasks (2D). Graph C summarises the difference in tetraspanin positivity (n=3), whilst graph C identifies sEV median size (B) through the ExoView software. The overall concentration of particles/ml from samples of 2D and 3D TFF purified secretome was analysed by NanoFCM and is presented in graph D.

Figure 28: Differences in 271 EVs concentration and size when isolated by TFF + SEC compared to TFF alone. A visual representation of the two different isolation methods and the resultant EV/secretome concentrate (1) and EV isolate (2) is illustrated in graphic A. Graph B portrays the difference in protein concentration between both isolation methods using a BCA assay, whilst graphs C, D and E employ NTA to initially assess both samples modal size and nanoparticle concentration. Graph B and D is plotted mean and SEM data from 3 technical repeats (n=1). Whilst graph C is plotted median of modal values for size distribution from 5 independent repeats (n=5).

Figure 29: Comparison of particle characteristics between TFF purified and TFF+SEC isolated Spinner Flask sEVs on Day 10 of collection. Lipid particles were labelled with Memglow 488 and three isolated batches analysed using the NanoFCM for concentration (A) and percentage staining (B) (n=3). From this data, the average median particle size was also plotted (C) (n=3). TFF vs TFF+SEC isolates were analysed through the ExoView software to fluorescently image (E) and quantify (D) this for tetraspanin positivity.

Figure 30: Comparing TFF and SEC fractions for lipid stained nanoparticle presence. Graph A outlines stained particle concentration, whilst B depicts what % fraction of all particles were lipid membrane bound and C compares the median size of stained particles in each sample. Graph D mean and SEM protein concentration data for each fraction was produced by 3 technical BCA repeats (n=1). Graphs A,B and C were plotted from means of a single TFF concentrated and SEC isolated batch (n=1).

Figure 31: Effects of MSC-EVs on 3T3 Fibroblast proliferation. 100µg/ml MSC derived EVs were incubated with 5000 Fibroblasts/cm² for 72 hours to determine their effect on cell

proliferation. (A) Graph highlights the CCK-8 live cell count readings between both 2D vs 3D derived and TFF vs SEC isolated EVs treated MSCs every 24 hours. In order to also assess the consistency in proliferation between these conditions, three independent MSC-EV cell lines were tested (B and C). (D) Representative enhanced (top) and ImageJ edited (below) Incucyte images show differences in fibroblast confluency under SEC and TFF isolation conditions. All plotted data in A, B and C representative of 3 technical repeats within 3 independent biological repeats (n=3).

Figure 32: Effects of 100µg/ml MSC derived EVs exposed to a fibroblast scratch wound for 24 hours. (A) Graph shows the scratch area percentage change over time in the presence of either the 2D and 3D culture derived EVs, as well as the SF media control. Additionally scratches were treated with EVs from 3 MSC cell lines isolated by SEC in (B) and TFF in (C) scratch area (%) was measured at both 10 and 20 hrs to give an indication of the rate of closure. (D) Representative examples a selection of scratch closure images from which the quantified percentage area values were derived. Summary graphs A, B and C represent 3 technical repeats within 3 independent biological repeats (n=3).

Figure 33: Effects of EVs on T cell proliferation. (A) Proliferation dye labelled PBMCs were incubated in the presence or absence of PHA and IL-2, and effects on proliferation assessed by flow cytometry. (A) shows the positive control flow cytometry gating for T lymphocytes, excluding monocytes and granulocytes which was set as a standard for all experimental conditions. Histograms from the gated control, illustrated in D, shows distinct peaks for each population for divided and undivided cells. Calculated proliferation index from each condition were plotted in B and C, assessing the differences between different MSC cell line EVs (B), EV isolation method and EV 3D vs 2D bioproduction (C) on PBMC proliferation. Images in E demonstrate the visual change between aggregated stimulated PBMCs and unstimulated PBMCs after four days of treatment. All plotted data in A, B and C represent seven technical repeats within one biological repeats (n=1), hence no statistical tests were performed for this data set.

Appendix figure 1: ExoView errors when performing EV tetraspanin analysis. Image A illustrates the effect of poor drying on chip appearance under a fluorescent microscope. Image B demonstrates background fluorescence from an unknown source, most likely drying effect from a droplet which remained on the chip after drying. Image C reveals how drying effect appears on a postscan of the chip, prior to fluorescent imaging for EVs. Image D shows a saturated chip, on which the sEVs are too concentrated and need diluting. Image E highlights the possibility of patchy sEV attachment to chip spots during the incubation stage. Finally F shows autofluorescence from a dust fragment bound to the chip surface.

List of Tables

Table 1: Stem Cell subtype advantages and disadvantages

Table 2: Categorising the three main extracellular vesicle subtypes

Table 3: The strengths and limitations associated with each isolation platform. Technique images and overviews adapted from the paper by Coumans et al [6]. Advantages and Disadvantages were taken from those listed in several review articles by Yamamoto et al [8], Chen et al [9], Xu et al [10] and Liangsupree et al [11].

Table 4: Reference table for basic materials and reagents information.

Table 5: Additional microcarrier details, including physical and chemical composition

Table 6: Bone Marrow Mesenchymal Stem Cells (bmMSCs) donor information

Table 7: Bioprocess conditions for SFs with modifications (highlighted in bold).

Table 8: Review of traditional EV characterisation methods

List of Abbreviations

bmMSC – bone marrow Mesenchymal stem cell

CM – Complete media

DLS – Dynamic light scattering

DMEM – Dulbecco's Modified Eagle's Medium

ELISA – Enzyme-linked immunosorbent assay

EVs – Extracellular vesicles

FBS – Fetal bovine serum

ILV – Intraluminal Vesicles

ISCT - International Society of Cell and Gene Therapy

ISEV – International Society for Extracellular Vesicles

MC – Microcarrier

MISEV – Minimal information for studies of extracellular vesicles

MS – Mass spectrometry

MSC – Mesenchymal stem cell

MVB – Multi Vesicular Body

NTA – Nanoparticle tracking analysis

PBMC – Peripheral blood mononuclear cells

PBS – Phosphate Buffered Saline

PP – Plastic plus

RC – Rooster collect

SC – Stem cell

SEC – Size exclusion chromatography

sEVs – small extracellular vesicles

SF – Spinner flask

TEM – Transmission electron microscopy

TFF – Tangential flow filtration

UC – Ultracentrifuge

XF – Xeno-free

Chapter 1: General Introduction

1.1 Basis of stem cell research

Since the pioneering Hematopoietic stem cell research in 1950s – 1960s by American researcher Dr E. Donnall Thomas, also known as the “father of bone marrow transplantation”, advancements in stem cell applications have soared [12, 13]. He performed the first human clinical trial on allogeneic bone marrow transplantations in 1957 and, although unsuccessful, monitored the progress of HLA-matching (mostly by van Rood et al) until he was able to create the first individualised leukaemia therapy programme [13, 14]. From this work many more centres for the treatment of hematologic malignancies opened, and later he received the nobel prize in 1990 for laying early research foundations for modern cancer immunotherapy treatments [13, 14].

This backbone research has now fed a plethora of studies into stem cell applications in regenerative medicine, *in vitro* organ/tissue modelling/tissue engineering and drug delivery etc [15].

1.2 Stem Cells

By definition, Stem Cells are unspecialised cells of a multicellular organism, capable of undergoing self renewal, maintaining stemness and differentiating [16]. Within this collective, subtypes of stem cell are classified by their level of potency, which controls their ability to specialise and is determined by their source of origin (figure 1). An example of a Totipotent Stem Cell is the fertilized egg (zygote), with the ability to specialise and differentiate into a Pluripotent Stem Cell (PSCs) and extra-embryonic structures [16]. These Pluripotent Stem Cells, which are derived from the Blastocyst Inner Cell Mass and also known as Embryonic Stem Cells (ESCs), are the precursors for the three Germ layers (Ectoderm, Endoderm and Mesoderm) [16]. Additionally, induced Pluripotent Cells (iPSCs) can also differentiate down the same lineages as an ESC but are generated artificially and engineered by reprogramming somatic cells [16]. Multipotent stem cells have a further narrowed spectrum of specialisation than PSCs towards select lineages. These include: Mesenchymal Stem Cells (MSCs), Hematopoietic Stem Cells (HSCs) and Neural Stem Cells (NSCs) [16]. Once differentiated, Multipotent stem cells can either become Oligopotent stem cells or Unipotent stem cells, meaning they either have considerably or completely restricted capacity to differentiate,

respectfully [16]. For example, Cardiac stem cells formed from an MSC, are oligopotent and able to form cardiomyocytes, smooth muscle cells and endothelial cells [17, 18]. Whereas cardiomyocytes are binucleated somatic cells, unable to further differentiate [17].

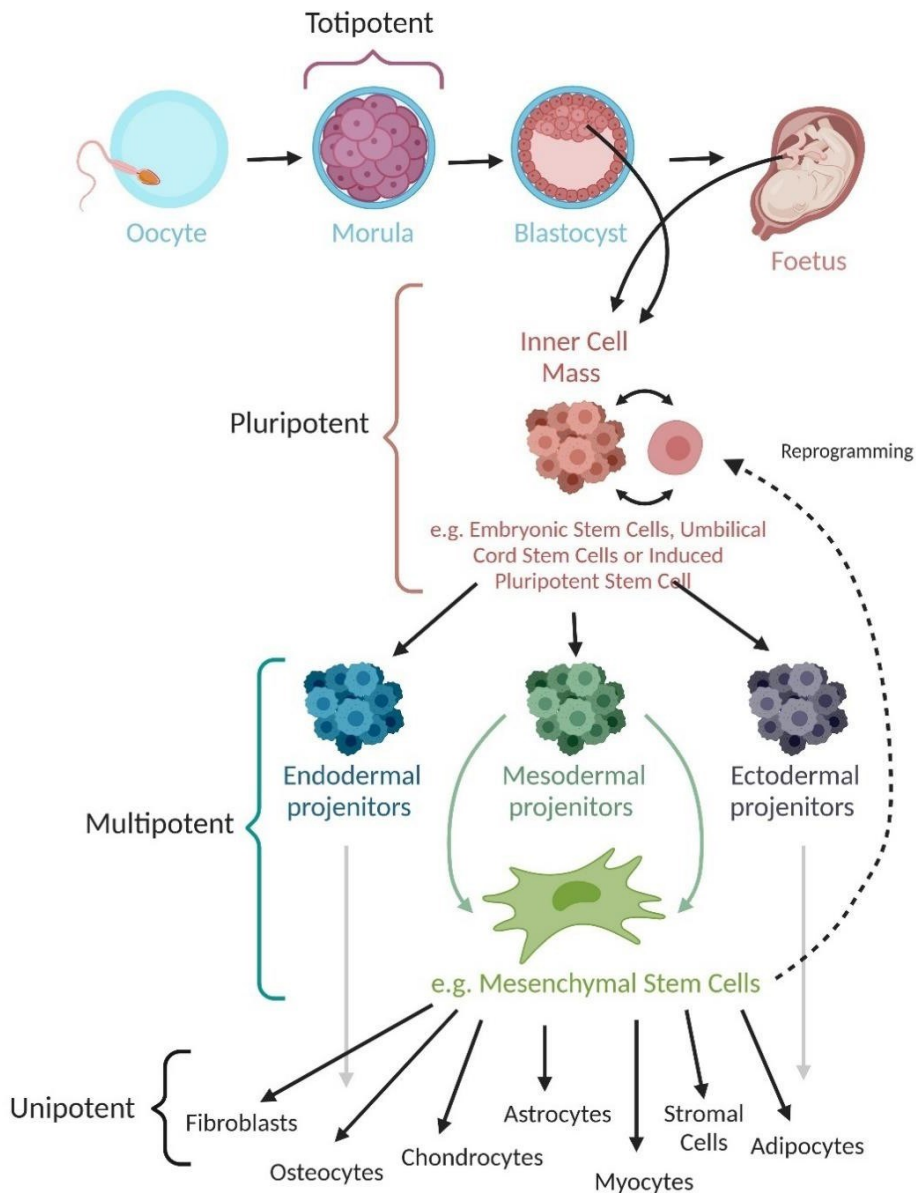


Figure 1: Stem cell hierarchy in regards to potency, with specific examples of MSC differentiation.

Stem cells as a collective have been extensively explored as biological therapeutics for replacement/engraftment and regeneration of impaired tissues. However, each has their own advantages and disadvantages which makes them preferable for use in specific fields of research, as outlined in table 1.

Table 1: Stem Cell subtype advantages and disadvantages

Cell Type	Advantages	Disadvantages	Reference
ESC	Pluripotency Unlimited self renewal and proliferation Abundant/Indefinite supply	Ethical/political concerns Potential for teratoma and tumour formation Immune rejection	[19-21]
iPSC	Pluripotency Autologous origin Reduced ethical issues Abundant sources Unlimited self renewal and proliferation	Potential for teratoma and tumour formation Inefficiency as difficulty controlling differentiation Instability Difficulty with cellular reprogramming	[19-21]
MSC	Ease of isolation Accessibility Immunoprivileged High yield from extraction from Adipose tissue Autologous origin	Limited replicative lifespan (loses potency) Low yield from extraction from Bone Marrow tissue Extraction can be painful (source dependent)	[19-21]

When choosing a stem cell subgroup from which to source our EVs, it was important that they were well characterised, scalable and their regenerative potential thoroughly understood and well documented. MSCs, as well as meeting these criteria, also possess stand out additional properties such as immunomodulation and anti-inflammation, which additionally endorse tissue repair [22-24].

1.2.1 Mesenchymal Stem Cells

International Society of Cell and Gene Therapy (ISCT) guidelines recommend that prior to studying MSCs, it should be illustrated that they fulfill the following cell-surface biomarker expression criteria: $\geq 95\%$ positive expression for CD73, CD90 and CD105, with $\leq 2\%$ expression within the population for CD34, CD45, CD11b or CD14, CD19 or CD79a finally and HLA class II [25]. In relation to MSC-EVs, it will be interesting to see if surface markers

such as CD44, CD73 and CD90 are expressed upon proteomic analysis, as other researchers have previously demonstrated their presence [26, 27]. Additional characteristics of MSCs are depicted in figure 2.

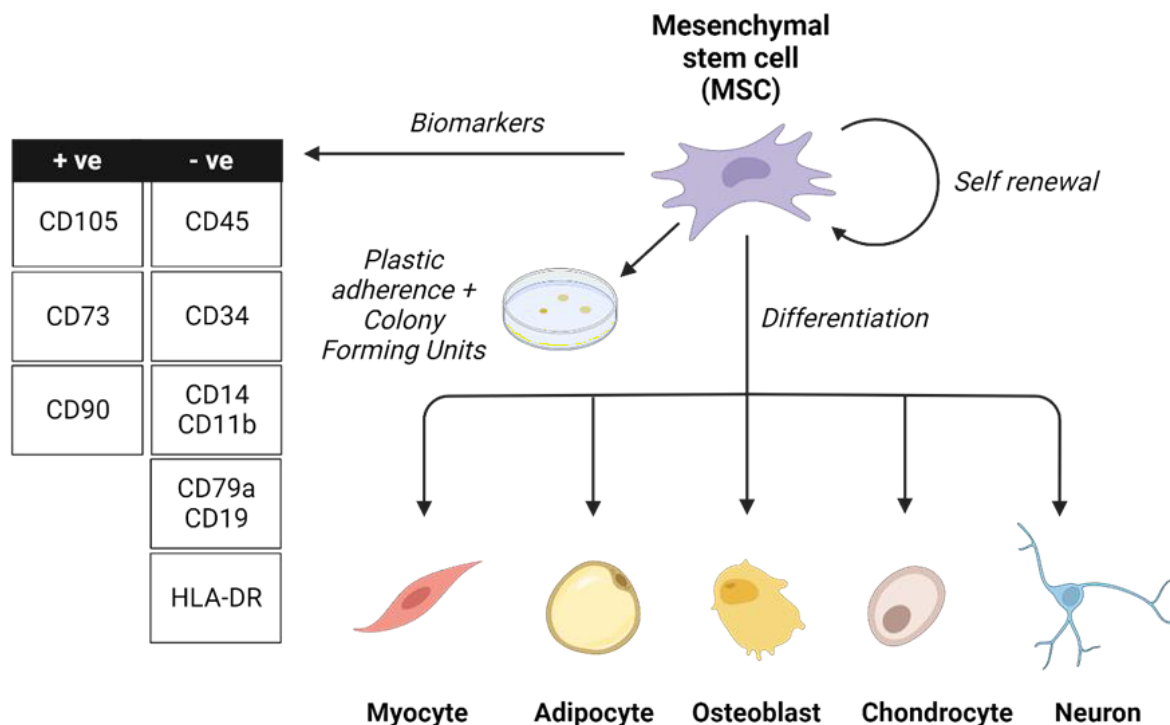


Figure 2: The minimum criteria used to define a human MSC as produced by the International Society of Cell and Gene Therapy (ISCT) and their clinical applications *in vivo* [1, 2].

Sources of MSCs and niches from which they could be isolated include: bone marrow, umbilical cord, cord blood, placenta, adipose tissue, tendon, Wharton's jelly and dental pulp [28-30]. Some may be more widely investigated *in vitro* rather than *in vivo*, depending on their safety and efficacy. For example, bm-MSCs were formerly the most widely applied subgroup, where they depicted the highest levels of multipotency and so had a wider range of implications. However there is a level of risk and pain to the extraction procedures to achieve a low cell yield of ~100cells/millilitre and in the case of the iliac crest, concentrations around 0.001–0.01% after purification [29, 31-33].

On the other hand, yield from adipose tissue derived from liposuction procedures can be 100-500 times higher than from the bone marrow [29, 32]. These banks of adipose MSCs are also a by-product of the procedure, where the tissue would normally be discarded as waste, and so their collection is deemed to be non-invasive and the cells highly accessible [34]. Additionally, some studies have shown them to have a higher proliferation capacity than bm-MSCs [30, 35]. However, bmMSCs are an attractive source for conducting research into cartilage and bone regeneration due to their preference towards these lineages [30, 35].

For the aims of this project nonetheless, the decision was to stick with the application of bm-MSCs due to their higher potency and the niche's homogeneous population of easily isolated MSCs, which are well characterised by the ISCT, as illustrated in figure 2 [36]. Their depth of documented research in the stem cell, scale up and Extracellular Vesicle research fields, as illustrated in the continuing sections, also makes bm-MSCs more attractive [37, 38].

1.2.1.1 Defining MSC

Prior to performing, presenting and reporting the MSC research, it was initially important to address how we wished to refer to the MSCs. This is due to the recent conflict surrounding their nomenclature, where their highly heterogeneous marker profile and variable potency has caused many groups to drop the use of "stem" [39, 40]. Specifically, this shift is towards Mesenchymal stromal cell and Multipotent progenitor cell [40-43]. In support of this change, in a therapeutic setting the term "Stem Cell treatment" is believed to be referred to as one in which the cells will offer a direct local response by remodelling healthy tissues. This however is not the case for MSCs as the trophic response is largely due to bioactive factors, suggesting employment of the term Medicinal Signaling Cells in replacement of Mesenchymal stem cells [44, 45]. For the purpose of this *in vitro* study however, where the purpose is for the MSCs to retain their stemness, we will be referring to them by their more well recognised naming of 'Mesenchymal Stem Cell'.

1.2.1.2 MSCs as therapeutics

The necessity to scale up Stem Cells comes from the high demand for therapeutically relevant doses which could later be applied *in vivo*. According to multiple review articles this minimal effective dose for IV transplantation was recorded to be between 70 and 190million MSCs/patient [46-48]. When this quantity is achieved, MSCs can be an appealing therapeutic, especially in personalised medicine [49]. When employed therapeutically, MSCs can be transplanted from the patient's own stem cell source (autologous) or extracted from an alternative individual, who has been MHC matched, and implanted in the patient (allogeneic) without inducing a cytotoxic response and transplant rejection [50]. They have the advanced capacity, unlike embryonic stem cells (ESCs) and induced pluripotent stem cells (iPSCs) of being moderately immunologically privileged and thus relatively safely implanted from a donor into a recipient [1, 51, 52]. This is due to regulated surface expression of transmembrane glycoprotein human leukocyte antigen-I (HLA-I), which allows MSCs to bypass CD8-

expressing T-cells [1]. Various regenerative study observations also recognised MSCs: anti-inflammatory action, promotion of macrophage plasticity through the TLR4 signalling pathway, depleted infiltration of white cells (neutrophils and macrophages) and preferment of the M2 macrophage phenotype [53-55]. This has led to their implementation in a wide range of clinical trials. Data from clinicaltrials.gov shows how at the end of 2019, just below 200 clinical trials with hMSCs were running, with 80% reaching phase I and II [56, 57]. Nevertheless, despite the high quantity of clinical studies, in 2015-2018 it was reported that only 13 hMSC-based products had achieved marketing authorization [56, 58]. Although safe and feasible, concerns into their therapeutic efficacy remain as they appear to show variable clinical impact [15] and hence struggle to make it through trials.

1.2.1.3 MSCs + EVs as immune-therapeutics

Continuing laboratory based studies into the different methods employed by MSCs which modulate physiological effects on other cells or tissues (cell-cell contact, release of soluble factors and enzymes as well as the paracrine release of factors) has shown the critical influence of the cell secretome. Their secretome is complex, encompasses soluble factors (growth factors, cytokines, chemokines and enzymes) and Extracellular Vesicles which have cargos containing soluble proteins, lipids, DNAs, RNAs and mitochondrial fragments [49, 59-61]. The particular ability of EVs within the cell secretome to maintain health through indirect cell communication has given them recognised potential as a nanoscale cell free therapeutic [49, 60, 61]. Specifically, MSC-derived EVs have shown to release immunomodulatory molecules such as IL-10, hepatocyte growth factor (HGF), transforming growth factor (TGF- β 1) which suppress T-cell proliferation and interact with other immune cells [163]. Additionally, their innate ability to reduce the proliferation, maturation, differentiation and activity (e.g. antibody production) of Natural Killer cells, Dendritic cells and B Lymphocytes suggests an Immune response inhibition affiliated to MSCs [62]. This recognises MSC-EVs potential to perform to the same or heightened standard to MSCs in clinical trials.

1.2.2 Cell culture of MSCs

MSCs can be expanded in culture in order to perform *in vitro* studies of their phenotype, secretome, regenerative potential, potency etc. The most basic form of this cell culture occurs in 2D on planar plastic culture surfaces, where the adherent MSCs can respond to a stimulus and then be assessed. This basic cell culture method however is laborious when expanding MSCs for large scale studies, producing therapeutic quantities of MSCs for assessment in

animal, 3D and organoid models. The same issues have been described more recently when attempting to collect suspended EVs from the cell culture media of planar T-Flasks at which the concentrations are too low for many of the analysis methods. Hence, especially when looking at scalability in this project we have chosen to move away from the use of traditional monolayer cell culture flasks and into systems that provide a larger culture surface area and expansion capabilities.

1.3 Scale Up and Scalable systems

The main considerations when working with MSCs and moving from a small scale cultivation system is to ensure that the platform provides: structural support for MSC adherence, as well as cultural stability to allow maintenance of MSC immunophenotype and multipotency. Furthermore, when generating large volumes of cell therapy product, there should be batch consistency and homogeneity and the system itself should be minimally labour-intensive, controllable and monitorable [63].

As a 2D set up, cell stackers (multi layered surfaces) are a simplistic, low cost way to perform compact scale up and are capable of achieving high cell volumes [63-65]. In particular the Nunc™ Cell Factory™ and Corning® CellSTACK® save incubation space and hence produce numbers of cells >100 times more than in a conventional T-flask [66]. However, this method is laborious and culture conditions difficult to monitor, especially when flasks or layers constitute their own distinct microenvironment [58, 63, 65]. Overall cell stackers provide a non-homogeneous culture chamber with restricted surface area, limiting overall scalability and fitting them for 'scale out' expansion [58, 65].

Unlike the constricted monolayer culture flasks, bench top suspension/agitated cultures can aid with generation of large volumes of cells/cell products in one chamber, where multiple flasks would normally be necessary. Specifically, bioreactors in comparison to spinner flasks (SFs) have increased volumetric productivity and so can facilitate a greater fold increase in expansion. Rafiq et al exhibited this by achieving a 6.02 and 7.02 fold expansion in 5L stirred tanks, in comparison to 3.66 and 5 fold in volume matched spinner flasks [67, 68]. As the requirements move further towards manufacturing or clinical scales, Bioreactors can facilitate production but with additional better monitoring and control over the culture process.

Commercially available bench top and industrial bioreactor types for adherent cells are shown in figure 3 and include mechanically driven (stirred tank, wave bed/rocker, vertical wheel, roller) and hydraulically/perfusion driven (hollow fibre bioreactor, fixed/packed bed) bioreactors [58, 63, 65, 69]. The use of dynamic bioreactors allows a continuous feeding cycle where agitated culture medium has consistent gradients, oxygen levels and distribution of nutrients [58, 63, 70, 71]. This allows for even maintenance of cells metabolic state and capacity to proliferate.

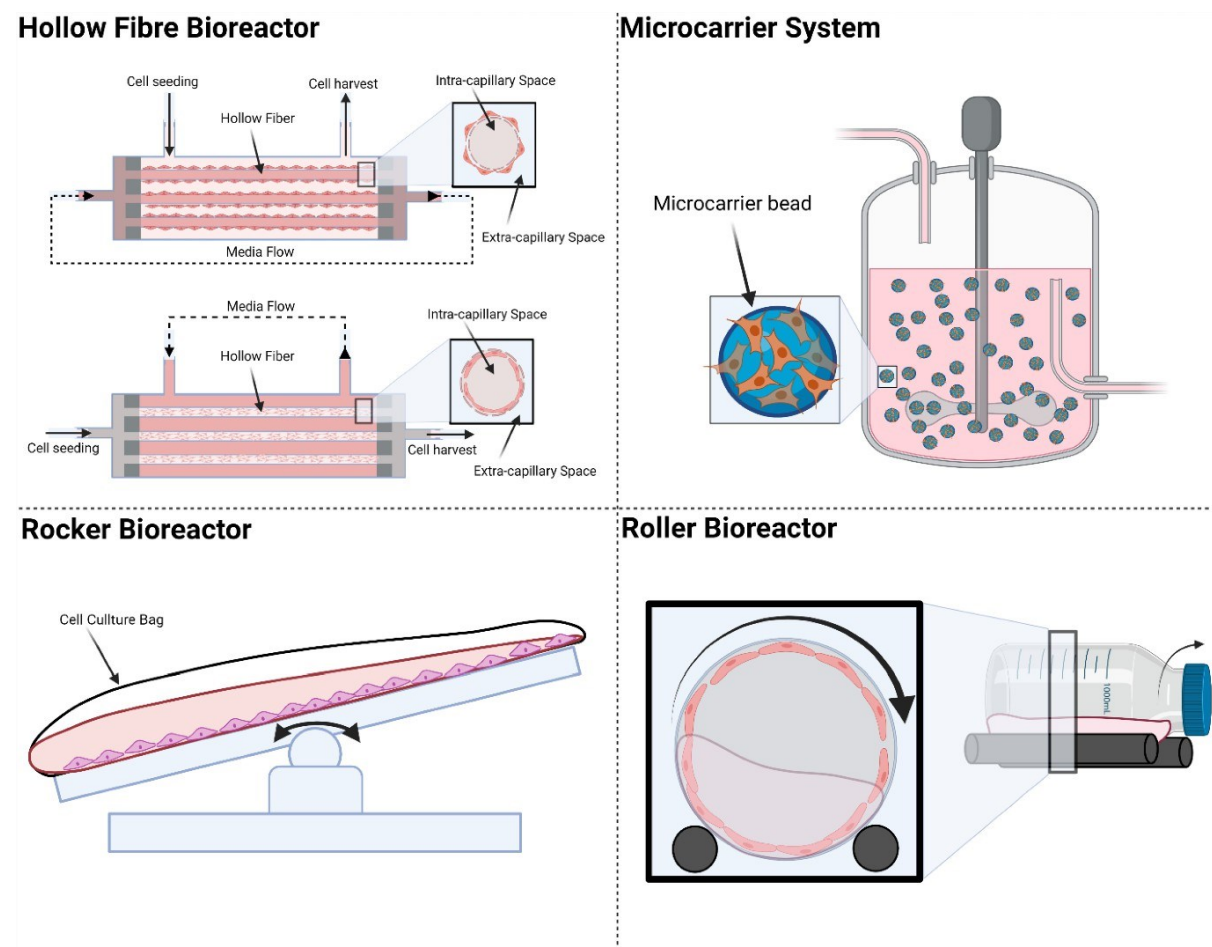


Figure 3: Schematic illustrating the potential bioreactor platforms and techniques to scale up MSCs and likewise EVs taken from an article by Chan et al (Chan WW, 2021). These include: Hollow fibre, Stirred, Rocker and Roller.

Achieving this agitated, homogenous culture relies on either the driving of liquid past cells (hydraulics) or mixing by means of impeller or the culture platform in motion [63, 69, 72, 73]. However, hydraulically driven systems are advantageous in that they generally depict low-level sheer stress, which minimises the risk of damage to the cells or lineage differentiation

[69, 73]. For example, fixed bed and packed bioreactors use a similar concept to planar flasks, where the cells grow in 2D layers on immobilised microcarriers (MCs), fibres or scaffolds. However, utilising a closed, perfusion feeding approach, the culture vessel has better parameter control, as well as homogeneity. Nevertheless, there are exceptions to the rule. In the case of hollow fibre bioreactors it is more difficult to maintain stable longitudinal concentration gradients as nutrients and oxygen becomes depleted along the fibre length [63, 74, 75]. Nonetheless, the closed cylindrical chamber provides an environment mimicking vesicular structures, by allowing cells to be inoculated and grow within the capillary space and on the fibrous surfaces [63]. This makes it an advanced method for scaling up cells, which thrive under these conditions *in vivo*, e.g. vascular, fibrous and cord tissues.

As generally less complex and inexpensive bioreactor systems, those that are mechanically driven use classic ways to scale adherent cells, whilst providing consistent gradients and levels of mass transfer through the system. Roller bottles provide a bench top scale up solution to static T flask cell culture, where cells grow in monolayers on the roller surface and during rotations are cyclically bathed in homogenous mixed culture medium [63]. Although the surface area is still restricted, deeming them unsuitable for clinical or industrial scale manufacturing [63, 76]. Rocker/Wave bed bioreactors use a platform, unlike the roller for the bottle bioreactor, to provide a pivoting motion to generate a flow of media over surface or matrices adhered cells [71]. Unlike a paddle driven bioreactor, the rocker movement creates low shear stress and thus makes it preferential when working with more sensitive cells [71, 77]. Moreover, the bag's connectable ports allows for optional feeding regimes (batch fed, repeated batch fed, and perfusion) and thus the bioreactor offers flexibility in performing large-scale cell culture [78]. Similar in some respects is the stirred tank bioreactor, which is also a closed, automated apparatus, with optional feeding regimes. Alike the rocker bioreactor, there is the choice for the stirred tank culture chamber to uphold various substrates for cell adherence, including MCs, as well as cells, spheroids or organoids in suspension [63, 79]. As suggested in the name, the bioreactor's agitation mechanism is operated by an internal impeller, which can make direct contact with the cells and hence give rise to shear stress [80, 81]. The same hurdles occur when expanding cells in spinner flasks that are used as a downscaled bench top stirred system. They are employed mostly to assess multiple factors and their effects on scalability, prior to testing in expensive bioreactors. However, the vertical wheel bioreactor was designed and commercialised more recently as a means of reducing the shear stress experienced in the classic stirred bioreactor [82].

Considering all these methods, as well as their outlined pros and cons, in order to evaluate the scalability of bmMSCs and their EV secretome, smaller scale 100ml spinner flasks were chosen as the platform to study. This gives the option following on from this to look to apply

our selected bioprocessing methods to larger scale, stirred tank bioreactors used in industrial applications.

1.4 Stirred flasks culture

1.4.1 Stirred flasks

Spinner Flasks (SFs) are highly adaptable, affordable, reusable (in most cases) culture vessels, which make them an ideal platform for performing studies that inform process development. The culture chamber and impeller can come in different shapes and with different capacities (ml-l scale). As a general culture vessel, it incorporates a conductive stir bar, with adjustable paddle, which when stimulated by the magnetic stirrer platform or overhead motor, creates an adaptable flow of fluid [83].

1.4.2 Microcarriers and Scaffolds for suspension culture

The initial manufacture and implementation of microcarriers (MCs) occurred in the late 60s-70s where Van Wezel demonstrated that anchorage-dependent cells could attach and grow on MC surfaces [84]. Commonly, their application is mainly in stirred-tank systems whereby culture conditions are flexible and adjustable to optimise harvest, but also in rotating wall bioreactors [85]. They are defined as small, spherical beads, as shown in figure 4, which act as a support matrix for cells to attach and duplicate in suspension [86]. These properties provides them with a high surface area to volume ratio, enhancing cell growth and thus cell/cell product yield. To be specific, they are manufactured to be $1.02 - 1.1\text{g/cm}^3$ to standardise minimum Njs and MC settling efficiency for flask sampling. Additionally applying MCs there is a decrease in cost ($\$0.044$ per cm^2) compared to stacked 2D plates ($\$0.061$ per cm^2) [87]. Thus, characterisation and employment of MCs is widest in industries concerned with the scale up of cellular therapeutics for clinical implementation.

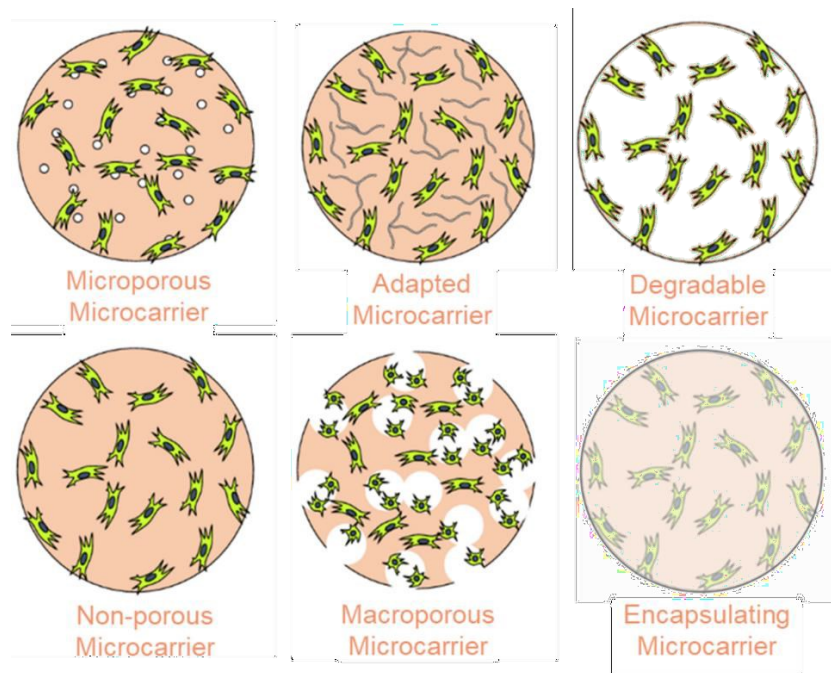


Figure 4: Comparison of common microcarriers with structural, topology and chemical differences. The image is adapted from that created by Koh et al [7].

Nonetheless, a distinct, preferential MC for culture of differing cell types has yet to be selected [88]. The difficulties in doing so occur because of the diverse range available and their varied performance dependent on culture conditions. MCs can possess varying physical properties including; stiffness, nanotopography, porosity, density, dimensions, surface topography and charge [88], synthetic or natural composition and functionalised groups (figure 4). Synthetic MCs are advantageous in terms of their low cost and high reproducibility in bulk, but they lack surface recognition and binding sites, which can enhance cell expansion [89]. Their base includes; glass, poly(lactide-co-glycolide) (PLGA), polyhydroxyethylmethacrylate, acrylamide, polystyrene and polyurethane [90]. In contrast, naturally sourced MCs are composed of biological polymers and derivatives, making them abundant and highly biocompatibility [91]. They include; gelatin, alginate, dextran, and collagen [92-94]. Additional physical characteristics, such as porosity, provides MCs with surplus surface area in which cells can adhere, as well as some shelter against intense hydrodynamic forces and shear stress in bioreactors [95]. However, some nano/microporous MCs offer pores too small for cells to easily enter and hence macroporous MCs or compartmental microspheres are preferential, offering greater cell infiltration, attachment and expansion [96, 97]. Yet, within MC pores nutrient and oxygen supplies have been shown to be depleted and thus less available to cells growing inside, affecting their quality and homogeneity [98]. Alongside these physical attributes, chemical functionalisation at the exposed MC surface can augment further their properties, leading to more rapid cell adhesion and expansion. Charged groups, including

Diethylaminoethyl (DEAE) or non-ionic animal proteins (collagen) and biological derived extracellular matrix components (glycoproteins including mouse laminin and human plasma purified fibronectin) are common examples [88].

Within chapter 4, the importance of MC selection is explored further by screening MCs which comply with the basic criteria of:

- Providing rapid cell attachment.
- Being cost effective.
- Tolerating shear stress in bioreactors with intense mechanical forces
- Maintaining even surface distribution of adhered cells.
- Facilitating or encouraging cell proliferation.
- Preserving cell stemness and functionality, discouraging differentiation.
- Ease of handling.
- Producing a consistent cell yield.

1.4.3 Stirred culture biophysics

In order to suspend these MCs in culture fluid, a physical force is needed. The aim of the mixing motion in the SF is therefore to both maintain the suspension of free/adhered cells, as well as to homogenise the molecular components of the culture media.

The N_{s1} (N_{js} or N just suspended) value by Zwietering, developed and demonstrated in the late 1950s, provides an effective way of balancing fluid flow force. It is defined as “the minimum impeller speed that just fully suspends the MCs at minimal shear stresses” and in brief, applies values to variables which can be attributed to shear stress in a stirred bioreactor. These include: particle size, particle density, liquid density, ratio of solids to liquids and Impeller diameter [99]. The importance of N_{js} has been demonstrated in cell cycle and DNA synthesis studies where shear stress created from fluid flow inhibited movement from G_0/G_1 to S phase [100, 101]. Luo et al., suggested that this cell cycle suppression and eventual arrest, so noticeable lack of expansion, may be a result of changes to cytoskeletal structures associated with the MAPK/ERK signalling pathway [100]. The links between physical stress and cell proliferation via this pathway has been described in endothelial cells and osteoblasts since by authors in related papers [102, 103]. Further to this, a review article by Tsai et al described research that reinforces how surface shear stress donates both chondrogenic and osteogenic lineage commitment, via a process called mechanotransduction [66]. Morphological responses to shear stress such as these can occur when exposed to forces of 0.013Pa or

more, thus making design of agitation protocols through computational fluid dynamics preferential [104]. For SFs running at even low stir speeds of 28rpm, a mean force of 0.0592 Pa was detected by Ismadi et al using Particle Image Velocimetry [105].

Although this data suggests that that mechanotransduction may occur at 30rpm, a lack of fluid flow below this speed has been evidenced to cause cell-cell collisions, which can henceforth cause spontaneous aggregation and clumping. Allowing MCs to collect and crowd the base of the flask during the log/exponential phase can lead to excessive bridging and MC agglomeration. Consequently creating zones of oxygen and nutrient deficiency, which compromises MSC viability [106, 107]. From a cell culture perspective, agitation of culture media in the stirred system drives the dispersion of critical gases and nutrients to create a homogenous microenvironment which meets cells metabolic demands [58, 63, 70, 71]. Adequate mixing is also important for homogenic dispersion of nutrients and gases through the culture vessel. Deprivation of these through inadequate mass transfer gradients prevents mitochondrial respiration from occurring and thus induces cell death by apoptosis [108-110].

In order to assess MSCs can maintain their potency after expansion on MCs in suspension culture, cell-MC interaction, cell metabolism was monitored and maintenance of stemness post-harvest was assessed. This allowed our group to conclude with certainty that the optimised bioprocess promoted MSC proliferation without any adverse effects on their profile or functionality. In addition, the project mainly focused also on the bmMSC secretome, collecting the spent media from bmMSC culture and isolating extracellular vesicle populations. Therefore any the assessment of the effects of MSC bioprocessing on MSC derived extracellular vesicle populations was also carried out across the suspension culture timeline.

1.5 Extracellular Vesicles

1.5.1 Historic timeline of EVs

Prior to their current definition as small Extracellular Vesicles (sEVs)/Exosomes, there are decades of research which focused on understanding their origin and bioactivity and harnessing their potential. Initially they were visually referenced to as sub-micron sized membrane bound vesicles in the extracellular space/matrix from early electron microscopy investigations [111-114]. One investigation described the existence of multivesicular bodies (MVBs) at the edge of the apical membrane and proposed potential fusion to expel packaged vesicles into the luminal space [114]. Research in the 1980s exposed a trafficking and sorting

pathway, now defined as the exosome biogenesis and secretion pathway and also the shedding of what they referred to as 'exosomes' from MVBs fused with the plasma membrane [115-119]. Although for a period of time, the role of these 'exosomes' was believed to be an 'apparatus' for waste disposal', and this was the accepted theory until pivotal investigations in the late 90s [120, 121]. These papers depicted sEVs from immune cells as antigen presenting and able to play physiological roles, be loaded and have therapeutic application [122, 123] .

1.5.2 EV definition

Leading us into the present day, Extracellular vesicles (EVs) are described as heterogeneous membrane capsules in the nano/micro-particle scale of between 30-10,000nm diameter [124]. Up to date evidence has illustrated their encapsulation of biological cargo key to maintaining healthy physiology (nucleic acids, metabolites, proteins and lipids) [121, 124]. Thus establishing their role in cell-to-cell communication between remote and neighbouring cells. This is in order to: maintain stem cell (SC) potency, regulate homeostasis, initiate immunological and inflammatory responses and promote tissue repair and regeneration [49, 60, 124]. They also have fantastic homing capacity and thus the small-scale vesicles are able to provoke a response at greater scale. Annually, new publications are further distinguishing their physical and biochemical properties and hence elucidating their potential as diagnostic indicators and therapeutics [125-127]. These investigations are increasingly attractive due to their presence in almost every cell variant and their ability to be isolated from physiological fluids including; blood, urine, saliva, bronchial lavage, breast milk, malignant ascites, cerebrospinal, amniotic and synovial fluid [49, 60].

At present, categorisation of EVs is based on factors such as their mechanisms of biogenesis and physical characteristics [61, 124]. Within the majority of the literature these are Exosomes, Microvesicles/Ectosomes and Apoptotic Bodies [49, 60, 124, 128]. Although, subgroups are yet to be fully defined due to the lack in robust clarification of their fabrication, structure and function. These are depicted by the wide range of studies in the table [61]. Intense research continues to be undertaken into the more specialised incorporation of unique cargo by each EV, hence affecting their roles within the cellular and extracellular microenvironment [129].

1.5.3 Subtypes

Table 2: Categorising the three main extracellular vesicle subtypes

	Microvesicles	Exosomes/sEVs	Apoptotic bodies
Size	Medium-sized vesicles 100-3,000nm [49, 61, 128, 130]	Generally the smallest vesicles 30-150nm [49, 121, 124, 128, 130]	Larger vesicles 50-5,000nm [60, 124, 128, 130]
Density	1.04 – 1.3 g/ml [131]	1.13 g/mL – B cell derived [132] 1.19 g/mL - Epithelial cell derived [132]	1.16–1.28 g/mL [131]
Profile	Morphology: Heterogeneous Markers: Lipid raft-associated species (phosphatidylserine-containing proteins), ARF6, VCAMP3, CD40, cholesterol, ceramide and sphingomyelin [49]. Contents: MiRNA, RNA, lipids and protein [49].	Morphology: Biconcave Membrane: raised lipid ceramide and aminophospholipid [131]. Markers: Alix, TSG101, heat shock proteins (HSP70, HSP60 and HSP90), CD9, CD63, CD81 and clathrin [60]. Contents: MiRNA, RNA and protein [49].	Morphology: Heterogeneous Markers: Exposure of Phosphatidylserine, TSP and C3b [60]. Contents: MiRNA, RNA, DNA, protein and cell organelles [49].

1.5.3.1 Apoptotic Bodies

Programmed cell death, also referred to as apoptosis, is the coordinated disassembly of aged, impaired, diseased or abnormal cells from the healthy host via membrane blebbing (figure 5). This occurs in order to maintain a balanced homeostatic environment, both routinely in normal and diseased physiological states [60]. Primarily apoptosis, ensuing cell cycle arrest, is

triggered by intrinsic factors, leading to the activation of the *p53*-dependent apoptotic pathway and thus pro-apoptotic factors, such as Bax [61]. Alternatively, extrinsic stimuli/factors initiate apoptosis through ligand binding to death receptors at the cell surface, such as those within the TNFR family [133]. In turn, pro-apoptotic caspase mediated signalling pathways induce the condensation of nuclear chromatin to be stored in apoptotic bodies, and execute cell death [121]. During the final stages, once the packaged cellular contents have passed through plasma membrane into the local environment, they are recognised by macrophage surface receptors and cleared by phagocytosis [61, 134, 135].

1.5.3.2 Microvesicles

Microvesicles arise from the external plasma membrane and function in modifying the extracellular environment and intercellular signalling pathways, as well as facilitating cell migration [121]. They contain ubiquitous cargo and, similarly to exosomes, are key regulators of cellular signalling [121]. The materialisation of microvesicles/ectosomes/shedding vesicles, as they are referred to in the literature, continue to be speculated. For example, there is evidence to suggest cytosolic Ca^{2+} dependent shifts in flippase, floppase, translocase, and scramblase activity triggers alterations to transbilayer lipid distribution, which subsequently leads to membrane curvature [124, 129]. A recent study by Stachowiak outlined similarly how peripheral protein crowding, and thus creation of lateral pressure, leads to bending of the surface [136]. Additional papers have stated the budding ensues from the binding of ESCRT-1 complex subunit TSG101 with arrestin domain-containing protein 1 (ARRDC1) tetrapeptide PSAP structural motif [137-140]. This interaction allows TSG101 to be recruited from Golgi body derived endosomes, to the lipid bilayer [121]. Here, collaboration between TSG101, ARRDC1 and glycosaminoglycans mediates reorganisation of the cytoskeleton [141]. This leads to microvesicle fission and discharge in a similar way to that indicated during viral budding [60, 121, 141]. Nevertheless, the most thoroughly described mechanisms of microvesicle fabrication and release is regulated by ADP-ribosylation factor 1 + 6 (ARF1 + 6), associated with the Ras superfamily of small GTP binding proteins [142, 143]. Stimulation of extracellular signal-regulated kinase (ERK) and Rho GTPases, facilitated by ARF6 (and ARF1), results in localisation of myosin light chain (MLC) kinase at the budding vesicle-membrane interface. This phosphorylates MLC, in RhoA's case via the Rho-associated protein kinase (ROCK) signalling pathway and successively activates the ATP dependent rearrangements of contractile actin and myosin machinery [144, 145]. This process induces microvesicle discharge as illustrated in figure 5.

1.5.3.3 small EVs/Exosomes

Exosomes direct short-range intercellular communication and are most commonly attributed to their regulation of local immune responses [121]. Once produced and secreted from exocytosis of multivesicular bodies (MVBs), they can be either be reabsorbed, internalised by local/neighbouring cells or alternatively they may enter systemic circulation to distal tissues. The process of exosome production begins with endocytosis, whereby early endosomes are formed that subsequently, upon invagination results in formation of late endosomes/ MVBs as depicted in figure 5. Inwards budding of MVBs generates intraluminal vesicles (ILVs) lined with membrane proteins/lipids, enriched with captured cytosolic constituents [128]. Rab GTPases, particularly, Rab11, Rab27 and Rab35, regulates intracellular spatiotemporal trafficking of the MVBs towards the cell surface [61, 146, 147]. Upon eventual fusion with the plasma membrane, ILVs are discharged from MVBs into the extracellular space and are henceforth referred to as exosomes [128]. Initially, the process of endosomal membrane blebbing and manufacture of ILVs for exosome release has found to be promoted by associations between Alix and ESCRT [132, 148, 149]. In addition, research has revealed that they have a role in cargo selection, along with syndecan [132]. Some studies have reported that incorporation of receptors into exosome membranes, as well as loading with bioactive cargo, can occur independent of ESCRT via both tetraspanin-enriched microdomains and tetraspanin CD81, though this is dependent on the initial cell source [132, 150]. Investigations reinforcing an alternative ESCRT-independent signalling pathway for organising exosomal bioactive contents into MVBs were based on microdomains enriched in sphingomyelinases [151]. These enzymes form the ceramides, one of the main constituents of exosomal membranes [132]. Functionally, ceramides can encourage negative curvature of the MVB, thus inducing budding [132].

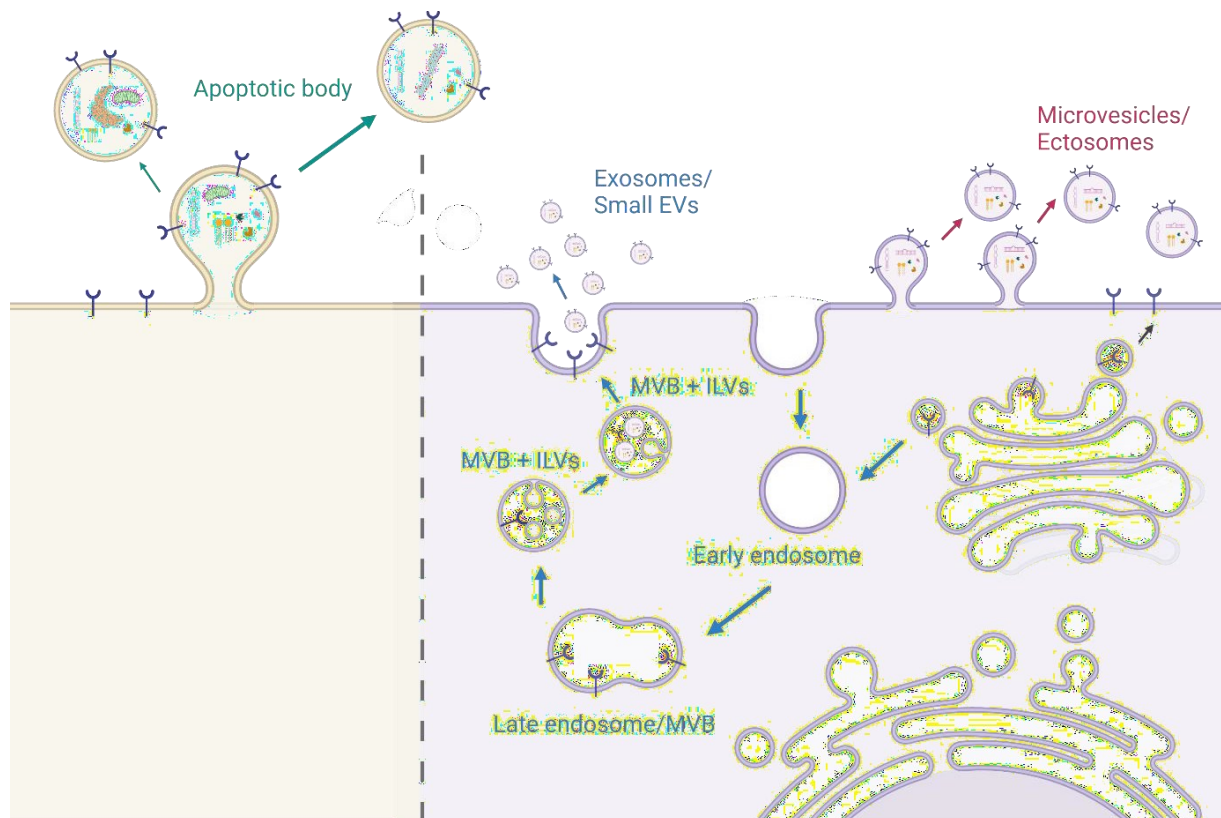


Figure 5: The biogenesis of all three main extracellular vesicle subgroups. The diagram illustrates how discharge of apoptotic bodies from apoptotic cells is comparable to the membrane blebbing observed in microvesicle formation. Exosome/small EV biogenesis involves internal MVB fusion to the plasma membrane, with no blebbing. Primarily specialised molecular signalling mechanisms facilitate late endosome/MVB internal budding and sorting of ILV contents. Following this, enzyme Rab GTPase mediates the transportation of MVBs to the plasma membrane, whereby after incorporation the ILVs are expelled as Exosomes/small EVs.

1.5.4 Extracellular Vesicles Therapeutic potential

EVs originated from stem cells have been demonstrated to incorporate their native biological components, thus mimicking a level of stemness depicted by their parental cell [12]. These features provide them with an innate, versatile therapeutic potential in regards to delivery of regenerative soluble proteins, growth factors and nucleic acids [152]. Unlike similar therapeutic platforms, such as liposomes or polymer-based nanoparticles, EVs are advantageous in that the lipid membrane-bound biomolecules are able to travel distally without themselves or their cargo being diluted and degraded. Their natural surface chemistry is recognisable to cells, hence permitting them to evade phagocytic clearing by the immune

system, which consequently prolongs circulation time and thus enhances both their stability and efficacy [132]. Prior to dodging local immune defences, EVs fail to provoke an initial immune reaction by their lowered immunogenicity and non-cytotoxicity [153-155]. Both these features increase their long-term safety *in vivo* in comparison to nanoparticle delivery systems. In addition, properties such as the small scale of EVs facilitates their ability to migrate to target sites through physical barriers. These include the hard to breach blood-brain barrier, that many larger drugs cannot cross, and dense extracellular matrix structures [156, 157]. However, multiple studies have demonstrated that, when unmodified, exosomes often accumulate in organs of the reticuloendothelial system (RES), including the spleen and liver, following injection [158, 159]. Hence, adaption of exosomes to augment their concentration at target sites is necessary. Investigations into the potential of EVs is increasingly attractive due to their consistent secretion by all cell types and their ability to be isolated from physiological fluids including; blood, urine, saliva, bronchial lavage, breast milk, malignant ascites, cerebrospinal, amniotic and synovial fluid [49, 60]. Furthermore, this has led to a plethora of scientific papers into their direction as both diagnostic indicators of disease and as cell-free therapeutics. [125-127].

Chapter 6 will focus on the implementation of sEVs in functional assays to showcase their regenerative, healing and immunoprivileged properties. Large volumes of research have been conducted regarding the role of EVs within skin surface wounds, be them in diabetic induced, wounded or severe burn rodent models. Much of this involves injection in/around the wound or loading natural/synthetic dressings and applying topically. According to the review paper by Cabral et al, most EVs are acquired from human umbilical cord, synovial or adipose MSCs and cultured for up to 48hrs until 80% confluent and applied in concentrations of up to 200 $\mu\text{g/ml}$ [160]. Generally, the hUC-MSCs EVs enhanced wound healing by normalising and heightening: re-epithelialisation, collagen deposition, endothelial cell migration, vascularisation and dermal fibroblasts proliferation [160]. Most importantly, nearly all of the studies noticed condensed scar formation at the macroscopic level and a profuse immunomodulatory response [160]. This enabled the wound site to be initially cleared of infection and predisposed a homeostatically balanced environment for regeneration. The immunological observations included: anti-inflammatory action, promotion of macrophage plasticity through the TLR4 signalling pathway, depleted infiltration of white cells (neutrophils and macrophages) and preferment of the M2 macrophage phenotype [54, 161]. Additionally, the activation and upregulation of STAT3 by hUC-MSCs prevents production of pro-inflammatory cytokines by THP1 monocyte cells and hence a prolonged pro-inflammatory response (typical of chronic wounds) [160]. Studies have also shown EV plays a role in immunomodulation under normal physiological niche [162]. For example, EV aid maintenance

of homeostasis through promoting the release of degraded RNA products and lipid trafficking [163]. Moreover, healthy cells can produce EVs that contains major histocompatibility complex (MHC)-peptide complexes which can activate T-cells and participate in immune-homeostasis [164, 165]. Specifically, MSC derived EVs have also shown to release immunomodulatory molecules such as IL-10, hepatocyte growth factor (HGF), transforming growth factor (TGF- β 1) which suppress T-cell proliferation and interact with other immune cells [166].

Although they show undisputable therapeutic potential, application of EVs is difficult until there is implementation of robust, standardised cell culture conditions and isolation methods for their production at scale. Ensuring optimised *in vitro* sEV production, purification and handling is prerequisite to generating consistent results in functionality assays, application to 3D models/organised and animal testing in research laboratories. Also maximising production of pure populations in Bioreactors is key to informing manufacturing of clinically viable therapeutics [167].

1.6 EV production

1.6.1 EVs from scalable culture

Within a small scale research laboratory, basic EV production relies on the expansion of cells in monolayers on flasks or culture plates plastic/glass. During cell culture the secreted EVs accumulate in waste media and this is retained to allow for EV isolation and purification.

There are many potential obstacles during the process of scaling up a biological product, due to their cellular derivative's innate sensitivity to environmental stimuli. Transitioning from static planar T flask cultures to agitated stirred tank/hollow fibre bioreactor system subjects cells to shear stress inducing forces, demonstrated to alter their phenotype [168, 169]. This includes their stemness or level of differentiation of both the cell and vesicle product (affecting composition and function) and production of apoptotic blebs, which can in turn contaminate the extracted EV fraction and thus decrease samples therapeutic potency [170, 171]. Consideration of fetal bovine serum exosome impurities is also imperative in both static and agitated conditions when delivering a pure, well-characterised and clinically applicable product. Thus, where possible, employment of xeno-free (XF) culture media, which by definition only contains human components, is highly advised as with serum-free [172]. Although serum-free can elicit an increase in EV manufacture, a complete lack of serum has exhibited modifications in exosomal biology with encapsulation of reactive oxygen species and stress induced proteins [172]. Nevertheless, overall, ensuring a stable bioreactor culture, with

little or no influence from confounding variables, can provide an excellent closed, scale-up platform, with high process control and reduced manually intensive handling [172]. Additionally perfusion-based systems can reduce liquid handling by the consistent removal of waste and culture replenishment it offers, further avoiding contamination risk and ensuring a concentrated EV rich media and hence purity of the product [173].


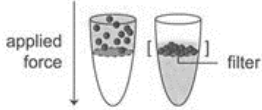
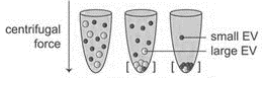
Once scaled up, Vesicle heavy secretome as a therapeutic product, are required to meet the International Council for Harmonisation of Technical Requirements for Pharmaceuticals for Human Use (ICH) guidelines. These are published on the official EMA website and outlined in Gimona et al review article [174]. Initially it is critical to identify what type of therapeutic vesicle fraction has been developed, be it a vesicular secretome fraction, a more non-specific fraction of vesicles, EVs, exosomes or microvesicles. This means characterisation of a well isolated and purified population.

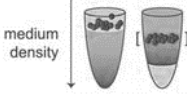
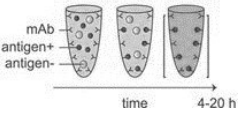
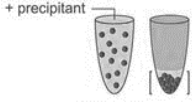
1.6.2 EV isolation and purification

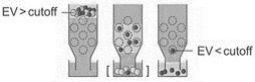
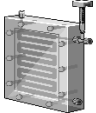
Ensuing their secretion, EVs can be isolated by a multitude of techniques outlined in table 3 [175]. The hierarchy of each method depends upon the sample type and purpose of isolation; each has a varying degree of sensitivity, specificity, expense, ease of handling, scalability, product purity, extraction yield and preservation of bioactivity [175]. Guidelines by the international society for extracellular vesicles (ISEV) [6] establish translatable high throughput, simplistic and scalable techniques, allowing for the generation of high purity EVs from heterogenous populations [9, 176]. These are referred to as the minimal information for studies of extracellular vesicles 2018 (MISEV2018) [177].

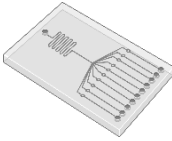
Previously, recognised methods for accessible particle separation based on their physical characteristics included ultracentrifugation (“gold standard” for EV isolation), ultrafiltration, size exclusion chromatography (SEC) and polymer precipitation [9, 10]. However, these approaches do not discriminate between exosome specific and general lipoprotein particles and so strategies with heightened specificity, such as affinity-based capture techniques are an exciting emerging option [178]. Table 3 lists the techniques most commonly employed by researchers.

Table 3: The strengths and limitations associated with each isolation platform. Technique images and overviews adapted from the paper by Coumans et al [6]. Advantages and Disadvantages were taken from those listed in several review articles by Yamamoto et al [8], Chen et al [9], Xu et al [10] and Liangsupree et al [11].

Technique	Overview	Advantages	Disadvantages
<p>Ultracentrifugation (UC)</p> 	<p>Centrifugation steps of increasing speed to remove cell fragments and dead cells, followed by UC at higher speeds to yield sEVs.</p>	<p>Well documented. Cheap to operate. No reagents required. Can take larger volumes.</p>	<p>Can damage sEVs. Poor repeatability. Time consuming. Requires expensive equipment.</p>
<p>Ultrafiltration</p> 	<p>External forces, such as pressure, centrifugation or both encourages soluble components to pass through a filter, whilst EVs larger than the pore size are retained.</p>	<p>Rapid process (0.5 hrs). Simple. Concentrates EV fractions up to around 240-fold.</p>	<p>Wide ranging EV recovery: 10-80%. Contamination. Reduced biological activity of EVs</p>
<p>Differential centrifugation</p> 	<p>Separation of EVs is based on both density and size with a selective increase in centrifugal speed determining the sedimentation of EVs.</p>	<p>Rapid process (3-9 hrs). Extraction can be performed at the litre scale. Simple.. Ability to process multiple samples in unison.</p>	<p>Wide ranging EV recovery: 2-80% Intense force from centrifugation can damage EVs. Aggregation of EVs and contaminants.</p>

<p>Density gradient centrifugation</p> 	<p>This method employs a density (size and mass/mass alone) gradient to extract EVs. The principle relies upon specific densities of EVs migrating along the substrate to an equilibrate zone.</p>	<p>Highly pure EV fraction.</p>	<p>On average only 10% EV recovery. Complex procedure and time intensive (16-90 hrs).</p>
<p>Immunocapture</p> 	<p>During immunocapture, surface bound monoclonal antibodies, specific to EV ligands are used to segregate the appropriate EV subpopulation.</p>	<p>Clinically applicable. Highly pure EV fraction. Highly selective.</p>	<p>Expensive. Wide ranging EV recovery: 4-20%</p>
<p>Precipitation</p> 	<p>The very simple procedure involves supplementing the sample with a precipitant (most commonly polyethylene glycol) which promotes precipitation.</p>	<p>Known to show an encouraging 90% EV recovery. Cheap. Simple process. Clinically applicable</p>	<p>Contamination can occur due to reduced specificity.</p>

<p>Size exclusion chromatography (SEC)</p> 	<p>SEC applies an exclusion matrix boasting a discrete pore size, to allow EVs to be separated based on size, in a distinct column. Generally elution of EVs occurs first, prior to soluble components.</p>	<p>Considerable more pure EV fraction than alternative methods (removes ~90% of non EV components). Rapid process (0.3 hrs). Clinically applicable. Minimal aggregation of EVs.</p>	<p>Wide ranging EV recovery: 40-90% Only works with small sample volume (μL-mL) at 1 sample per column. Additional apparatus essential. Complex process. Expensive.</p>
<p>Tangential Flow Filtration (TFF)</p> 	<p>Separation of particles by use of longitudinal cross-flow forces and movement across a semipermeable membrane [11, 179]. The molecules smaller than the MWCO filter pass through the membrane (filtrate) and particles larger than the MWCO, including EVs, are recirculated through the TFF and concentrated (retentate)[11].</p>	<p>High recovery Adaptable Concentrating not diluting Scalable Simple to operate Low-cost</p>	<p>Low purity Less extensively researched</p>

<p>Microfluidics</p> 	<p>Manipulation of liquids within channels. Physical filtration based techniques where driving forces push smaller particles through pores whilst larger particles are retained. Particles were encouraged down specific trajectories, shifted in orbit (acoustic-wave forces), attracted to field regions based on microelectrode voltage. Also immunoaffinity based isolation with interactions between antigens and antibodies to capture sEVs</p>	<p>High purity. High efficiency (fast separation and high throughput)</p>	<p>Device is complex, needs additional equipment and optimising. Expensive.</p>
--	---	---	---

More recent recommendations for the best isolation outcomes are to combine techniques which suit the project aims and have opposing, counteracting pros and cons. Many researchers have trialled combining UC and SEC [180-182]. However for projects which focus on scalability, techniques such as TFF alongside secondary SEC allow production of an enriched, lipoprotein and protein aggregate free suspension [183, 184]. Nonetheless, this particular method was also attributed to the dramatic 30-70% reduction in total particle number [184]. This nonetheless is a general finding with alternative isolation and purification methods hence, to prevent loss of therapeutic potential, any compromise in regards to purity can be overcome by reference to the EV fraction as 'the process is the product' [174]. This definition is used commonly when generating early biologicals and so is feasible when, on the whole, MSC populations discharging the EVs are heterogeneous, somewhat unpredictable and non-clonal [185].

Nonetheless, regardless of the protocol used, the MISEV guidelines state the importance of summarising an extensive procedure for EV isolation to ensure repeatability by other research groups. Chapter 4 and 5 describe how TFF with SEC was chosen as a 2 step complementary and scalable method for isolating pure sEV populations.

1.6.3 EV storage

To minimise the number of variables effecting EVs characteristics and functionality, many researchers, upon isolation of EVs, advise to analyse them or apply them fresh [186, 187]. These variables, which can influence yield, physical properties and performance *in vitro/vivo*, include: cryoprotective agents (CPA), lyophilisation, temperature and freeze/thaw cycles [188]. Thus, following these findings, although the 2013 MISEV addition suggested -80°C preservation in PBS within siliconized vessels, the 2018 updated document did not provide standard guidelines [189, 190]. It does however highlight the importance of documenting storage conditions (e.g. sterility, temperature, protectants etc.) for standardisation, reproducibility and to ensure the stability and safety of the therapeutic product prior to administration [174]. Additionally, the conditions must be practical and achievable for the ease of external shipment and internal distribution.

A study by Görgens et al. aimed to clarify appropriate storage for sEVs as there had been shown to be no official consensus reached. As -80°C storage has been reported to cause a decrease in EV concentration over time, an increase in contaminant protein and a change in EVs size and morphology, it is recognised that storage buffers, which can act to cryopreserve, should be employed. Of the popular buffers tested, they concluded that PBS with human albumin and trehalose was most effective at maintaining stability and improving recovery [191, 192]. As a non-penetrating cryoprotectant, trehalose is an osmolyte, as well as an inhibitor of aggregation, which can also form hydrogen bonds with water (water replacement hypothesis) to stabilise the EV lipid membranes [193, 194]. Hence, for our research we employed trehalose in PBS when storing our EVs at freezing temperatures.

1.6.4 EV characterisation

Succeeding the isolation and storage of EVs, there must be 'extended characterisation' to verify their surface/cargo profile (biomarkers, cytokines and mRNA/miRNA, DNA and metabolome), morphology and size. There are strict guidelines implemented by MISEV which outlines both these and the analytical techniques recommended to measure for them [190]. This was done to standardise as stringently as possibly the way each research group profiles their EVs/Exosomes in order to maintain consistent findings and repeatable methodologies.

A full comparison of these techniques was performed in chapter 5 introduction and provides insight into why each technique we employed was selected.

1.7 Conclusions and Gaps in Knowledge

This literature review has outlined the well-documented research into the bioprocessing and scale up of MSCs in stirred tank bioreactor systems using MCs as well as the advantageous therapeutic potential of MSCs in regenerative medicine. Nevertheless, it also identifies the qualities associated with sEVs as a novel cell-free therapeutic. Where sEVs show great promise, the lack of published data into the effects of bioprocessing in suspension culture on sEV scale up and reference to optimised stirred bioreactor production of sEVs is evident. Additionally, a comprehensive characterisation profile of these sEVs, both along the bioprocess timeline and following harvest, has yet to be performed from optimised culture of MSCs on MCs in SFs. For example, a study performed by de Almeida Fuzeta et al compared the effects of MSC expansion in a Vertical Wheel Bioreactor to 2D planar culture of sEVs, but did not measure sEVs across the culture timeline and only following harvest [195]. They also achieved higher concentration of sEVs and general productivity in the scalable system and stated to have a more robust downstream purification process [195]. Additionally, a paper by Haraszti et al again assessed 2D vs 3D SF culture of MSCs on sEV concentration, size, biomarkers and protein profile but failed to do this across the culture timeline and only upon harvest [196]. Additionally, they did not release data on the optimisation of the bioreactor system and neither did they compare the yield and characterisation of MSCs against sEVs [196].

Further thorough investigation into these research gaps would provide abundant data on how EV production from MSCs is affected by an agitated suspension culture, as well as the effects the 'scaling up' process has on sEV functionality.

Chapter 2: Aims and Objectives

As platforms facilitating the scale up of MSCs, many forms of bioreactor have been demonstrated to be extensively researched in this literature review. This however also revealed the variable effects of physical adaptations on cell expansion and hence the importance of optimising the bioprocess to specific upscale culture requirements, individual to each research group. Once this had been achieved, augmented bioreactor protocols were shown to encourage proliferation of MSCs whilst retaining their characteristic profile and potency.

More recently the potential for retrieving higher yields of MSC-sEVs from suspension 3D in comparison to planar 2D culture had been exhibited [197-199] and thus made platforms such as stirred tank bioreactors an appealing method for producing sEVs at scale also. However, prior to beginning this project there had been little research, bar use of traditional practices, into not only the upstream but scalable downstream isolation of pure sEV populations and their functional potential in regeneration, healing and immunological *in vitro* assays.

In particular there was also limited documentation into the biophysical effects of agitated culture on MSC derived sEVs and the changes in sEV profile across the bioprocess timeline. Furthermore, the novelty of the project was mainly from the assessment of both protein and tetraspanin profile across the small scale bioreactor culture timeline, which provided intel into the capabilities of sEVs collection throughout the upscale process. Once optimised and standardised, with minimal batch-to-batch variation, the platform could be augmented to encourage sEV secretion and the upregulation of proteins which could enhance the sEVs therapeutic effect.

Further benefits of the platform itself include providing a bench scale solution for enhancing sEV yield within university research laboratories at low cost and high simplicity. The scalable system should provide the potential for streamlining into a continual process from bioreactor inoculation to MSC harvest and sEV isolation. In addition, by investigating the culture of multiple cell lines batch by batch within the optimised bioreactor and measuring the effects of each upstream and downstream bioprocessing parameters on sEV characteristics, we can reach confident conclusions in the potential of our scale up platform, as well as it's reproducibility.

Therefore, this project aims to develop a reproducible scalable upstream and downstream bioprocess, specifically applying SF stirred bioreactors, for the effective generation of therapeutic MSC-sEVs.

In order to attain this aim, the individual objectives of this project were to:

1. Produce an optimised bioprocess, using SFs, to support MSC expansion on MCs at scale, maintaining their potency and further allowing for the collection of MSC-sEVs across the culture timeline.
2. Demonstrate batch reproducibility of the scalable platform in relation to MSC and MSC-EV concentrations across the culture timeline.
3. Confirm maintenance of MSC stemness and potency and apply multiple methods to characterise MSC-EV profile following SF culture.
4. Investigate the effects of the SF culture process along the culture timeline on EV characteristics and protein profile.
5. Following the application of a downstream bioprocess for sEV purification and isolation at scale, measure the effect of sEVs in *in vitro* functional assays.

Chapter 3: Materials and Methods

3.1 Materials and Reagents

Table 4: Reference table for basic materials and reagents information.

Identified use	Material	Manufacturer	Details	Use
Complete Growth Media (DMEM + 10% FBS + 1% UltraGlutamine + 1ng/ml bFGF)	Dulbecco's Modified Eagle's Medium (DMEM)	Gibco™	Supplemented with 1g/l (0.1% w/v) Glucose and free from L-Glutamine and phenol red.	Cell culture
	Fetal bovine serum (FBS)	Sigma	Fetal Bovine Serum non-USA origin, sterile-filtered Cat No° F7524-500ML Batch BCBX5042. Cat No° F7524-500ML Batch 0001640139	Cell culture
	UltraGlutamine	Lonza biowhittaker	200mM in 0.85% NaCl solution	Cell culture
	basic Fibroblast Growth Factor (bFGF)	Peprotech		Cell culture

	DPBS (Dulbecco's Phosphate Buffered Saline)	Dulbecco's	Without Calcium or Magnesium.	Cell culture
	Trypsin-EDTA	Gibco	0.25% modified with • EDTA • Phenol Red	Cell Passage
	Accutase	Sigma		Cell culture – Flow Cytometry
	Cell culture treated flask	Corning	T225, T75, T25cm2	Cell culture
	Tissue culture treated well plates	Corning	96, 48, 24, 12 well plates	Cell culture
	Micro-Carrier Spinner Flask with Bottom Dimple 100mL + Impeller Assembly	Bellco		Agitated cell culture
	5 Position Magnetic Stirrer Compact	Bellco		Agitated cell culture
	Microcarriers	Solohill (PALL)	Selection in Table 2	Agitated cell culture
	SigmaCote	Sigma		Agitated cell culture
	Trypan Blue	Sigma		Cell counting
	Cell counting chamber/ haemocytomete r	Marienfield		Cell counting
	Sterile PES Syringe Filter	Fisher	0.2um	EV isolation and sterile filtration

	Plastic syringes with needles	Fisher		Filtration
	Steriflip® Sterile Centrifuge Tube Top Filter Unit	Millipore	50 mL process volume, 100.0 µm pore size, hydrophilic nylon net membrane	Separation of cells and microcarriers
	Via 1 cassette	Chemometec		Cell count and cell viability
	Live dead cytotoxicity viability kit	Invitrogen	Stains for Live (Green Calcein AM) + dead (red ethidium homodimer-1) cells.	cell viability
	Cell counting kit 8	Sigma	Uses WST-8 (2-(2-methoxy-4-nitrophenyl)-3-(4-nitrophenyl)-5-(2,4-disulfophenyl)-2H-tetrazolium, monosodium salt)	cell viability
	Deionised water	Millipore		Cell Staining
	Fixation buffer (4% para-formaldehyde)	Thermofisher		Cell fixation
	0.1N Hydrochloric Acid (HCl)	Sigma		Cell Staining

	99% isopropanol	Sigma		Cell Staining
	Adipogenic differentiation kit	Gibco,		Adipogenic differentiation
	Chondrogenic differentiation kit	Gibco,		Chondrogenic differentiation
	Osteogenic differentiation kit	Gibco,		Osteogenic differentiation
	Silver nitrate solution	Sigma	2.5% solution	Osteogenic Staining
Reagent X	Naphtol AS-MX Phosphate Alkaline solution	Sigma		Osteogenic Staining
	Fast Violet B salt grade III	Sigma		Osteogenic Staining
	Alcian Blue powder	Sigma		Chondrogenic Staining
	Oil Red O powder	Sigma		Adipogenic Staining
	Triton-X-100	Sigma		Immunocytochemistry
	Trehalose	Sigma		EV storage
	PHA-P	Sigma		PBMC
	IL-2	Peprotech		PBMC
	Ficoll paque plus	Ge healthcare		PBMC
	CellTrace™ Violet (lyophilized powder) (Cell Trace pb450)	Thermofisher	1:2000 dilution	PBMC
	CellTrace™CFS E FITC	Thermosisher	1:2000 dilution	PBMC
Memglow 488 stock	MemGlow 488 (2nmol)	Universal biologicals	20µM stock solution when reconstituted	

			with 100µl of anhydrous DMSO	
	CD34 – PerCP Clone 581 mIgG1	Biologend	1/100	Flow Cytometry – Phenotyping Antibody Panel
	HLA-DR – APC Clone Tu39 mIgG2a		1/100	
	CD45 – APC- Cyanine7 Clone 2D1 mIgG1		1/500	
	CD105 – FITC Clone 43A3 mIgG1		1/100	
	CD90 – Brilliant Violet 650 Clone 5E10 mIgG1		1/100	
	CD44 – Brilliant Violet 605 Clone IM7 ratIgG2b		1/250	
	CD73 – PECy7 Clone AD2 mIgG1		1/250	
Flow Buffer (PBS + 0.5% BSA + 2mM EDTA)	Bovine serum albumin (BSA)	Fisher		Flow Cytometry
	Ethylenediamine tetraacetic acid (EDTA)	Sigma		Flow Cytometry

Table 5: Additional microcarrier details, including physical and chemical composition

	Matrix	Density	Diameter (um)	Surface area (cm ² /mg)	Micro carrier /g	Surface coating	Charge	Porosity
Plastic	Polystyrene	1.02	125-212	0.36	4.6 x 10 ⁵	None	None	None
Plastic Plus	Polystyrene	1.02	125-212	0.36	4.6 x 10 ⁵	None	+	None
Star Plus	Polystyrene	1.02	125-212	0.36	4.6 x 10 ⁵	None	+	None
Collagen	Polystyrene	1.02	125-212	0.36	4.6 x 10 ⁵	Type 1 porcine collagen	None	None
FACT III	Polystyrene	1.02	125-212	0.36	4.6 x 10 ⁵	Type 1 porcine collagen	+	None
Hillex II	Dextran	1.11	160-200	0.515	?	Trimethyl ammonium	+	Micro pores on surface

Table 6: Bone Marrow Mesenchymal Stem Cells (bmMSCs) donor information

Line name/ WCB lot	Supplier	Sex	Age	PDLs	Potency assay (Tri-lineage)	Cell Surface Antigen (% positive)
AM2	N/A	Hispanic Male	21 yo	N/A	N/A	N/A
AM4	N/A	Male	24 yo	N/A	N/A	N/A
144	N/A	Caucasian Female	26 yo	N/A	N/A	N/A
Serum derived cells #MSC- 003 310263	RoosterBio	Female	20 yo	9.3	Pass	CD34 (<10%) CD45 (<10%) CD90 (>90%) CD166 (>90%)
Serum derived cells #MSC- 003 310267	RoosterBio	Male	19 yo	9.4	Pass	CD34 (<10%) CD45 (<10%) CD90 (>90%) CD166 (>90%)
Serum derived cells #MSC- 003 310271	RoosterBio	Male	25 yo	10	Pass	CD34 (<10%) CD45 (<10%) CD90 (>90%) CD166 (>90%)

3.2 Methods

*Refer to materials section for details on materials and reagents mentioned below.

3.2.1 Basic Cell Culture

3.2.1.1 Thawing Cells:

Vials of cells were rapidly thawed by immersion in a 37°C water bath until visibly defrosted and only few frozen fragments remained (seconds - minutes). Following this, within the sterile cell culture hood, the cell suspension was slowly dispersed into a falcon tube containing 9mls of warm complete growth media (CM). Cells were pelleted at 300g for 5 minutes and the supernatant was removed. The cell pellet was then resuspended in a set volume of media to perform a cell count (1 million cells/ml).

3.2.1.2 Cell counting

From a cell suspension stock, 10µl was transferred to a microcentrifuge tube with 10µl Trypan Blue, mixed, and 10µl dispensed onto the grid of a haemocytometer. Upon microscopic visualisation of the haemocytometer cells in all 4 corners and the 1 central grid, counts were made and an average and cells/ml calculated (see calculation below). From the equation below, cell suspension volume required for reseeding was calculated and the necessary volume made into a fresh stock.

$$\text{Cells/ml in suspension} = \frac{\text{average no. cells in haemocytometer grid}}{2} \times 10,000$$

3.2.1.3 Cell Passage:

bmMSCs were media exchanged every 2-4 days and passaged once confluent (80-90%). Once confluent, medium was removed and cells washed with DPBS (Dulbecco) in order to remove any remaining serum. Following removal of DPBS, the addition of 40µl cm² of 0.25% Trypsin-EDTA (Gibco) proteolytic enzymes was added and incubated for 5 minutes to promote the detachment of cells from growth surfaces. Following microscopic observation (EVOS microscope) of floating and attached cells, some physical agitation of the contents of the flask

was necessary to dissociate the cells. Once successfully trypsinised, cell suspensions were immediately diluted and neutralised with fresh CM. Once mixed thoroughly the suspension was transferred to a centrifuge tube for centrifugation (300g for 5 minutes) to form a cell pellet. Subsequent to pellet formation, supernatant was removed and the pellet resuspended in 1ml DMEM/planar flask. From this a cell count was performed and new flasks inoculated at ~4000 – 5000 cells/cm², or frozen as described in section 3.2.1.4.

3.2.1.4 Cell Freezing:

Cell suspensions of known concentration (usually 1×10^6 or 2×10^6) were distributed between freezing vials in a freezing reagent composed of 10% DMSO in FBS. Cell pellets were resuspended in freezing media, and aliquots of 0.5×10^6 cells frozen in individual vials. Vials were placed immediately in a 'mr frosty' freezing container and then placed in the -80 freezer in order to achieve an optimal cooling rate for cell preservation ($-1^\circ\text{C}/\text{min}$).

3.2.1.5 Cell Fixation:

Cells were initially washed using PBS to remove media, then fixed with 4% para-Formaldehyde (PFA) solution for 20 minutes at room temp. This resulted in formation of protein crosslinks within the cells, strengthening the cells structural bonds enough to maintain their current biological state and withstand further processing. Once fixed, cells were washed multiple times and eventually stored in PBS at 4°C until ready for staining or further analysis.

3.2.2 Microcarrier Screening

3.2.2.1 Coating 96 well plates for low attachment pupose

Flat bottom 96 well plates (CoStar) were POLY-HEMA (P3932, Sigma Aldrich) coated aseptically in order to prevent MSCs from adhering to the polystyrene growth surface. POLY-HEMA stock was first made by dissolving in 95% ethanol by shaking (~150 rpm at $\sim 37^\circ\text{C}$) for 24 hours. The solution was then filter sterilised and $25 \mu\text{l}/\text{well}$ added to each well in the plate. Once coated and subsequently UV sterilised for 24hrs, the plates were wrapped in foil and stored at room temperature ready for each screening experiment.

3.2.2.2 Microcarrier aggregation screening experiment

MCs were conditioned in complete media for approximately 1hr prior to seeding with cells. MC stock volumes were calculated by measuring the surface area required per $100 \mu\text{l}$ media in

order to form monolayers within 96 well plates (10mg/ml or 1% w/v). After 1hr, passage 4/5 hMSC cells were seeded at 5000cells/cm² with the MC suspensions in triplicate and combined by gentle mixing to create a total volume/well of 200µl. Control wells were MC only and cell suspension only. Plates were transferred into the 37°C, 5% CO₂ Incucyte plate reader and incubated for 7 days. Images and videos were shot every hour at x4 and x20 magnifications. Additionally batch matched cells were seeded and left overnight to adhere on uncoated polystyrene 96 well plates at seeding densities between 0 and 15,000 cells/cm² to create a standard growth curve.

The Incucyte images of aggregation were quantitatively analysed using paint 3D and Java imageJ software. Using paint 3D, fill tolerance was toggled (to between 1 and 8% where necessary) to allow for nude areas to be visually isolated from large areas of MC aggregation. Following this, using the imageJ application, Images with tightly packed monolayers on day 0 were converted to an 8-bit type format, threshold set to 100 and the image fraction measured. These readings were subtracted from the time point 0 values and plotted.

3.2.2.3 CCK-8 Cell Viability Assay

CCK-8 assays were performed to assess cell viability. The assay uses WST-8 (2-(2-methoxy-4-nitrophenyl)-3-(4-nitrophenyl)-5-(2,4-disulfophenyl)-2H-tetrazolium, monosodium salt), which upon enzymatic dehydrogenase reduction yields an orange formazan dye. A colour change and fluorescent output reading directly reflects metabolic activity and correlates to live cell numbers. 10µl of CCK-8 solution was dispensed into 100µl of each experimental and control well consistently, and the 96 well plate incubated for 3 hours. Reduction was measured using a Spark® multimode microplate reader (TECAN).and absorbance measured at 450 nm.

3.2.3 Spinner Flask studies

3.2.3.1 Siliconising Spinner Flasks

Spinner Flasks (SFs) were siliconized in order to prevent MSCs adhering to the SF surfaces. Prior to each experiment, SFs were disassembled, cleaned with neutracon (decon) and hot water, left to dry overnight, reassembled and sent to autoclave. Once cleaned, SFs were moved to the fume hood and 10ml sigmacote siliconizing agent was evenly dispersed across all interior components and walls of the flask. Excess sigmacote was aspirated off and flasks

left to dry before being rinsed and scrubbed thoroughly with hot water and neutracon to eliminate HCl by-products. These were then air dried for a second time in the fume hood and the required surface area of MCs (500cm²/100ml final volume) were suspended in sterile PBS (1.39g MCs in 30ml) added to each flask and autoclaved in preparation for the experimental run.

3.2.3.2 Spinner Flask protocol

3.2.3.2.1 Seeding and expansion of MSCs in Spinner Flasks

Following sterilisation of MCs within SFs, they were returned to the cell culture hood on the day of cell seeding and PBS replaced with 50ml CM for 2hrs to condition the MCs (37°C, 5% CO²) with 30rpm constant stirring. During this process, MSCs were passaged and counted and later CM within the SF was replaced with a predetermined preliminary volume of media (as outlined in table 7). SFs were then inoculated with MSCs at either 5000 cells or 6000/cm² of MC, dependent on the cell line used. The SFs arm caps were loosened by 1.5 turns, to permit gas exchange, and placed in the incubator (37°C, 5% CO²) on a spinning platform. Whilst optimising the bioprocess, SF runs often used modified procedures, as bolded in table 7. All protocols included a hold period, which was an initial period encouraging attachment of MSCs to MCs. Succeeding the hold period, as a standard 100ml culture in SFs were stirred for 10 days at 30rpm and they underwent an 80% media exchange 2/3 times over this time course during periods of MSC counting, imaging and metabolic measurements.

Table 7: Bioprocess conditions for SFs with modifications (highlighted in bold).

MSC Cell Line	MC	Sir speed (rpm)	Hold time (hrs)	Initial media (%) -first 24 hrs	Media Type
AM4	Plastic	30	2, 4, 24	100	CM + RC
AM4, 263	Plastic	30	24	50	CM + RC
263	Plastic Plus	30	24	100	CM + RC
263, 267, 271	Plastic	30	24	100	CM + RC
263, 267, 271	Plastic	30	24	100	UC + RC
263, 267, 271	Plastic	30	24	100	TFF + RC

3.2.3.2.2 Spinner Flask Cell measurements

0.5-1ml media only samples were taken every 2/3 days for glucose and lactate measurements alongside samples of cell-MC suspensions for images and cell counts. Live cell counts were performed by lysing cells directly on the MCs and performing nuclei counts (NucleoCounter NC-3000). 200µl of MSC-MC samples were placed in a 1.5ml centrifuge tube and cells lysed by adding 200µl reagent A100 (lysis buffer) and 200µl reagent B (stabilising buffer) and mixing well. This suspension was then drawn up into the Via1-Cassette and stained within by immobilised acridine orange and DAPI to assess both live and dead cells. Samples were counted by the NucleoCounter NC-3000 and total SF cell counts deduced. Measurements were supported by phase contrast and live dead fluorescent stained (Invitrogen) images of cells attached to and bridging over MCs. Alongside this, the glucose and lactate measurements for MSC metabolism were made using an Accutrend Plus meter (Roche) as instructed by the device manual.

3.2.3.2.3 Spinner Flask harvest

On the final day of the SF experimental run, MSCs were harvested from the culture system. The process involved two initial PBS washes (50ml PBS at 35rpm for 10 minutes) and following this cell dissociation from MCs using enzymatic dissociation. Two reagents were chosen for 35rpm agitation; 40ml trypsin-EDTA for 10 minutes or 40ml Accutase for 20 minutes total exposure. Often when maximum detachment was not achieved, and free floating cells not observed, MSC-MC suspensions were exposed to the enzymatic digestion for

another 20 seconds at 250rpm until free floating cells were visualised. The activity was neutralised immediately following detachment by addition of equal volume of CM and using a 0.1 μm steriflip filter and a vacuum pump, MSCs were separated from the MCs. Recovery was then established by a second "Viability and Cell Count" measurement of MSCs in suspension using the Via1-Cassette and NucleoCounter NC-3000. In addition to these readings, MSCs were characterised by setting up Colony Forming Unit (CFU) assays, Trilineage Differentiation, Flow Cytometry and PBMC assays.

3.2.4 Mesenchymal Stem Cell Characterisation

3.2.4.1 Colony Forming Unit (CFU) Assay

The CFU assay relies upon every MSC in a population's ability to undergo unlimited division. Cells were seeded at 5-10 cells/cm² (100-200 cells per T25) and left for approximately 14 days to form colonies, feeding every 3 days. These flasks were fixed using 4% PFA and subsequently stained with crystal violet (0.5% w/v), which stained the nuclei of cells and highlight their clustered colony forming growth pattern. Images of these were taken using the EVOS microscope at 4x objective.

3.2.4.2 Trilineage Differentiation

Cell suspensions were reseeded at 10,000 cells/cm² for adipogenesis and 5000 cells/cm² for osteogenic differentiation in either 24 or 12 well plates, ensuring the monolayer was evenly covered with CM. After 24 hours incubation, CM was replaced with 1-2ml/well of prepared Adipogenesis or Osteogenesis differentiation media (StemPro™) respectfully. In contrast, chondrogenic differentiation plates rely upon a unique droplet seeding technique with enhanced cell-cell interactions and increased hypoxia to drive differentiation. To achieve concentrated spheroids, MSCs were respun and suspended at 10,000,000cells/ml in 200 μl complete media and from this 5 μL droplets dispensed per well. These micromasses were then incubated until attachment of cells was occurred at the edges (approximately 1-3 hrs), ensuring the media did not evaporate and cells remained hydrated. Following this observation, the wells were cautiously filled with prepared StemPro™ Chondrogenesis differentiation media, avoiding disturbing the micromasses. All differentiation plates were then media

changed every 2-4 days for a minimum of 14 days and until differentiation was visible, before being fixed and stained.

3.2.4.2.1 Osteogenesis staining

Following fixation of the cells, a method comparable to Von Kossa staining was employed in order to quantitatively detect Osteogenic mineralisation properties. A 4% v/v solution (reagent X) was prepared by combining Naphtol AS-MX Phosphate Alkaline solution and Fast Violet B salts solution. Primarily, the storage solution of D-PBS was replaced with 1ml/well of 4% v/v Reagent X and incubated at room temperature for 45 minutes under light protection. Following this at least 3 deionised water washes were necessary to remove excess stain and then 1ml/well of 2.5% silver nitrate solution added to reveal brown or black staining of mineralisation/alkaline phosphate deposition. This reaction took 30 minutes under the light and the stained cells were visualised under an EVOS light microscope.

3.2.4.2.2 Chondrogenesis stain

Prior to staining, cell collectives shed from micromasses should depict a core of condensed cells, with more of a spherical morphology, indicative of dense matrix production, and at the edges of these aggregates cells with an elongated appearance. Therefore if chondrogenic, these acidic polysaccharide (mainly glycosaminoglycan) rich shed aggregates should stain blue under Alcian Blue staining. The 1%wt/vol Alcian Blue solution is prepared by dissolving the Alcian Blue powder in 0.1N HCl and filtering through a 0.2 µm filter until it runs clear. After removing the D-PBS from the fixed Chondrogenic differentiation wells, 1-2ml/well of the Alcian Blue stain was dispensed onto each well and the plate left to incubate at room temperature for 60 minutes. Once 60 minutes had passed this was then rinsed away with 3x 0.1N HCl washes to remove excess stain and then 2x deionised water washes to reduce acidity. The blue staining was then visualised and images taken under an EVOS light microscope.

3.2.4.2.3 Adipogenic staining

Firstly, a stock was made by combining 150mg of Oil Red O powder to 50mL of 99% isopropanol until it is completely dissolved and then pass through a 0.2 µm filter until the solution

runs clear. The stock was then converted to a working solution by diluting 3:1 with deionised water, incubating at room temp for 10 minutes and filtering for a second time until the solution again runs clear. PBS in the adipogenic differentiation wells was then replaced with enough of this working solution to cover the well surface and left at room temperature for 5 minutes before being rinsed off with deionised water repeatedly until no excess stain remains. Cells were left hydrated in PBS to allow for imaging of the stained lipids and lipoproteins within adipocyte vacuoles using a light microscope.

3.2.4.3 Flow Cytometry

MSCs harvested from the bioreactor were phenotyped to quantify changes in known cell surface proteins by flow cytometry. Cells were detached with accutase, resuspended in Flow Buffer and a new cell count performed and suspensions adjusted to 1×10^6 /ml. 100 μ ls were added to a round bottomed 96-well plate for all samples. Plates were centrifuged at 300g for 5 minutes to pellet the cells which were then subsequently resuspended in 100 μ l of directly conjugated antibodies diluted in flow buffer (see 3.1 table 4 for details on antibodies and dilutions). Incubation occurred in the dark, on ice for 30-60 minutes. Cells were pelleted and washed with ice cold PBS twice, followed by resuspension in 100 μ l flow buffer. Surface marker expression was quantified using a Cytoflex-S flow cytometer (Beckman Coulter) and at least 10,000 events per sample were collected.

3.2.4.4 MSC-PBMC Assay

Peripheral blood mononuclear cells (PBMCs) were isolated from NHS leukapheresis cones. The specimen was then transported to the laboratory and once diluted slowly layered onto 20ml Ficoll, which previously had been centrifuged (1000g for 1min) to create a gradient. This was then centrifuged at 450g for 45 minutes at 20 degrees, with slow braking to prevent the disruption of the cell layer at the interface of the blood and ficoll. The PBMC layer was removed and cells washed twice with PBS, before counting. PBMCs were resuspended at 10×10^6 cells per ml in prewarmed PBS containing 2 μ M (1:2000) CFSE. Cells were incubated in the dark for 20 mins at 37C before quenching labelling with CM, and incubated for a further 5 mins. Cells were washed twice and added to pre-plated MSCs in a 24-well plate (left to adhere overnight) at defined ratio 1:1 in the presence of 10 μ l/ml PHA and 0.4 μ l/ml IL-2, which were added to induce T cell proliferation. Positive control wells were stimulated PBMCs in the absence of MSCs and negative controls were unstimulated cells. These cultures were

incubated in the dark for 5 days and then plates analysed by Cytoflex-S flow cytometer (Beckman Coulter)

3.2.5 Extracellular Vesicle Preparation

3.2.5.1 EV Concentration and Isolation

Medium was collected from SFs and firstly spun at 300g for 5 minutes in order to remove live/dead cells and MCs, where a second spin at 2000g for 10 minutes removed cell debris. This cleared suspension was then run in 80ml volumes through the Polyethersulfone (PES) Ultrafilter (VF05P4) 100kDa Sartorius TFF cassette to concentrate samples twofold to 40mls. Secretome was concentrated and purified in Serum Free media for functional studies and concentrated and resuspended in PBS for characterisation. For standardisation of bioprocessing, the TFF was run at a maximum of 2.5 psi at a flow rate of 200-400ml/min as suggested in the user manual.

In order to further isolate small EVs/Exosomes from the concentrated secretome, the Cell Guidance Systems EX01 Exo-spin™ mini columns were further implemented. These combine both Size Exclusion Chromatography (SEC) and Precipitation, in order to isolate Exosomes between 30 and 300nm in size. Concentrated EV samples were spun at 16,000 × g for 30 minutes in a microcentrifuge tube to allow for removal of any residual cell debris. Supernatant was then mixed with Exo-spin™ Precipitation buffer and incubated overnight at 4°C. The mixture was centrifuged at 16,000 x g for 1 hour, supernatant discarded and the EV containing pellet resuspended in 100µl of PBS. Once the Exo-spin™ column had been washed with PBS as directed in the manual, the 100µl of exosome-containing pellet was added to the top of the Exo-spin™ column, drawn through by gravity and larger waste EVs collected at the base as the first EV fraction. Following this, washing the column gently with 180µl PBS (characterisation studies) or Serum free media (functional studies), allowed the elution and so isolation of a second fraction containing sEVs/Exosomes. Upon washing of the column, all the eluted extractions were kept for analysis in case of loss of sEVs and finally columns stored on the final wash in 20% ethanol in PBS.

3.2.5.2 EV storage

Samples were all stored in their TFF isolated state for short term (up to 7 days) at 4°C and for long term storage (over 7 days and up to 1 year) in the -80 freezer. Additionally, samples that were being used for functional work were stored in rooster collect and those used for

characterisation in PBS and 25nM Trehalose. No samples were freeze thawed more than once.

3.2.6 Extracellular Vesicle Analysis

3.2.6.1 Nanoparticle Tracking Analysis (NTA)

The NS300 Malvern Panalytical NanoSight uses Nanoparticle Tracking Analysis (NTA) to measure nanoparticles in solution between 10nm -2000nm. A minimum liquid volume of 250µl containing 1×10^6 to 1×10^9 particles per mL was loaded via syringe pump into the sample chamber. Here dispersed particles move using Brownian motion. The principle of this in determining size is that small particles collide more frequently with solvent molecules, thus giving them greater energy transfer and causing them to move at greater speeds. Brownian motion is visualised by light scattering from their illumination with a laser beam and detected using a sCMOS camera. The Stokes-Einstein equation was then applied by the system to determine size by tracking movement of particles. Prior to performing sample analysis, LGC Colloidal gold nanoparticle (LGCQC5050) was used to calibrate measurements (nominal diameter 30nm and concentration of 1.47×10^{11} NP/g). Between samples and each 3 individual repeats PBS was also used to flush the system.

3.2.6.2 Dynamic Light Scattering (DLS)

Particle size distribution and concentration measurements were made using the Multi-Angle Dynamic Light Scattering (MADLS) zetasizer ultra (Malvern Panalytical Ltd., Malvern, UK) at LGC. This detects a wider proportion of the sample and so is advantageous in that it can measure multiple angles of a heterogeneous particle population without misinterpreting sizes, thus generating a more complete size distribution. The instrument was equipped with a 10mW 633nm wavelength He-Ne laser to analyse 1 mL samples within disposable cuvettes (DTS0012, Malvern Panalytical Ltd., UK). The instrument combines the auto correlation size measurements at each angle automatically using the ZS XPLOER software (Malvern Panalytical Ltd., UK).

3.2.6.3 NanoFlowCytometry (NanoFCM)

Both stained (Universal Biologicals MemGlow™ 488: Fluorogenic Membrane Probe - MG01-10) and unstained samples were analysed by NanoFlowCytometry (NanoFCM) to determine nanoparticle concentrations and size distributions. The Nano flow cytometry analyzer (NanoFCM Inc., Nottingham, UK), takes up a sample <10µl by the capillary into a sheath fluid stream, which passes single file, particle by particle through a set of 488nm and 640nm lasers. This signal was then detected by 3 single-photon counting avalanche photodiode detectors (SPCM APDs), one measuring the scatter signal of nanoparticles and the other 2 simultaneously measure the fluorescence emitted by stained particles, both of >40nm in diameter. Optimal event rate for sample acquisition was recording between 2,000 and 12,000 events during a single minute timeframe, whilst sampling pressure was 1.0 kPa. Prior to this, to determine true nanoparticle concentration, the machine was calibrated for flow rate by adopting a 250nm silica bead standard at a concentration of 1.99×10^{10} particles/ml (NanoFCM Inc., 250nm Std FL SiNP). Unknown nanoparticle size distributions were calculated by plotting the standard curve from a polydisperse assortment of non-fluorescent silica nanoparticles at a concentration of $\sim 3 \times 10^{10}$ particles/mL (NanoFCM Inc., S16M-Exo). This standard curve, created using V2.0 software, was based on these bead populations: 68, 91, 113 and 155 nm.

Memglow 488, staining was performed at 100nM for 30 minutes at 4 degrees with no free dye removal step as the stain is self-quenching.

3.2.6.4 Bicinchoninic Acid (BCA) protein assay

Protein concentration was established for many EV characterisation and functional assays by bicinchoninic acid (BCA) protein assay (Pierce). The reduction of Cu^{2+} to Cu^{1+} by protein was colorimetrically assessed by absorbance reading at 562 nm on the Spark® multimode microplate reader (TECAN). The technique was performed in line with the manufacturers manual and measurements were made of standard curve standards (working Range = 20–2,000 µg/mL), unknown samples and a blank, with unknowns being read from the standard curve.

3.2.6.5 Enzyme-linked immunosorbent Assay (ELISA)

ExoLISA™ CD9 (EX501) CD63 (EX502) CD81 (EX503) Exosome Detection Assay (CellGuidance systems) was performed by capture of sample exosome antigens between a Biotinylated antibody bound to streptavidin coated plates and Europium-labeled antibody. The technique was performed in line with the manufacturers manual and following incubation, samples were then read using the Spark® multimode microplate reader (TECAN) under a Time-Resolved Fluorescence (TRF) setting with 337nm excitation and 615nm emission filters.

3.2.6.6 ExoView

The ExoView™ R100 (UnchainedLabs, UK) was used to perform sizing, counting, and biomarker detection at the single EV level. EVs from 20µL sample incubated overnight on chips containing triplicate of each immunocapture spot tetraspanins (CD81, CD63, CD9) and an IgG control. After washing chips using manufacturers instructions, they were subsequently fluorescently stained and probed by the same 3 secondary labelled antibodies for assessment of colocalisation. Detection of fluorescence was performed using the Exoview R100 and analysed for also both tetraspanin count and size by means of the ExoScan 2.5.5 acquisition software (NanoView Biosciences, UK).

3.2.6.7 Transmission electron microscopy (TEM)

The JEM1400 **Transmission electron microscope** (JEOL) coupled with an XR-80 digital acquisition system (AMT) was used to assess EV morphology and size. 20µl Samples were Physisorbed via drop casting on a 200 mesh carbon-coated copper formvar grid (Agar Scientific, UK) and images acquired.

3.2.6.8 Proteomics and Mass Spectroscopy

SEC isolated and concentrated (0.5mL 3kDa Amicon spin columns) MSC-sEVs underwent mass spectrometry (MS)-based proteomics to reveal their proteomic cargo. The samples were initially quantified using a micro-BCA assay in order to ensure EVs were highly concentrated to meet MS requirements.

In preparation for gel electrophoresis, the isolated MSC-sEVs were firstly reduced and alkylated in Laemmli buffer (65°C for 15 minutes) and following this loaded at 30µg or less on 10% SDS-PAGE gel (10 pockets 1 mm thickness) for molecular weight-based separation of proteins. following this we performed the overnight staining at 4°C with 0.5% Coomassie G250 brilliant blue dye (Pierce) in 40% aqueous methanol and 5% glacial acetic. Gels were

then repetitively de-stained in 10% aqueous ethanol and 7.5% glacial acetic acid prior to cutting.

All samples were excised and divided into 5 sets of bands dependent on size (kDa). Excised and diced (approximately 2x2x1 mm in size) gel pieces with stained protein bands were transferred into polypropylene tubes (1.5 ml, LoBind PCR clean, Eppendorf). Protein bands were fully de-stained with varying volumes (100-200 μ l) of 50% acetonitrile in aqueous 50mM ammonium bicarbonate, dehydrated in acetonitrile until rock solid and vacuum dried in preparation for in-gel digestion. For proteolytic in-gel digestion gel pieces were re-hydrated in 40 μ l of trypsin solution in at a 25:1 protein to trypsin ratio (Trypsin Gold, sequencing, Promega, UK), followed by the further hydration in 150 μ l of 3 mM ammonium bicarbonate. Fully immersed gel pieces were left overnight at a thermoshaker at 550rpm and 37°C.

Succeeding digestion, the process for extracting peptides involved gentle increase of acetonitrile percentage in the sample tubes followed by the 15 min sonication. Closely, 50-70 μ l of acetonitrile was added and samples were sonicated. Liquid containing extracted peptides above gel pieces was carefully collected into separate tubes. Gel pieces were covered in 50% acetonitrile in 50mM aqueous ammonium bicarbonate and sonicated. This step was repeated once and each time extracted peptides were collected in the corresponding polypropylene tube. Finally, gel pieces were fully dehydrated in 100% acetonitrile to achieve maximum peptide extraction and this extract was combined with the other. Total peptide extracts were subsequently vacuum dried and stored (-20 °C) prior to MS analysis.

Once ready for processing using liquid chromatography-coupled tandem MS (LC-MS/MS) analysis, dry samples were initially reconstituted in 30 μ L of 3% aqueous acetonitrile and 0.1% formic acid. The sample peptides were separated and evaluated through a nano UPLC system (Acquity M class, Waters) coupled with 5600 TripleTof (AB Sciex, UK) operating in information dependent analysis mode.

10 μ l peptide solution was injected and trapped onto a trap column (nanoEase M/Z Symmetry C18 Trap Column, 100A, 5 μ m, 180 μ m x 20mm, Waters) for a total of 3 min at 15 μ l/min of 1% acetonitrile in aqueous 0.1% formic acid. Peptides were separated on an analytical column (nanoEase M/Z Peptide BEH C18 Column, 130Å, 1.7 μ m, 75 μ m X 150 mm, Waters) with a flow rate of 0.5 μ l/min and a gradient of 1%-45% acetonitrile in aqueous 0.1% formic acid in 45 min, followed by the steep gradient increase 45%-90% acetonitrile in 0.1% aqueous formic acid for 5 min, isocratic separation for 5 min at 90% acetonitrile in 0.1% aqueous formic acid and 12 min re-equilibration to the initial conditions. Samples were directly infused into mass spectrometer using a PicoTip™ emitter (New Objective, Germany) and a fine electrospray was formed at 2500V. The 10 most intense multiply charged ions were selected from each MS

survey scan (200 ms) for a high sensitivity collision induced fragmentation. Analysed ions within 50 mDa tolerance were temporarily excluded from further MS/MS analysis for 30 s. The mass spectrometer was fully calibrated before the measurements.

Once data was collected, relative quantification of peptides was performed using Progenesis Q1 for proteomics software (version 4, Nonlinear Dynamics, UK). Acquired files were processed using multi-fraction setup allowing for data normalisation to account for possible differences from run to run and achieve the most accurate relative quantification. After merging the sections 1-5, exported files were searched against the SwissProt database using MascotDeamon (ver 2.5) using *Homo sapiens* taxonomy, allowing for maximum three peptide mis-cleavages and allowing for variable modifications on methionine (oxidation) and cysteine (carbamidomethylation). Only protein-unique peptides with a confidence higher of 95% and score higher than a threshold for identity were exported back to Progenesis. Keratins as a result of possible contamination during sample handling were manually excluded from data analysis. Relative quantification of was allowed only from protein-unique peptides. Merged with information on relative protein abundances for each sample were exported as .xml file and post-processed for gene ontology analysis with FunRich software.

3.3 Statistics

Data storage, plotting and analysis was performed using GraphPad Prism 8. All figure legends reference how data are presented, number of repeats performed and statistical significance. Most data are displayed as mean \pm standard error of the mean (SEM) or rarely as mean \pm standard deviation (SD). As a range of techniques have been applied in this project, N=3 can be described broadly as featuring at least 3 assessments of 3 different batches of sample or 3 different experimental runs. When working traditionally in plates N=3 referred to atleast 3 well repeats (technical repeats) performed on 3 separate occasions in separate experiments (biological repeats). The majority of data was statistically assessed by one way ANOVA with Tukey's multiple comparisons to define differences in statistical difference between the means of n=3 repeats. On occasion, and where referred to in the figure legend, t-tests were applied when comparing the means of two populations or one population against a control. Within all statistical tests, equal SDs/SEMs and gaussian distribution was assumed with the application of a 95% confidence level ($\alpha=0.05$). When determining statistical difference, p values larger than 0.05 were indicative of no statistical difference, whereas p values less than 0.05 were indicative of a statistical difference. Dependent on the p value, significance was referred to as: $p < 0.05 = *$, $p < 0.01 = **$, $p < 0.001 = ***$, $p < 0.0001 = ****$.

Chapter 4: Bioprocessing of MSCs and MSC-EVs from Spinner Flasks

4.1 Introduction

The success of scaling up any biologicals in a bioreactor culture environment is dependent upon initially engineering an optimised upstream system. In regards to the scale up of MSC derived sEVs, the downstream bioprocessing considerations were also key to maintaining yield whilst achieving purity. Henceforth factors such as: stir speeds mixing times, MC selection, media selection and sEV isolation technique were adapted and optimised in this chapter to support MSC expansion, EV collection and maintenance of potency.

4.1.1 Upstream Bioprocessing

Scale up optimisation of Stem Cells in Bioreactors, including MSCs, is well publicised, with the main focus being that small changes to the bioprocessing/physical features of the Bioreactor can have a major impact on Cell yield/viability/phenotype etc. Hence, the main considerations when working with MSCs and moving from a small scale cultivation system was to ensure that the platform provides: structural support for MSC adherence, as well as cultural stability to allow maintainance of MSC immunophenotype and multipotency. As alluded to in the introduction section 1.3-1.4, within the culture platform it is important to perform sufficient microcarrier selection and optimise both physical agitation and chemical media composition parameters as part of the bioprocessing optimisation.

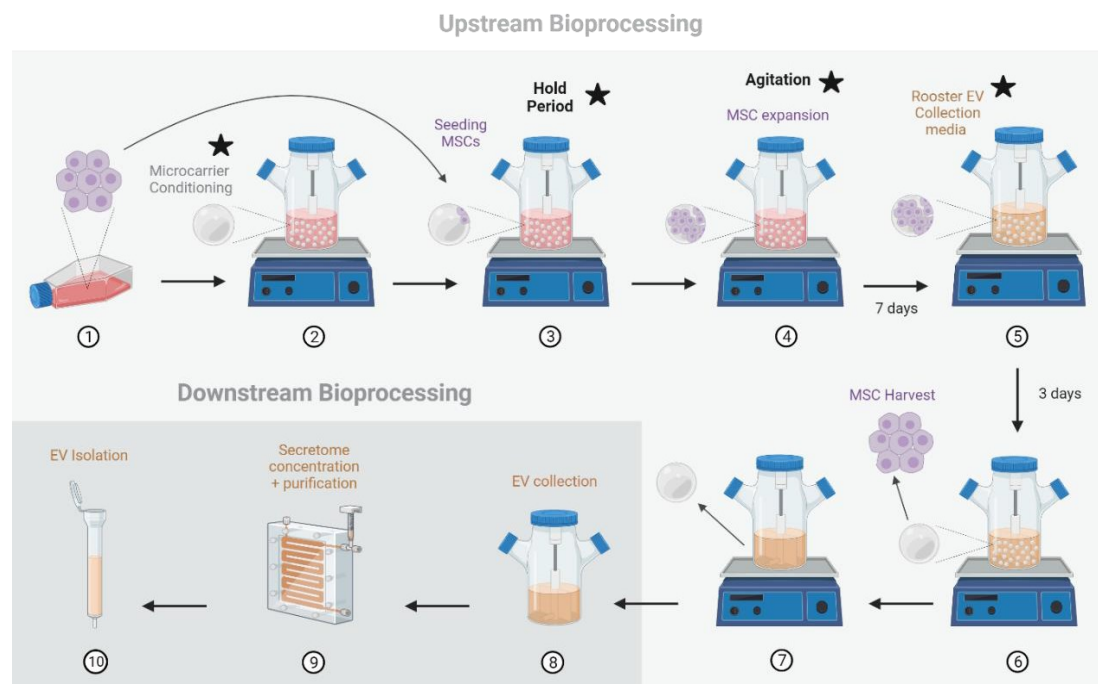


Figure 6: Upstream and Downstream Bioprocessing of MSCs in SFs. Scalable Upstream bioprocessing to enhance MSC yield relies upon the adaptation of culture parameters, which are pinpointed with a star. These include; MC type, hold period, agitation speeds and MSC expansion media. Surrounding these is an upscale procedure consisting of steps which need to be completely controlled in order to ensure batch repeatability.

4.1.2 Bioprocessing factors

4.1.2.1 Microcarriers

Microcarriers are small, spherical beads commonly applied in stirred-tank systems to allow anchorage-dependent cells to attach and grow on/in their matrix [84, 86]. These properties provides them with a high surface area to volume ratio, enhancing cell expansion and thus cell/cell product yield. As previously referred to in section 1.4.2, some MCs convey adapted surface topography and chemistry to further escalate cell attachment and expansion, which is what we wanted to investigate by screening six unique MCs (Solohill). A similar study was performed by Rafiq et al, which compared both Solohill and other commercial MCs together. They concluded that Collagen, Plastic and Pronectin - F promoted the highest viable cell number with performance of these MCs in 2D planar culture closely mimicking their performance in 3D suspension culture [200]. Reinforcing this was a study by Navaei et al who found MSCs expanded using SoloHill Collagen MCs displayed maintained >90% viability post

harvest and during Bioreactor culture cell density was greatest on Corning Synthemax MCs [201]. In comparison, both Loubière et al. and Van Beylen et al. selected Star-Plus and Plastic-Plus MCs as their most promising MCs for culturing Umbilical Cord MSCs and human periosteum-derived progenitor cells [202, 203]. This was based on a similar criteria of initial cell attachment, proliferation, viability and harvest efficiency. Interestingly, despite this data, a review article by Tsai and Ma documented substantial preference towards Cultisphere S, Synthemax and Cytodex MCs for expansion of MSCs in Bioreactors [204].

Evaluating findings from other research groups suggested the need to reassess selected Solohill MCs for bmMSC scale up suitability. To do so, monolayer 2D screening investigations were initially performed before moving into agitated 3D suspension SFs. These are highly adaptable, affordable, reusable culture vessels that closely emulate the fluid flow and shear stress forces experienced in a Stirred tank bioreactor, making them an ideal platform for assessing different bioprocesses and batch-to-batch run consistency.

4.1.2.2 Agitation

Critical factors that need to be optimised and controlled during MSC expansion on MCs in SFs comprised stir speeds and agitation protocols. As previously mentioned, stir speeds were determined by the N_j / N_{S1} calculation, as well as previous work conducted by our research groups and well documented in papers (see section 1.4.3). Although some studies found that variations in stir speed showed no significant difference in cell expansion, it was determined that once this exceeds the optimal N_{S1} range, cells fold-increase can decline [205]. Generally, for MSC culture in SFs these boundaries were considered to be 25-90rpm, with stir speeds of 30-45rpm employed most often [205-207]. These speeds achieve complete suspension of MCs, encourage attachment and increase overall MSC yield, support glucose consumption and thus active metabolism [66, 105, 208-210]. Nonetheless, this does vary dependent on Bioreactor vessel size/type MC and cell type and without doubt it is imperative that this parameter is optimised internally for all types of bioprocessing research [105, 210, 211]. This prevents exposure to high levels of shear stress or settling and clumping of MCs from inhibiting cell growth [212, 213].

To further assist initial MSC attachment to MCs, stirring patterns and stir/static hold period protocols are often employed by research groups looking to maximise yield. Strategies used varies extensively between authors from prolonged [76, 83, 214] and interval static attachment periods [212, 215] to slow stir speeds [68, 88, 216, 217]. Specifically a 1 hour to 3hrs to 16-

24hrs intermittent stirring all resulted in the reduction of the initial lag in cell expansion [214, 218-220]. Rafiq et al, after multiple papers assessing optimisation of stirred bioreactor culture, settled on the employment of a hold time of 3 hours with intermittent 5 minute spinning every 30 minutes in order to enhance cell yield. Applying this method they observed a >150% increase in viable cell density post 24 hrs in culture in comparison to their original conditions [221].

From reviewing literature it is clear that implementing a hold period can force greater MSC adhesion to MCs, which consequently has a positive impact on expansion and final yields. Thus as part of the bioprocessing we decided to trial 2hr, 4hr and 24hr intermittent spinning hold times. Alongside this, we wanted to trial lowering the initial media volume (%) for the first 24hrs of culture with the hypothesis that it would concentrate MCs into a reduced area, encouraging increased contact between cells and MCs and hence further promoting initial cell attachment.

4.1.2.3 Media composition

Once the SF agitation protocol had been optimised for the scale up of MSCs, selection of chemical media composition was then necessary for the continuous collection of secretome across the culture timeline. To ensure sEVs collected from secretome were MSC derived it is important to consider the effect of well documented fetal bovine serum (FBS) sEV impurities and so employ either XF, serum free or EV depleted FBS culture media [172, 222, 223]. Examples of those which that were popular amongst other academic groups, was outlined in a literature review by Almeria et al. These included: Ultracentrifugation (UC) depleted media, Amicon ultra-15 centrifugal and Merk Millipore Ultrafiltration (UF) depleted media; hollow fiber-modified polyethersulfone (mPES) membrane Tangential flow filtration (Repligen KR2i TFF) depleted media; Fibrinogen and fibrin depleted FBS and Commercially available EV-depleted media/serum (MesenCult™-ACF Plus, System Biosciences Exo-FBS™, Oxium™EXO and RoosterCollect EV Pro™) [224]. Of these options, alongside switching to serum free media, generally, the defined commercial collection medias appear to be most commonly applied. Serum free media typically provided a simple method for EV collection, whilst also shown by many to elicit an increase in EV manufacture, without altering the EVs size or physical properties [225]. However, it has been shown to alter factors such as EV cargo (encapsulation of reactive oxygen species, alteration of RNAs) and proteome (stress induced proteins) [226-228]. Additionally, recent research into chemically defined XF media implied that although, similarly to serum free media, there is consistency and so reproducibility between batches,

the media exerts the same effects on EV release profile (greater release of particles but with altered miRNAs) [229].

However, when working at scale or wanting to collect EVs over a time course, UC, UF and TFF depletion methods can allow for more affordable and adaptable cell culture. Nonetheless, studies have shown conflicting results into the effect that depleted FBS has on population doubling and viability, as well as if the advantages outweigh the disadvantages, which includes MISEV's recommendations to avoid FBS where possible [230-232]. For example a study on neurological cell types both an initial lag and sustained reduction in cell expansion, in comparison to complete media, with a significant decrease in viable cell number after 48hrs culture in depleted FBS [231]. Thus this study appears to make it clear that circulating EVs in serum play a key role in supporting cell survival and growth during culture, but does argue that it does not suggest depleted FBS exerts a toxic effect on cells. In contrast, an UC-MSC focused study demonstrated that population doubling time (PDT) was unchanged across all donors sustained in the FBS and UC-FBS media (but not in UF-FBS) and consistency in cell viability as well as MSC surface marker presence across all media compositions [230]. Specifically literature reviews and experimental papers are in agreement that short-term or transitional use of depleted and FBS-free media is comparable in performance to complete FBS media when culturing MSCs [233]. Unlike UC-FBS, there is little recorded application of TFF-FBS, especially that using the Sartorius Vivaflow TFF. Documented use of 500kDa hollow fibre TFF came from in house optimisation from a paper by Wolf et al, where they alluded to it's levels of depletion being equivalent to that seen using UC , with benefits including its scalability and ease of handling [234].

The scrutinisation surrounding the use of any form of FBS (including depleted) in EV derived cell culture, made it difficult to select a media composition for SF studies. However, by employing both depleted FBS for the bulk of MSC expansion and a defined XF EV collection media once MSCs reached close to confluence, analysis of a purer EV population could be made on day 10 of culture from MSC secretome.

4.1.2.4 Feeding regimes

When working with a small scale, manually operated bioreactor (SFs), this is a more limited option of feeding regimes to replenish nutrient and remove waste products. Again, feeding regimes are restricted further by the necessity for this platform to permit consistent collection of sEVs across the bioprocess timeline. Hence both restrictions prevented us from being able

to adopt a fed-batch technique, which is the addition of media only and dilution of metabolic waste, and instead adopted an ~70-80% batch-feeding protocol (complete media exchange). However, it must be acknowledged that the current standard method for batch feeding involves closer to a 25-50% exchange every 2/3 days (draw-fill protocol) [235]. This was shown to be advantageous in regards to both decreasing costs, reducing MC loss and maintaining a consistent osmolarity range by conserving MSC secreted cytokines and key growth factors, which are enhancers of cell expansion and functionality [218, 235, 236]. Generally, batch culture is ideal for process development studies at smaller scale as media exchanges can be performed around screening MSC-MC interactions, MSC proliferation and metabolic changes, whilst permitting collection of MSC-EV rich secretome [237]. However, once optimisation of stirred culture had been achieved, it would be wise to consider perfusion mode culture as it has been evidenced to produce greater MSC yields, whilst maintaining potency. For example a study by Cunha et al. demonstrated 14.6 fold expansion under perfusion culture, in comparison to 11.5 fold expansion under batch feeding [238], whilst Dos Santos et al. achieved 5.0×10^5 cells/ml after 11 days of culture, where batch feeding attained 1.5×10^5 cells/ml after 7 days [239]. If the relationship between MSC numbers and sEV concentrations correlate, perfusion feeding in litre scale bioreactors would provide an excellent platform for scalable MSC-sEV production.

4.1.3 Characterisation post Bioprocessing

Following scale up, it was important to ensure MSCs met the ISCT guidelines for characterisation post exposure to suspension culture forces, FBS depletion and harvest stress. Thus these were seeded for phenotyping to look for known +ve and -ve MSC biomarkers, differentiation assays (Adipogenic, Osteogenic and Chondrogenic differentiation), colony forming unit and T lymphocyte suppression assays. Although, it appeared to be unlikely that these would be affected by agitation stress as years of bioprocessing research, a large selection of which was detailed in the Hassan et al. review article, overwhelmingly reports that MSCs retain their stemness and functionality post SF and Bioreactor culture [48]. However, as we are more focused on the MSC secretome and EVs as a scalable therapeutic product from SFs, the assessment of MSC characterisation was precautionary and secondary to the EV research.

4.1.4 Downstream bioprocessing

4.1.4.1 EV concentration, isolation and purification

Isolation of sEVs from the wider cell secretome is important to determine the results from the assessment of protein cargo, surface chemistry and EV functionality can be amounted to the sEVs/Exosomes and not excess protein or Microvesicles. As already mentioned, there are various techniques that can be employed which have varying degrees of cost, scalability, product purity, extraction yield, ease of handling and preservation of bioactivity [175]. This makes the selection of both media composition and isolation technique, key to the production of high yields of pure sEV populations from scalable suspension bioprocess. A detailed review of all sEV isolation techniques was alluded to in the thesis introduction (1.6.2) but within this study it was decided that Tangential Flow Filtration (TFF) and Size Exclusion Chromatography (SEC) with precipitation were suitable, complementary isolation methods. The TFF is not limited by maximum volumes, unlike SEC, and can concentrate media down, whilst sustaining yield of EVs [240-243] and causing negligible physical damage to their integrity, as illustrated by UC [244]. Although the time efficiency, ease of handling and scalability of TFF, make TFF a preferential method for filtering EV rich secretome, it's insufficient purification of sEVs makes it better suited in a 2 part combined isolation method [243, 245].

4.2 Aims

The aim of this chapter of the thesis was to show MSCs can be scaled up successfully in small scale Bioreactors (SFs) using an optimised protocol. To achieve this, multiple bioprocesses were assessed that both encourage attachment and expansion of MSCs (upstream bioprocessing), whilst also allowing the collection of sEVs across the culture timeline and downstream bioprocessing of them.

More specifically, the aims of this chapter were to:

- 1 Screen selected MCs in 2D for their ability to support MSC expansion.
- 2 Optimise SF bioprocesses to maximise MSC harvest.
- 3 Characterise MSCs post SF harvest to ensure maintenance of stemness.
- 4 Test various media compositions for EV collection across the bioprocess timeline.
- 5 Concentrate and purify EVs from SFs.

4.3 Results

MC screening experiments suggest Star Plus and Hillex 2 are not suitable for facilitating MSC culture

A selection of 6 Solohill MCs, all with varying surface compositions and charges, were initially screened for their ability to support AM2, AM4 and 144 MSC expansion in 96 well plates. The well surfaces were coated with sigmacote to prevent MSC attachment and 5000 cell/cm² seeded with concentration standardised monolayers of MCs. This experiment would eventually predispose which MCs were employed in SFs.

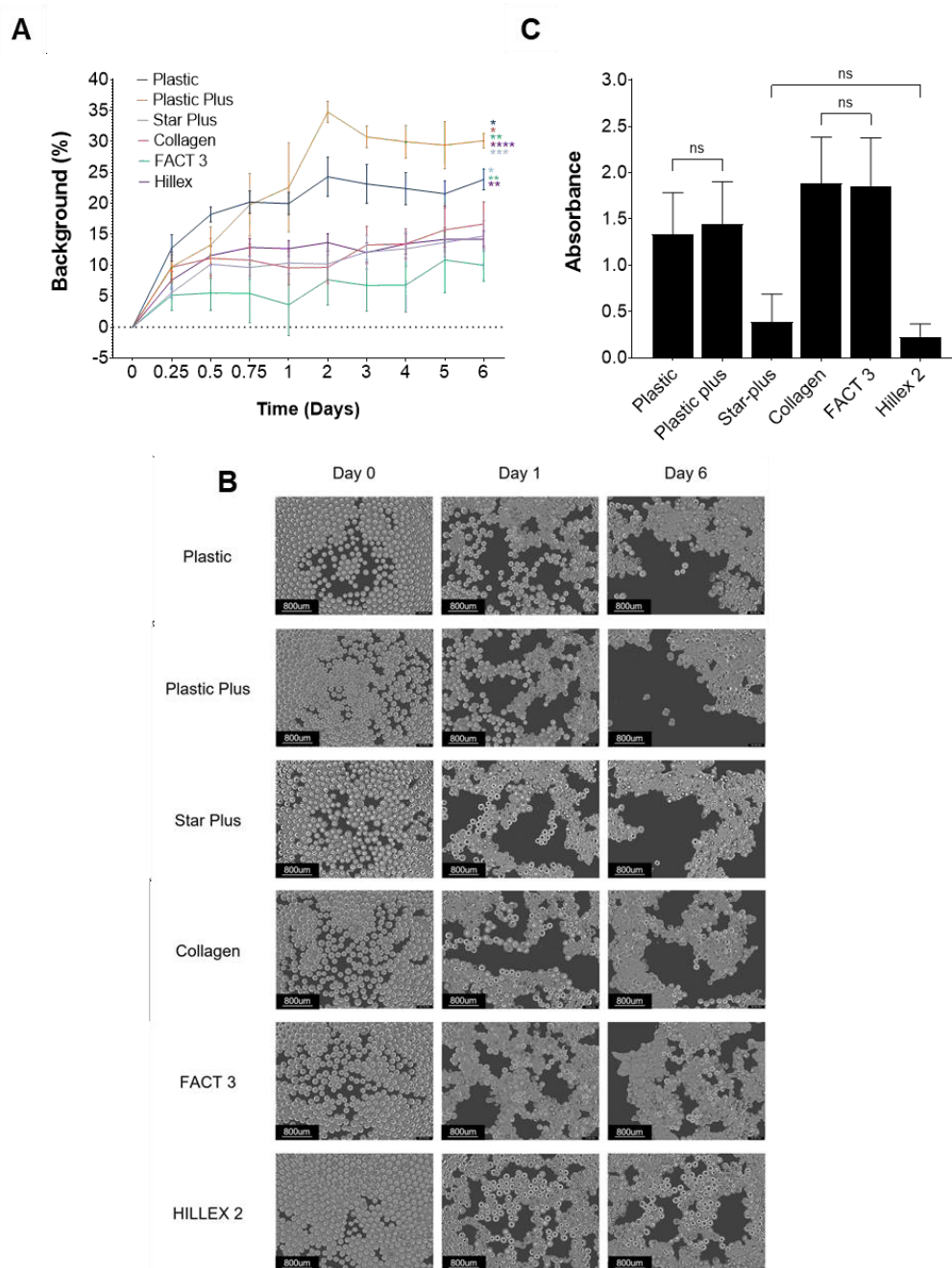


Figure 7: MC screening in 2D planar culture. Quantification of MC-MSC aggregation (A) and a selection of AM2 images from which aggregation was quantified (B). Monolayer MC dispersions were incubated with AM2, AM4 and 144 bmMSCs in 96 well plates at 5000cells/cm² for 7 days and snapshots were taken at 4x objective across this timecourse. The Incucyte snapshots were then quantified by background (%) unoccupied by aggregates, which indirectly reflects MC aggregation. On day 7, CCK-8 measurements were also made of cell viability post incubation and are outlined in C. Graph A and C means were plotted with SEM (A) and SD (C) from 3 technical repeats and 3 independent biological repeats for cell lines AM2, AM4 and 144 (n=3).

Fig7B images were taken at 4x objective using the incucyte software and edited so the nude area/background was more visible. The images were further edited using imageJ in order to allow for quantification in fig7A. The microscopic snapshots depict how within 24hrs the monolayer of MCs move to form aggregates and zones free of MCs begin to form (fig7B). Visually, there appears to be minimal difference in background (%) and MC aggregation on day 1 but this is more apparent by day 6, where plastic and plastic plus MCs congregated together into densely packed areas. Hillex 2 on the other hand has a lower percentage total nude area with only small pockets of plate background. The quantified values for background (%) from the images in fig7B are presented in fig7A and depict how both plastic plus and plastic MCs show the highest levels of aggregation. Specifically plastic plus shows significant more aggregation than all other MCs at day 10 and plastic shows significantly more aggregation than Star plus, Fact 3 and Hillex 2 (fig7A). Of all the MCs, Fact 3 consistently at all time points shows the lowest levels of aggregation.

On day 7 of MSC-MC culture, CCK-8 solution was added to each well and AM2, AM4 and 144 live cell count was assessed using absorbance readings produced by Spark® multimode microplate reader (TECAN). From the 6 solohill MCs, both Star-plus and Hillex 2 MCs show the lowest absorbance readings (fig7C). These are significantly different to Plastic, Plastic plus, FACT 3 and Collagen's absorbance readings, from which the latter two produce the highest absorbance readings and hence highest proportion of live cells (fig7C).

A 24hr hold time, with a protocol employing plastic MCs in 100% media volume generates the highest levels of MSC expansion and eventual cell yield.

AM4 MSCs of passage 3-5 were seeded into SFs at 4-5000cells/cm² MCs post MC conditioning using selected bioprocessing conditions. Figure 8 demonstrates the adaptation and optimisation of the upstream bioprocessing conditions to meet the demands of the scale up study.

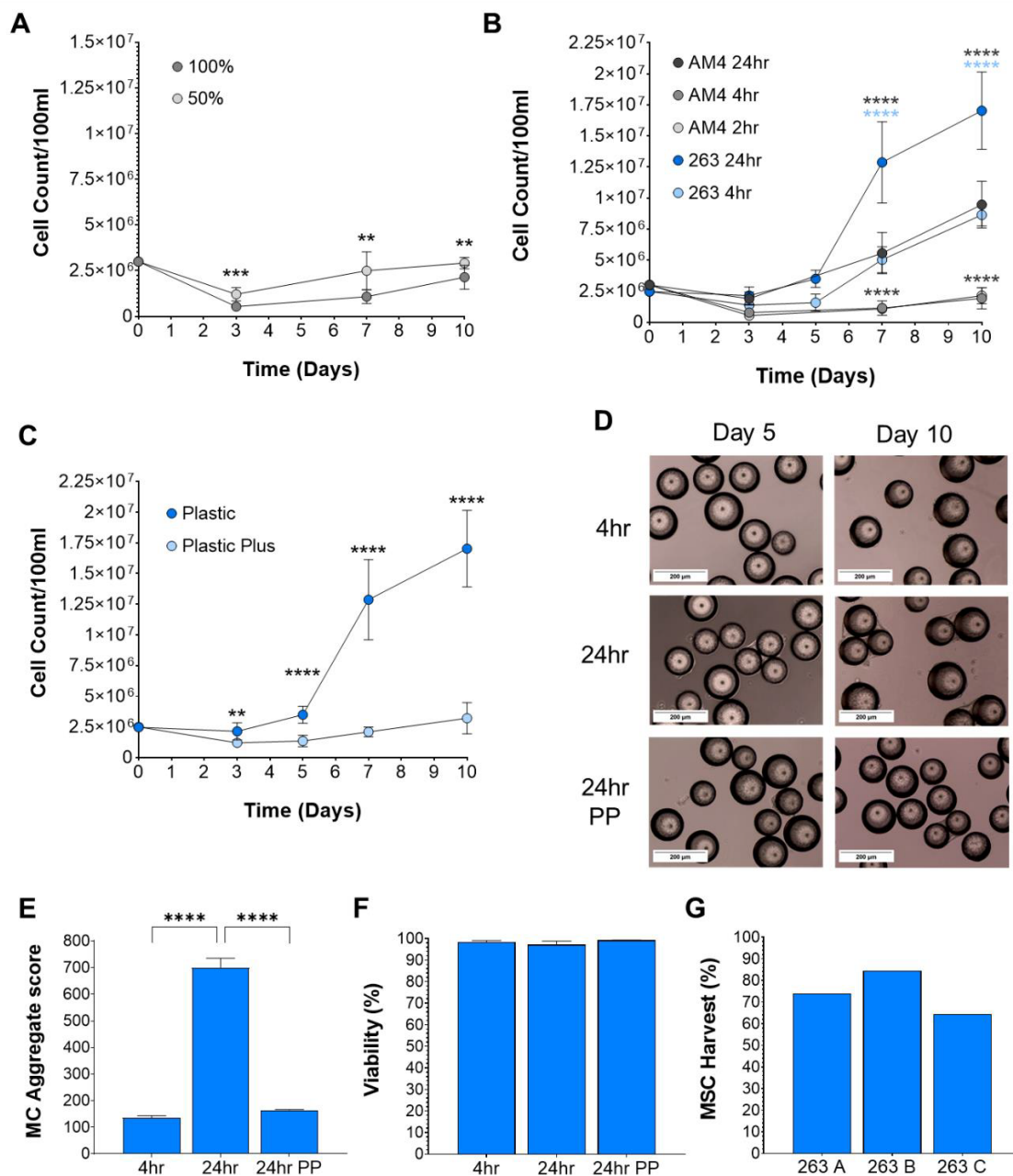


Figure 8: Optimising the bioprocess parameters to increase MSC expansion and yield from SFs. Graph A shows the effect of reducing the initial media volume (%) on AM4 MSC cell count over the course of the cell culture timeline. Graph B shows the effect of different hold period lengths in 2 cell lines on MSC expansion. Of these protocols, the most effective was employed with both plastic and plastic plus MCs. Each of these conditions were repeated on three separate occasions atleast with different batches of MSCs. A selection of 20x objective microscopic images are presented in D to illustrate the difference in MSC-MC bridging and aggregation across different protocols. Additionally E shows this aggregation quantitatively using a standardised procedure/equation/method and F highlights the MSC viability post harvest from each bioprocessing protocol, all measured using the nucleocounter software.

Finally graph G acknowledges the harvest (%) of 3 batches of 263 24hr hold plastic bioreactor runs. Graphs A, B, C and F mean and SEM values were plotted from 3 technical repeats of 3 independent SF runs (n=3). Whilst graph E mean values with SEM was plotted from 1 technical repeat of 4 days combined calculations from 3 independent SF runs (n=3). Unpaired T-tests were performed

Initially a 2hr hold time was applied to encourage some MSC attachment, which involved 25/30rpm stirring for 5 minutes following every 25 minutes of static culture over the course of the hold time. Applying this controlled hold period, initially, all three batch repeats of this condition showed no evidence of population doubling or expansion above the initial seeding density. Therefore, decreasing the % of media over the first 24 hrs of culture, alongside this hold period was trialled to see if this forced more MSC adherence to and growth upon MCs. Graph A illustrates the comparison between both 50% and 100% complete media volumes for the first 24hrs of culture where, although there is a significant difference between the two media volume (%) at all time points, the MSCs maintained low levels of cell number at a plateau.

Following this, it was acknowledged that adjusting the SF hold time would have a greater impact on MSC yield than % volume. Graph B describes the effects of old and new selected hold period lengths on AM4 and 263 MSC cell count over the course of 10 days SF culture. It was apparent from the data that the longer hold period (24hrs) dictates a significantly greater AM4 ($p < 0.0001$) and 263 ($p < 0.0001$) MSC cell count on day 7 and 10 of culture in comparison to shorter hold times. In addition to this the rooster 263 cell line illustrated greater MSC expansion to AM4 with significantly different cell count measurements at day 7 ($p < 0.0001$) and day 10 ($p < 0.0001$) under the 24hr hold period protocol. Applying the 24hr hold time protocol, graph C conveys the difference in 263 MSC growth rates between plastic and plastic plus MCs, with plastic supported MSCs showing significantly greater cell numbers at day 3 ($p < 0.01$), day 5 ($p < 0.0001$), day 7 ($p < 0.0001$) and day 10 ($p < 0.0001$). To reinforce these results, images of MSC-MC aggregation were taken at all media exchange time points with day 5 and 10 for line 263 4hrs, 24hrs and 24hrs pp being exhibited in (D). These images were quantified in (E) using a standardised calculation inclusive of all types of aggregate (bridging between 2, 3 and 4+ MCs). This data describes how 24hr plastic MCs convey significantly greater aggregation than plastic plus (24 PP: $p < 0.0001$) and 4hr plastic MCs (4hr: $p < 0.0001$). Nonetheless, the viability of 263 MSCs post harvest from SFs remains high at between 95-100% and shows no significant difference between these 3 conditions. From the optimal 24hr plastic protocol, MSCs of three different batches were harvested from three different runs and the harvest % calculated. Graph G recognises that this could be as low as 64% and went no higher than 84%.

TFF depleted FBS does not sustain 263 and 271 MSC expansion in SFs whereas UC depleted FBS promotes comparable growth to complete media.

Following the creation of an optimised SF scale up platform, in order to collect MSC derived EVs from across this culture bioprocess timeline, an alternate FBS-EV free media had to be developed. Ideally this would be extensively depleted of any FBS derived sEVs but contain biological components to maintain MSC metabolism.

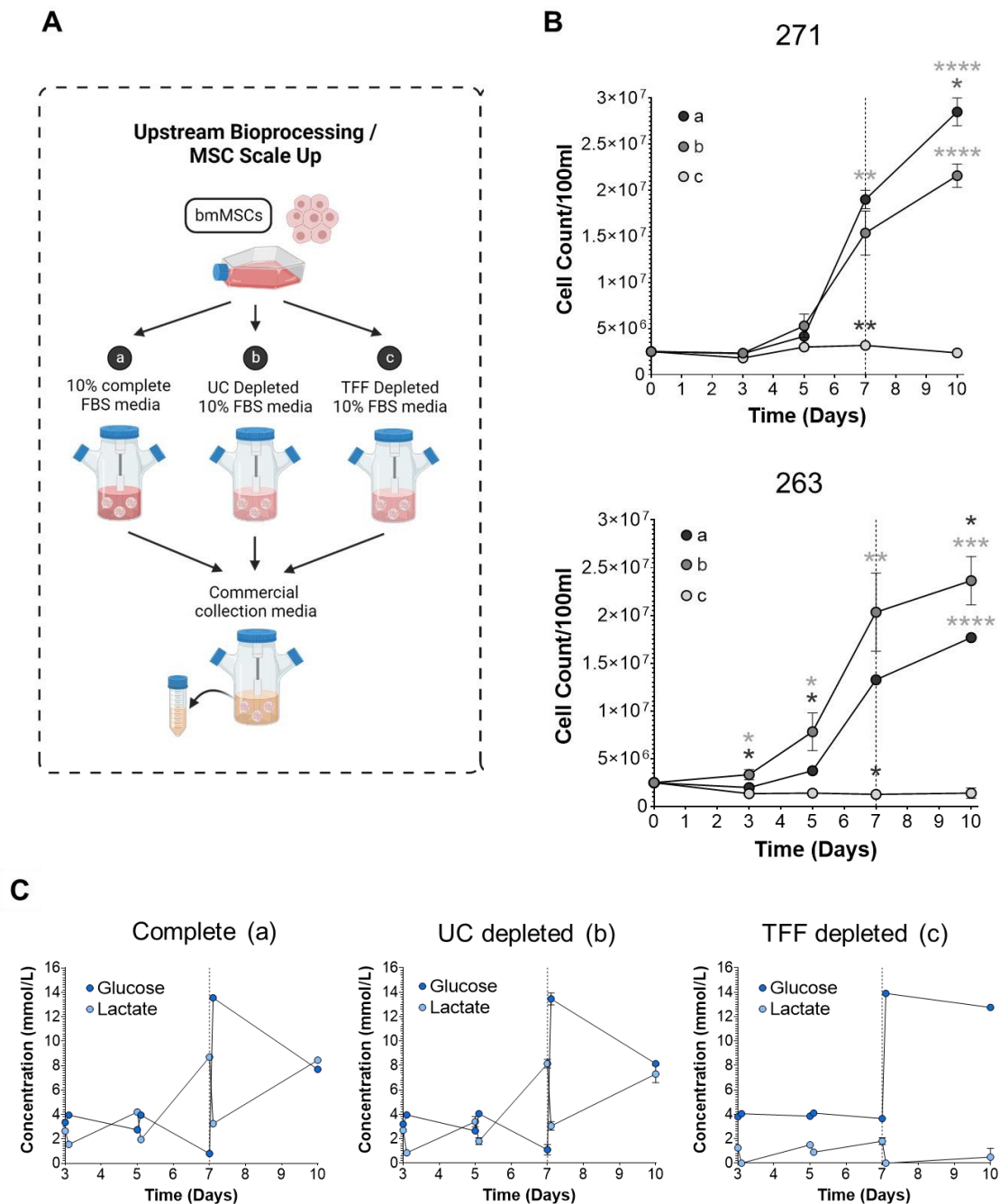


Figure 9: MSC expansion in SFs under three different conditions used for EV collection. Graphic A describes the growth medias as; complete 10% FBS media (a), UC depleted FBS

media (b) and TFF depleted FBS media (c), all with a switch to Rooster collect (RC) collection media at day 7. Graphs B both assess the effects of growth media protocols a, b and c on MSC line 263 and 271 expansion. Whilst MSC line 263 Glucose and lactate measurements across the culture timeline for all conditions are illustrated in graphs C. Graphs mean values and SEM in B were plotted from 3 technical repeats of 3 independent SF runs (n=3). Whereas graph C (a,b and c) display 3 technical repeats and SEM of glucose and lactate measurements from 1 independent SF run (n=1).

As described in fig9A, a UC depleted FBS (b) was added to culture media at 10% alongside a TFF depleted FBS (c) at 10% and compared to an complete 10% FBS culture media (CM). MSCs were cultured under these conditions for 7 days before switching to Rooster Collection media (RC), which is XF and so also suitable for EV harvest. Fig9B show how both 271 and 263 MSCs exhibited an increase in cell count over time with both media (a) and (b), whilst there appeared to be a consistent plateau in cell count and so no growth with media (c). Specifically media (b), which is advantageous to EV collection, depicts a significant difference to media (c) equal to that of established CM (a) at time points day 7 (a and b: $p < 0$) and 10 (a and b: $p < 0.0001$) for cell line 271. Similarly, EV collection media (b) appears to out perform (a) for MSC expansion with significant difference to media (a) and (c) on day 3 ($p < 0.05$), 5 ($p < 0.05$) and 10 (a: $p < 0.05$ and c: $p < 0.001$). Alongside cell counts, Glucose and Lactate measurements identified that whilst Glucose concentrations fell and lactate rose greatly following each media changes with (a) and (b), media (c) evoked barely any variation in Glucose and Lactate levels (fig9C).

UC depleted FBS has the highest particle concentration of all EV collection medias but of these only ~5% on average are lipid (EV) particles.

Determining the biological contents of the collection medias allowed us to ascertain the success of the lipid (EV) particle depletion process and also the composition of the RC commercial collection media. Henceforth, samples of the collection medias, RC, UC FBS and TFF FBS were analysed by NanoFCM both unstained and lipid stained for nanoparticle size and concentration.

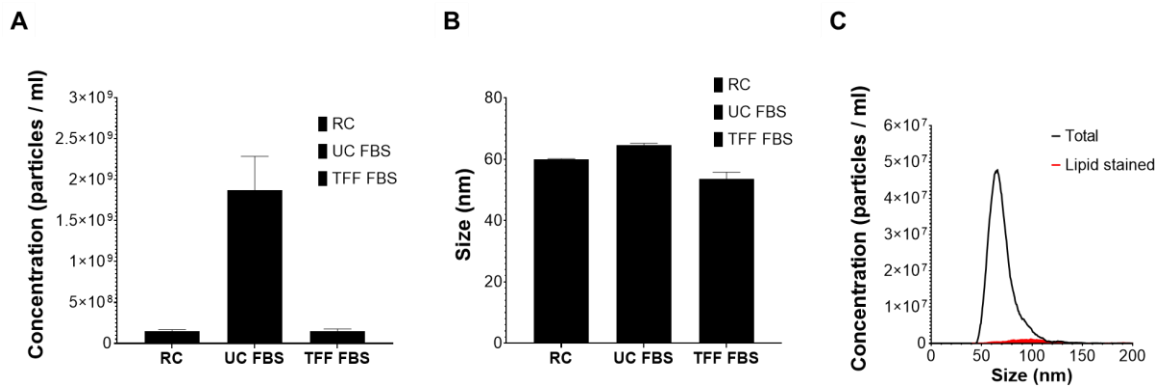


Figure 10: RC, UC depleted and TFF depleted nanoparticle compositions as assessed by NanoFCM. At least 2 batches of each media were sampled and analysed for concentration (A) and median size (B) and both mean and SEM values plotted (n=2). 3 batches of UC FBS were sampled and Memglow 488 lipid stained particles size distribution measured, with mean values plotted in (C) (n=3).

Initially, fig10A illustrated that UC FBS contained a much greater concentration of nanoparticles than both RC and TFF FBS. However, when Memglow 488 lipid stained vesicles from 3 batches of UC FBS were measured in fig10C, it was apparent that on average only 4.9% were lipid stained. In regards to size, all three media times contained similar sized particles also of a mean of ~55-65nm (fig10B).

Complete media (a) and UC depleted media (b) illustrate MC-MSC aggregate formation across the culture timeline, whereas TFF depleted media (c) does not.

MSC-MC samples were taken from SFs prior to each media change and visualised for MC numbers, MSC adherence, formation of aggregates with bridging MSCs, MC clumps (any macroscopically visible formations) and floating debris etc. This allowed us to check the status of the suspension culture and reinforce cell counts previously measured on the nucleocounter.

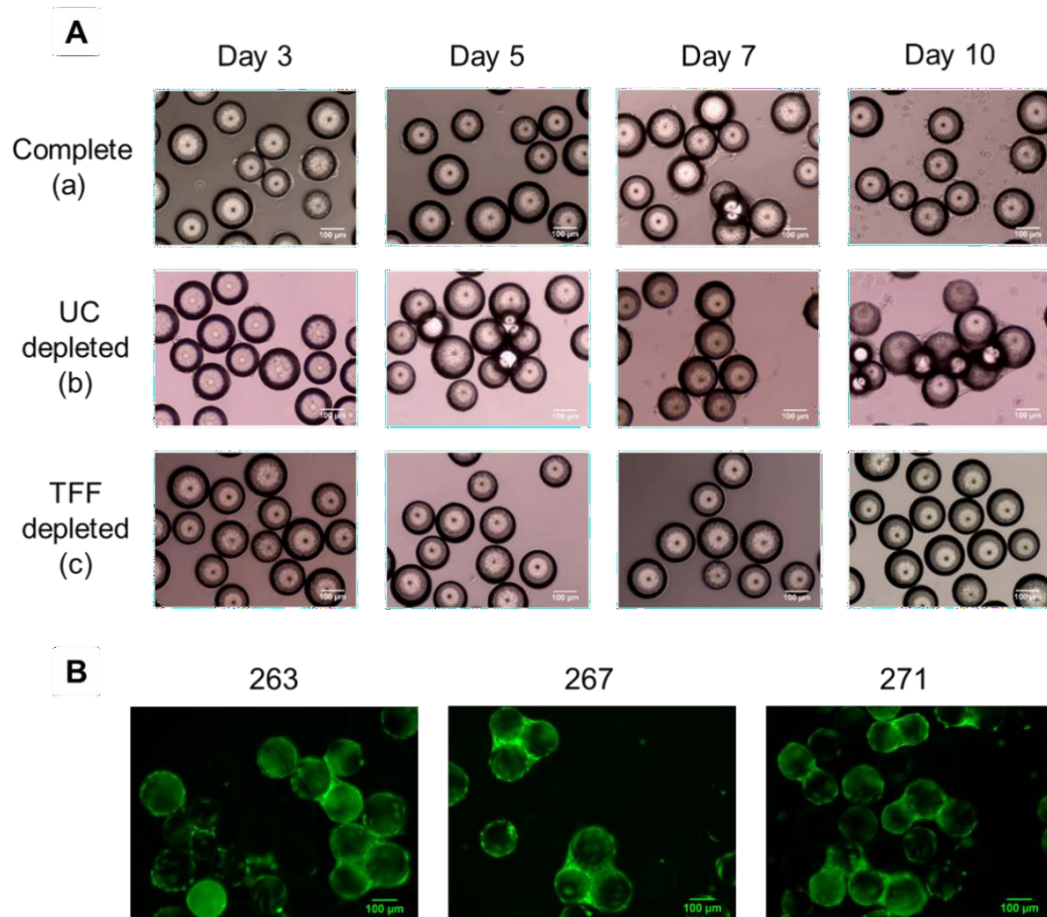


Figure 11: Images of 263 MSCs bridging across MCs and forming MC aggregates across the culture timeline. EVOS Light microscopy images of bioreactor samples of 3 media compositions, as well as Live stained (Calcein AM) samples on harvest day 10 from 3 cell lines run using method (b).

By day 7 both media (a) and (b) show considerable aggregate formations varying in size of 3-5 MCs, whilst media (c) revealed no MC aggregates across all days of the culture timeline (fig11A). By day 10 of culture, although there are still areas of MSC-MC aggregation, there appears to be a large amount of floating cells in culture media (a), with some also present in (b). Fig 11B demonstrates live cell (Calcein AM green fluorescence) bridging across MCs at day 10 for samples taken from media protocol (b) and how MSCs within aggregates, with reduced exposure to media components, continue to show signs of permeability and metabolism as a result of the presence of esterases.

SF harvested MSC cell lines 263, 267 and 271 depict a biomarker profile characteristic of their stemness.

MSC cell lines were harvested from SFs on day 10 and seeded in plates for antibody staining and following this run on the flow cytometer. This was in order to measure expression post SF of MSC markers defined by the ISCT.

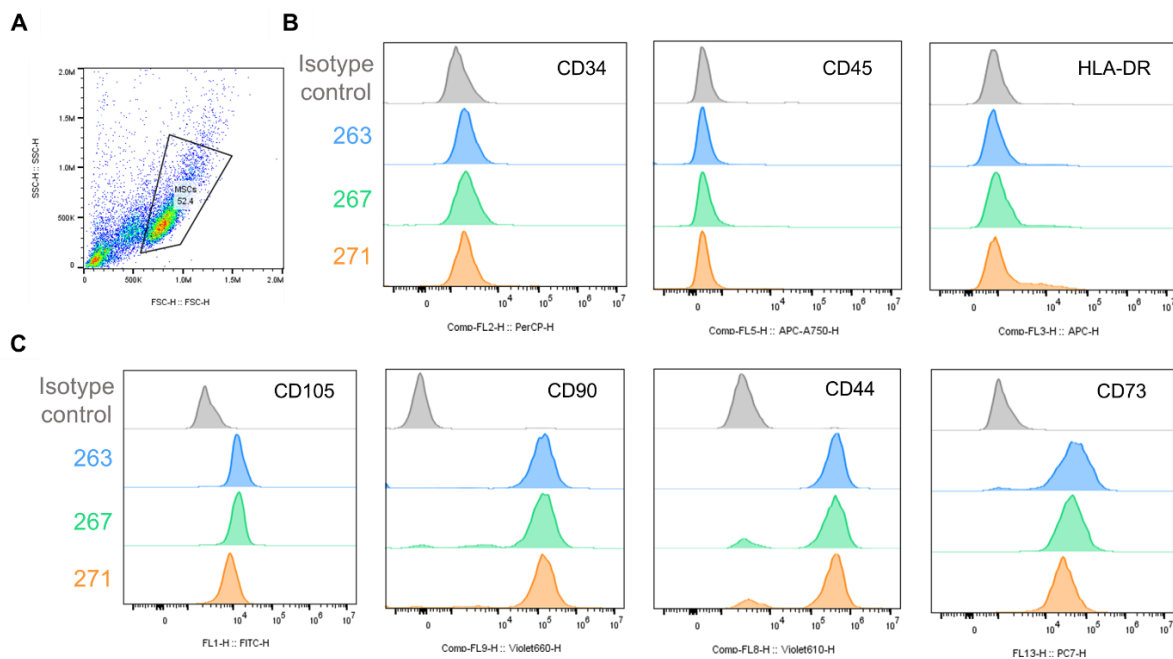


Figure 12: Full characterisation of bmMSCs from harvested SFs. Histograms illustrate Flow Cytometry staining for 4 positive bmMSC markers (CD105, CD44, CD73 and CD90) (C) as well as negative markers (CD34, CD45 and HLA-DR) (B). To determine expression against the isotype control, donors 263, 267 and 271 were gated as shown in A.

Once analysed, MSCs were gated for the larger population (as shown in fig12A) and from this MSCs were defined as negative or positive dependent on how they compared to the negative isotype control. Histograms shifted right from the negative control (fig12C) depict positivity for CD105, CD90, CD44 and CD73. However, a small population of the cells appear to be unstained and fall into the negative region. Upon quantification, this was shown to be most prominent for CD105, with % positivity below 95% in all cell lines, 73% being the lowest. For CD90 the highest population which falls into the negative region was in cell line 267 (4.4%) and for CD73 it was in cell line 263 (7.2%). This means that all cell lines show ISCT defined positivity for CD90, whereas all lines excluding 263 are positive for CD73 and no lines were ISCT positive for CD105. The same cells reveal undisputed negativity for biomarkers CD34, CD45 and HLA-DR in fig 12B.

MSCs exhibited a significant difference in proliferative index compared to a stimulated positive control and thus evidenced an ability to suppress T lymphocytes

Lymphocytes from PBMCs were either intentionally unstimulated (-ve control), stimulated using of PHA and IL-2 , (+ve control) or cultured in the presence of MSCs to determine the immunosuppressive potential of MSCs post SF harvest.

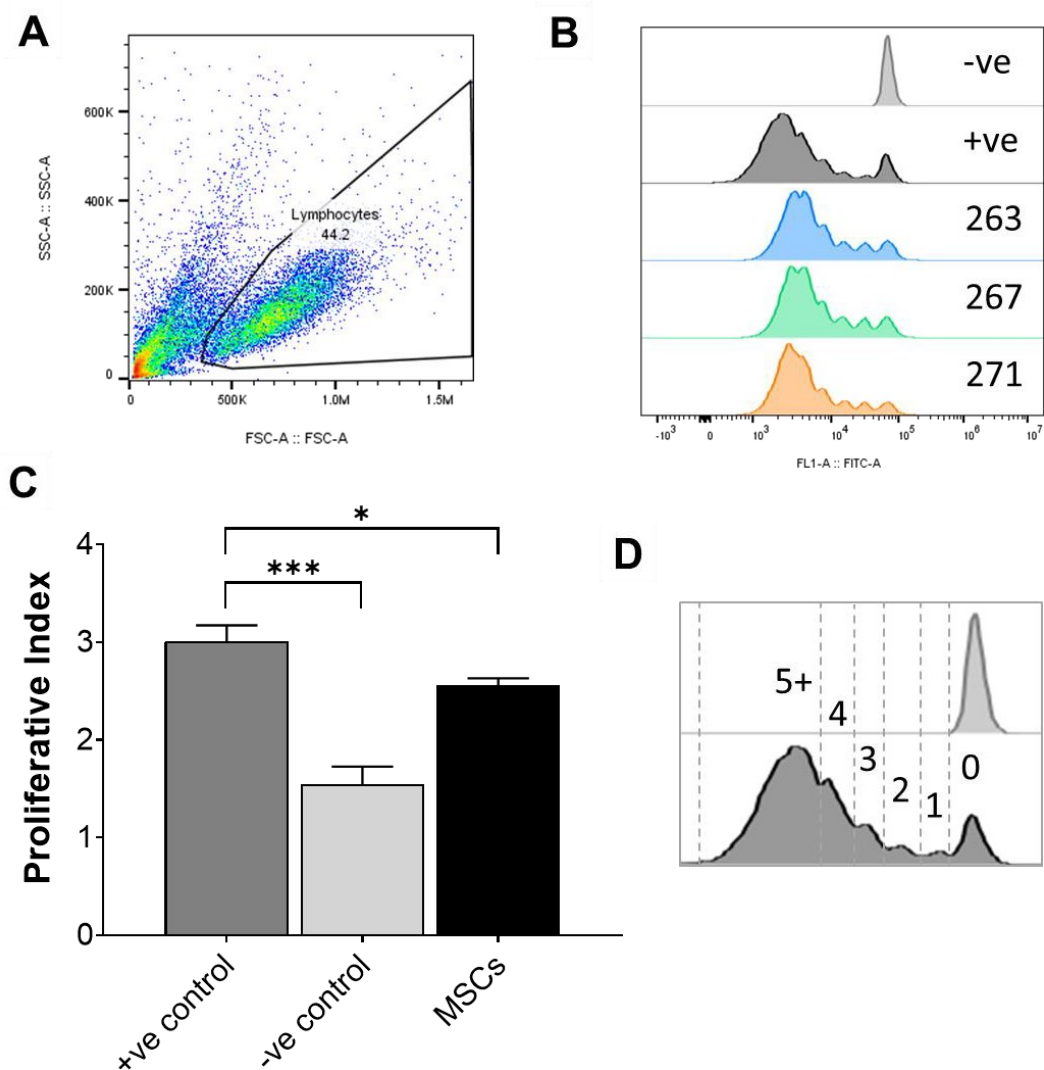


Figure 13: PBMC assay of MSCs post SF. MSCs and lymphocytes were cultured for 5 days and proliferation index quantified using cell divisions, annotated in (D) from gated lymphocytes (A). This was applied to MSC cell lines 263, 267 and 271 (B), following their harvest from agitated culture. Graph C represents the mean and SEM values for 263, 267 and 271 results combined and statistical analysis was performed using an unpaired T test (n=3).

From the CFSE (FITC) stained gated lymphocytes (fig13A), divisions were plotted (fig13B) and cells/division quantified. Applying these values, cells in division, division index and then proliferation index was calculated for each cell line as annotated in fig13D. From the data the -ve unstimulated control demonstrated the most significant difference in lymphocyte proliferation to the stimulated lymphocytes (+ve). Likewise, MSCs 263, 267 and 271 when cultured with PBMCs also demonstrate a significant difference ($p < 0.05$) in lymphocyte proliferative index compared to stimulated lymphocytes, cultured with PHA and IL-2 (fig13C).

MSCs were able to form colonies post SF harvest.

The three MSC cell lines 263, 267 and 271, which had been expanded in SFs for 10 days, were harvested and seeded in T25 planar flasks at low cell densities of 100-200 cells/25cm² for 14 days until they formed distinct colonies. These were stained with crystal violet (A) and imaged microscopically to highlight the colony forming unit capacities of MSCs grown on MCs in agitated conditions.

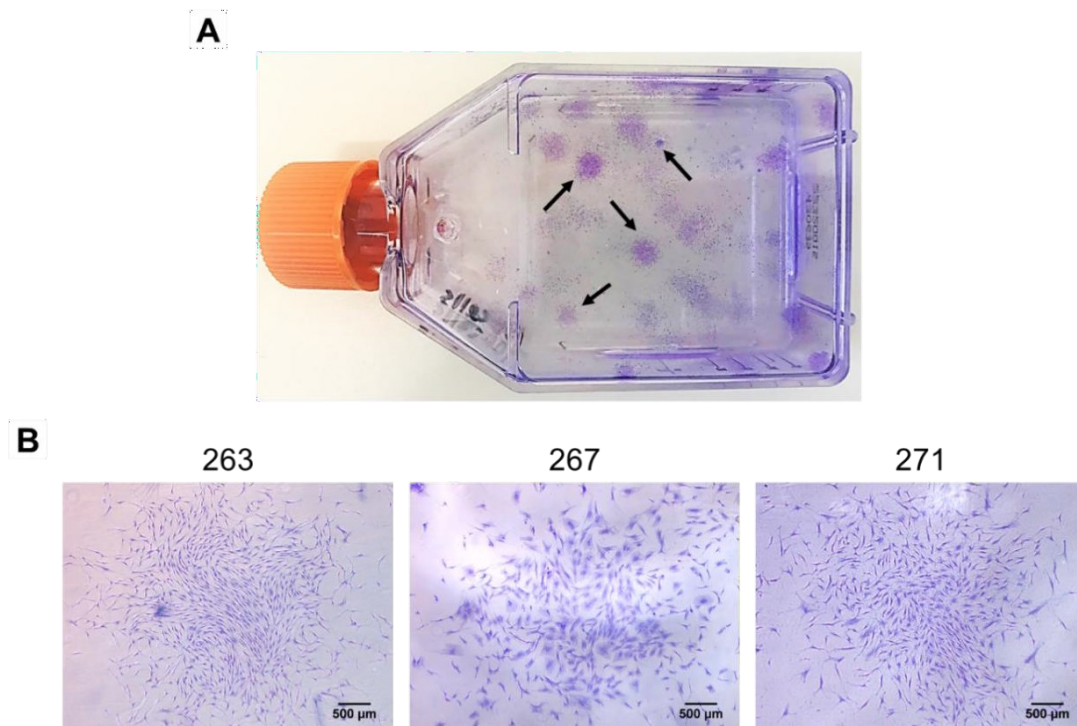


Figure 14: Post harvest 263, 267 and 271 MSCs colony forming units stained with Crystal Violet. Three cell lines cultures using media protocol (b) were seeded for colony forming unit assays post SF run and stained with crystal violet as shown macroscopically in A and microscopically in B.

Macroscopically, segregated colonies of all different sizes and densities are pinpointed by arrows in fig14A. Close up microscopic images taken at 4x objective identify colonies which are centrally dense and sparser at the edges, fixed before colonies merge but once they are have formed recognisable aggregated, circular collectives of cells (fig14B).

MSCs maintained their trilineage differentiation potential following harvesting from SFs.

Following SF harvest, MSCs of three different cell lines (263, 267 and 271) were differentiated down three different lineages into; adipogenic tissue, osteogenic tissue and chondrogenic tissues to demonstrate they retained their differentiation potential.

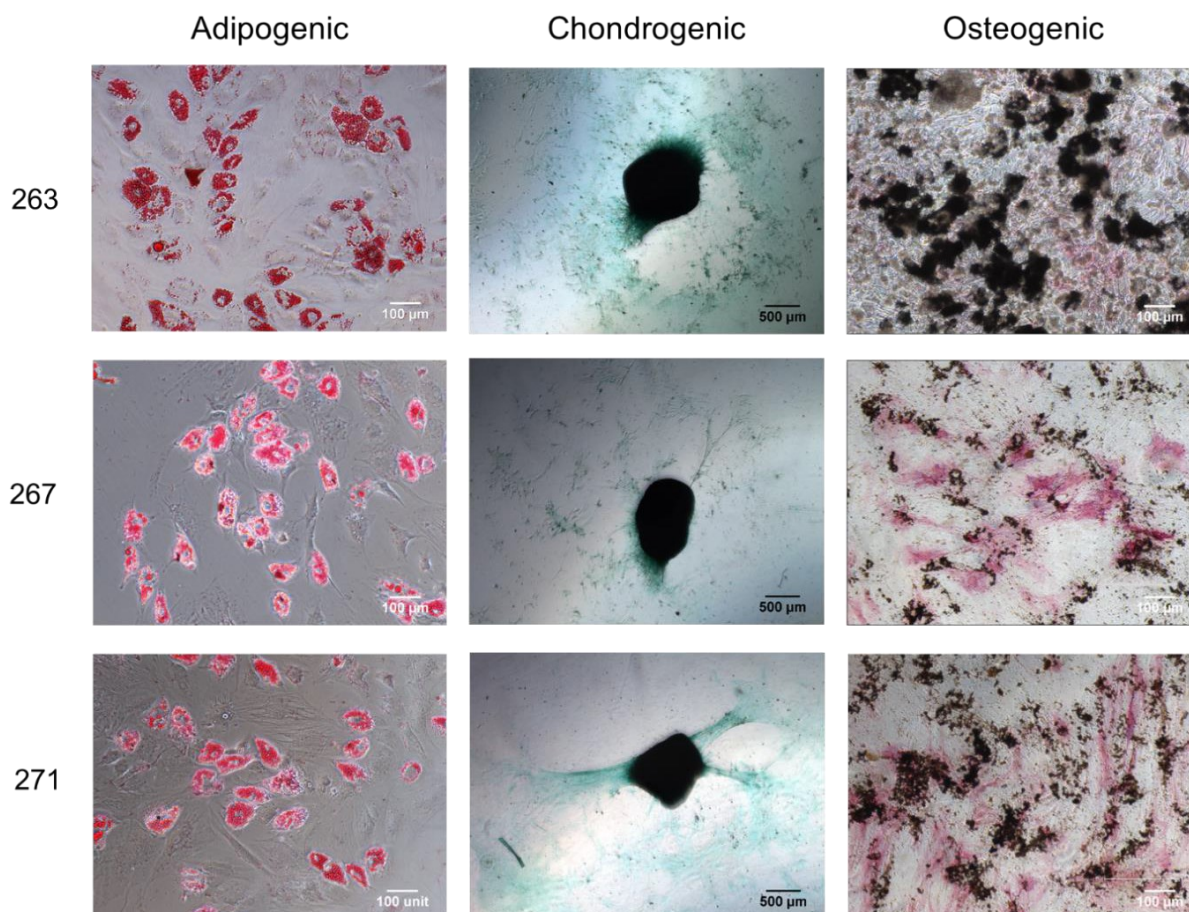


Figure 15: Trilineage differentiation potential of MSC cell lines 263, 267 and 271 from the optimal SF EV collection protocol (b). 10x, 4x and 10x objective images show respectively how once harvested, MSCs were able to be differentiated down three lineages: Adipogenic, Chondrogenic and Osteogenic.

Fig 15 10x Images of mature Adipocytes shows cells stained with Oil Red O to highlight accumulation of lipid vesicles within their fat reservoir, whilst the same batches of MSCs formed Von Kossa Fast Violet B stained Alkaline Phosphatase and silver nitrate stained brown or black staining of mineralisation structures, stereotypical of osteogenesis. Fig 15 4x objective snapshots illustrate MSCs which have formed chondrocyte micromasses stained with alcian blue for glycosaminoglycan deposition.

TFF Filtrate contains trace numbers of EV size particles but does contain protein.

Subsequent to harvesting and characterising MSCs from SF culture, the EV rich secretome was initially concentrated and purified by TFF in preparation for storage prior to characterisation and functional studies.

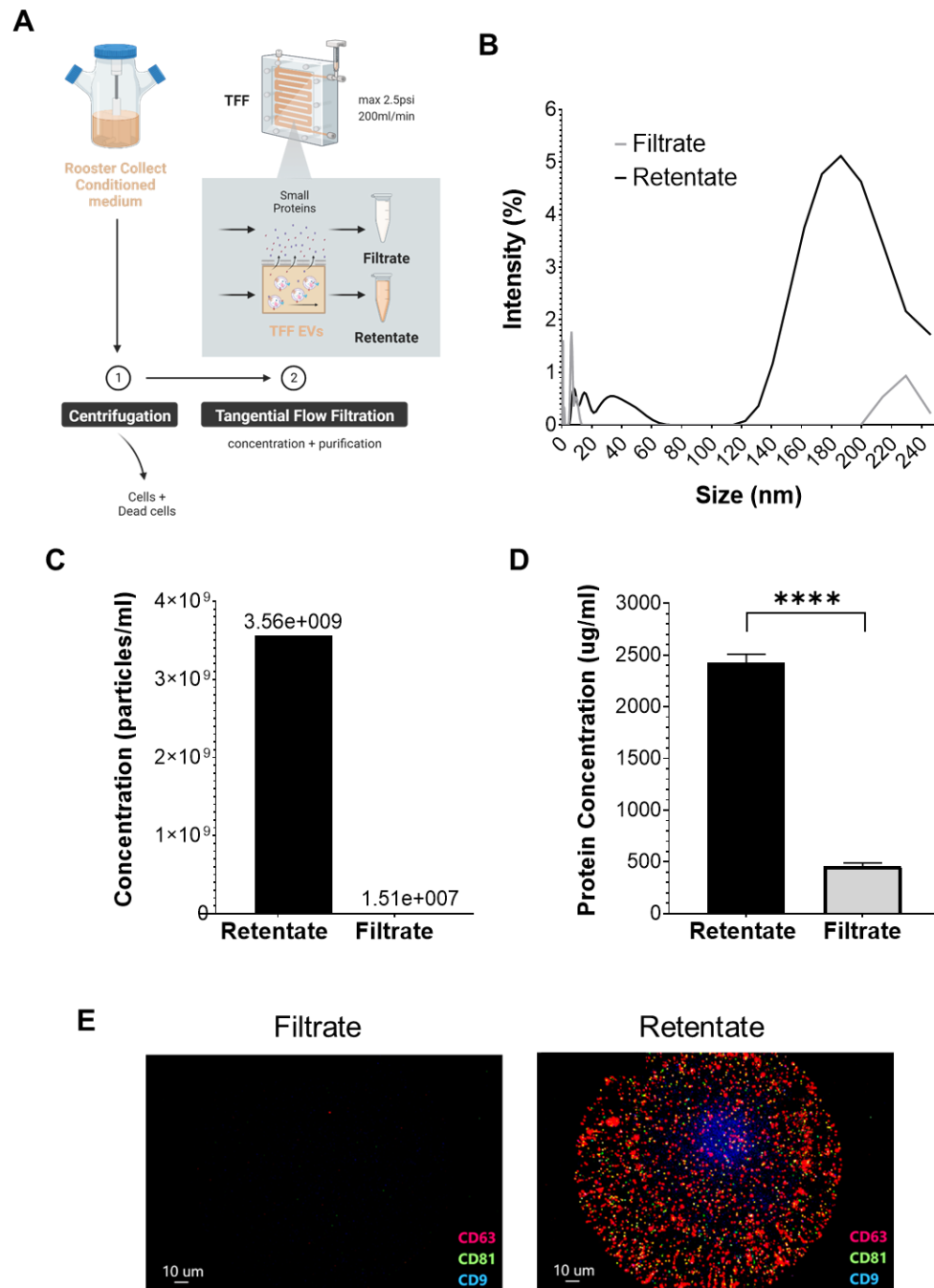


Figure 16: EV concentration and purification from SF media via Tangential Flow Filtration (TFF). Graphic A describes the initial protocol used to isolate EVs (retentate >100kDs) from the other media components (filtrate <100kDa). The difference in the size distribution (DLS

measurement) and particle concentration (NanoFCM measurement) of the filtrate and retentate is shown in graphs B and C respectively. Images E depicts the difference in filtrate and retentate samples visually by ExoView spot CD63 binding and Graph D shows the difference in protein concentration assessed using a BCA assay. Graph D is plotted mean and SEM data from 3 independent batch repeats (n=3). Statistical analysis on this data was performed using an unpaired T test (n=3).

The method used for EV secretome purification and concentration, which included an initial centrifugation step and secondary TFF filtration, is outlined in fig16A. Fig16C demonstrates the contrast between TFF retentate and filtrate particles/ml, with retentate containing 235x greater concentration particles, as also alluded to in DLS graph fig16B, where filtrate's greatest particle size peak is at ~10nm. This can be seen visually by the images of samples bound to a CD63 ExoView spot, of which the filtrate shows negligible binding to tetraspanins or fluorescence from the secondary antibody. Finally, fig16E measured the difference in protein concentration between TFF Retentate and Filtrate, depicting the presence of ~2500µg/ml protein (retentate) and ~500µg/ml (filtrate), closer to a 5x difference.

4.4 Discussion

Initial screening studies of MCs in 2D planar culture were useful to speed up the process of MC shortlisting for SF studies. The MTT viable cell count assay was applied as a classic method for determining cell growth on MCs, whilst background % and aggregation quantification was a unique method performed alongside this to ascertain if results were comparable. The values for background % and aggregation were highly variable and all MCs showed a degree of aggregation that did not necessarily reflect the MTT absorbance readings at day 7 (e.g. collagen and FACT-3 low aggregation but high MTT live cell viability) (fig7A and C). Hence, it was concluded that another purely quantitative method would be more useful for screening studies (e.g. cell counts over time/metabolic measurements). Additionally, the findings from MC planar screening studies did not reflect that seen in suspension for plastic and plastic plus. There was no significant difference in MC aggregation at all time points in 2D and live cell absorbance on day 7 for plastic and plastic plus MCs (fig7A and C), whereas there was a recognisable significant difference between their ability to facilitate MSC expansion at all time points in SFs (fig8C). This lack of correlation suggests that it is necessary to reassess the ability of selected MCs to support MSC cell culture in agitated, 3D conditions. However, proliferation of MSCs following attachment to MCs was comparable to that seen during regular 2D expansion and so their performance was adequate for bioprocessing studies

and MSC scale up [7] (fig8C). In addition, Plastic/Polystyrene based MCs appeared to be generally popular amongst other academic groups for application in bioreactors, as well as being affordable and adaptable (with surface coatings) if necessary [204, 246, 247]. The ability of cells to expand on MCs was mainly assessed by nucleocounter cell counts and confirmed by microscopy imaging of samples. However, from these images MC aggregate calculations proved a convenient and novel way to predict differences in MSC expansion on MCs (fig8E). This was shown by the resemblance in MC aggregate number and significant difference between 24hr with plastic MCs and both 24hr hold time with PP MCs ($p < 0.0001$) and 4hr hold time with plastic MCs ($p < 0.0001$) (fig8E).

Whilst MSCs have some preference to MCs in SFs, it is well documented that an initial lag phase in MSC proliferation can occur as cells undergo attachment to MCs [214, 218-220]. To increase attachment post MSC inoculation, bioprocessing experiments identified a 24hr hold time as the optimum for reducing the lag time and significantly increasing MSC count by day 7 and 10 (fig8B). Although some study findings aligned with ours, a variety of hold periods and slow stirring attachment phases were employed in several research papers, as listed in a review article by Tsai et al [248]. For example, there are some groups whose results contradict those in this project, even though the majority of the bioreactor setup was comparable [221]. This implies that there is no defined 'optimal' strategy for cell culture in agitated bioreactor environments as many groups adopted their own protocol which balanced promoting proliferation and avoiding large aggregate formations [235]. Again, this makes the consideration of hold times imperative to the growth of MSCs on MCs in Bioreactors, and something that must be re-evaluated with every substantial change in protocol.

Following the optimisation of SF agitation protocol, the next step was to consider the extraction of secretome and EVs from the MSC culture media. One issue that scientists face when culturing MSCs for EV production is maintaining cells in media free of extraneous, FBS derived, vesicular structures, which could contaminate the MSC-EV population. From the documented alternatives to complete FBS rich media, we decided to deplete our FBS of vesicles using 2 methods, TFF and UC. Of these, 263 and 271 MSCs grown in UC media illustrated comparable cell yields to CM at day 3, 5, 7 and 10, making it a feasible alternative to CM in terms of encouraging MSC attachment, proliferation and metabolism (fig 9B and C). This suggests that UC depleted media, unlike TFF depleted media, contains enough proteins/factors to allow MSCs to grow and thrive. The particle contents of UC depleted and TFF depleted media were assessed to confirm the levels of proteins/lipids by nanoFCM as shown in figure 10A. Figure 10C most importantly confirmed that on average only 4.9% of nanoparticles were lipid stained in UC depleted FBS and so this indicates that the medium was in fact protein rich and thus able to meet the metabolic demands of MSCs in culture whilst

being 'EV free'. Lipid particle depleted UC media is also advantageous in that it permits the collection of MSC secretome across the culture timeline without effecting scalability. This allows the performance of investigations into the change in the EV profile as MSCs adapt to suspension culture and multiply under the stress of agitated conditions over time, which is something other research groups have failed to investigate and thus comprises a large gap in the literature [238, 249, 250].

In terms of the proficiency of RC to sustain the MSCs, it appears that the rate of expansion slows upon it's addition at day 7 (fig9B), as well as causing cells to detach from MCs and MC aggregates to separate (fig11A). This is most likely a result of the XF, highly pure nature of the media, which was shown in figure 10A from the trace amounts of particles at the lower detection level of the NanoFCM detected in both RC media and TFF depleted FBS. Attention should be drawn to the drawbacks of a complete absence of animal (including human) derived components in media, as these protein and lipid based molecules are key to assisting MSC adhesion and proliferation on MCs [88]. In addition to the detachment of MSCs from MCs implying the cells were under considerable levels of stress, it also highlights the effects this would have on day 10 MSC-EVs cargo and protein profile, as well as the quantities of sEVs secreted by MSCs. In order to overcome these issues with cell detachment, Rafiq et al alluded to the possibility of coating MCs with an attachment substrate when applying serum-free/depleted or XF media [76].

As there is potential for the stress of the SF environment to also effect MSC phenotype, it was important to characterise cells after harvesting to ensure they had retained their stemness and multipotency. Figures 12, 13, 14 and 15 described how live MSCs showed a traditional profile of negativity (CD45, CD34, and HLA-DR) and general positivity (CD105, CD44, CD73 and CD90), potency for Adipogenesis, Osteogenesis and Chondrogenesis as well as an ability to form colonies. The presence of a negative population in a rare case for CD73, which resulted in positivity falling outside the 95% cut off, does however mean cell line 263 cannot technically be defined as MSCs with full potency for CD73 under ISCT guidelines. Additionally, although expression of CD105 was considerably weaker than other positive MSC markers and overlapped with the negative control, this had been shown to occur in other Bioreactor and SF studies, dropping to below 95% and as low as 88% in one [246]. The overall academic opinion on this was that this could be a result of damage to/removal of these markers under agitation shear stress or during enzymatic detachment of MSCs from MCs. Thus in order to confirm this further investigation was necessary by characterising MSCs pre-inoculation in suspension culture and characterising MSCs throughout the culture whilst attached to MCs. Future studies will focus on maintaining the potency of MSCs in bioreactors for all cell lines, in order to demonstrate that MSCs can maintain their stemness in agitated suspension culture. Fig13C

also highlighted the immunosuppressive capacity of SF derived MSCs by the significant difference in T cell proliferation capacity upon co-culture in comparison to stimulated T cells. Maintenance of these characteristics was in accordance with the ISCT guidelines and illustrated that bioreactors can promote scalable cell proliferation and expansion, without forcing differentiation or causing loss of recognized properties, which make them preferential therapeutically e.g. immunosuppressive capabilities.

Finally, in order to retain the concentration of our final product (the retrieved EVs), a scalable downstream purification and isolation protocol was implemented. As alluded to earlier, TFF has been shown by many researchers to provide a convenient and scalable platform for concentrating and purifying EVs, without resulting in damage to or loss of sEVs [251]. Results of figure 16 demonstrate that the TFF filtered out negligible nanoparticles within the EV size fraction (fig16B and C) but was able to filter out some protein (fig16D). This made it valuable for the concentration of sEVs for storage, whilst sustaining yield (fig16E), but left scope to further purify the TFF-EVs of any excess protein. Hence, application of a TFF with a larger size filter of 300-500kDa may show greater depletion of small proteins contaminants and thus provide us with a purer sample. These size filters have proven effectiveness for concentrating and purifying EVs as shown by various research groups [183, 252, 253].

In addition, there is also the option of applying multiple isolation methods, as has recently become popular, and so employing widely used SEC to purify the TFF-EVs and isolate only the sEV fraction for functional and characterisation studies. This will be explored in chapter 5.

Chapter 5: Analysis of MSC-EVs from optimised SF bioprocess

5.1 Introduction

Ensuing the success of the optimised SF platform for MSC expansion in chapter 4, its affects on MSC-EV secretome was assessed in this chapter. This included the influence on sEV biomarkers, protein profile, size and numbers. In addition, at the end of chapter 5, the sEVs from this process which have been further isolated by SEC will also be characterised, prior to their application in functional studies (chapter 6).

5.1.1 sEV isolation

From the table of isolation techniques described in chapter 1, SEC, microfluidics and immunocapture produce an end product with high purity but can only process at small volumes. Hence, they complement an initial technique suitable for working at scale. As extensive research has shown SEC, when combined with precipitation, has excellent reproducibility of purified sEVs free of protein contaminants, this procedure was adopted [254-257]. Although SEC, in all its commercial and personalised variations, is now one of the most commonly adopted platforms, it was nevertheless important to assess the affects of this technique on EV physical characteristics [11, 258].

5.1.2 EV characterisation

5.1.2.1 MISEV characterisation guidelines

Subsequent to optimisation of MSC bioprocessing and EV purification, as mentioned previously in chapter 4, it is crucial to perform full characterisation of the nanoparticle population, as well as illustrating how both the upstream and downstream bioprocessing affects the secretome composition. To characterise MSC-sEVs from MSC-secretome, the ISEV guidelines defines criteria [190] which includes:

- A minimum of three positive protein markers of EVs, aiming for at least one lipid-bound/transmembrane protein and one cytosolic protein.
- At least one negative control protein marker.

- Two unique but complementary single particle analysis techniques to assess EV size, morphology, homogeneity, number etc.
- One microscopic image of EVs.

These principles have been endorsed by 97% of MISEV2018 survey respondents and thus were adopted in this section of the thesis [190]. Applying the official guidelines, the chosen criteria for defining EVs within our purified secretome was as follows:

- Positivity for three surface tetraspanins, commonly expressed by sEVs using ExoLISA and ExoView (CD63, CD81 and CD9).
- Lipid membrane staining of vesicles with Memglow 488.
- Negativity for Mouse IgG (ExoView).
- Single particle analysis using NTA and NanoFCM (particle number and size) and TEM (size and morphology). General protein concentration (BCA) and in depth fingerprint protein assessment (Mass Spectrometry).

As much of the specialised software and techniques used to define EVs have been recently developed, both a novel and more classical ‘complementary’ method for characterising our EVs was adopted, as suggested in MISEV 2018 [190]. All characterisation techniques apply their own principle or mechanism and have individual advantages and disadvantages as reviewed in table 8.

Table 8: Review of traditional EV characterisation methods

Technique	Analysis type	Principle/mechanism	Advantages	Disadvantages
Electron Microscopy (EM) [259-261]	Single particle analysis Imaging (size and morphology)	Focused electrons scattered by specimen and detected. SEM detects reflected electrons TEM detects transmitted electrons	Requires small sample High resolution	Expensive Sample prep dehydration process and vacuum causes shrinkage of EVs.
Atomic Force Microscopy (AFM) [175, 262, 263]	Single particle analysis 3D Imaging (size, morphology and topography)	Non-contact force interaction between sample and cantilever tip. Tip movement is calculated using a laser and photon to produce a three-dimensional image.	Requires small sample No prior fixation or staining required. Can coat surface a specialised surface with antibodies for subpopulation biomarker identification.	Sensitive to analysis conditions (temperature, forces, scan speeds etc) which can impede its accuracy.
DLS [264-267]	Particle size distribution and concentration)	Measures real time Brownian motion of suspended particles using lasers and detection of scattered light using a photon detector (whole sample evaluation).	Accessible Simple to use Little sample preparation.	Unreliable for highly polydisperse suspensions as small particles may be obscured by light scattering from larger particles.

<p>Tuneable resistance pulse sensing (TRPS)</p> <p>[265, 268]</p>	<p>Single particle analysis (particle size distribution, concentration and surface charge)</p>	<p>Applying voltage to an electrolyte solution filled reservoir causes an ionic current, which increases the particles electrical resistance and henceforth creates a resistive pulse as they pass through it.</p>	<p>Fast</p> <p>Little sample preparation.</p>	<p>Difficult parameter set up with heterogeneous samples.</p>
<p>NTA</p> <p>[190, 265, 267, 269, 270]</p>	<p>Single analysis particle by particle of many particles simultaneously (particle size distribution and concentration)</p>	<p>Measures real time Brownian motion of suspended particles using lasers and detection of scattered light using a camera (single particle analysis).</p>	<p>Little sample preparation.</p> <p>High specificity when samples are very pure.</p> <p>Fluorescent detection can be performed with antibody conjugation.</p>	<p>High optical background and unreliable for highly polydisperse suspensions as small particles may be obscured by light scattering from larger particles.</p>
<p>Flow Cytometry</p> <p>[190, 267, 270-272]</p>	<p>Single particle analysis (particle size distribution and concentration)</p> <p>Specific molecules analysis (Biomarker characterisation)</p>	<p>Stream of particle suspension passes through a laser and detects both the forward-scattered light (FSC), measuring relative size, and side-scattered light (SSC), measuring granularity.</p>	<p>Accessible</p> <p>High Throughput</p> <p>Fast</p> <p>Requires small sample</p> <p>Measures a multiple parameters, including surface biomarkers by antibody-fluorophore conjugation.</p>	<p>Classic flow cytometers cannot detect sizes <300nm</p> <p>Standard Flow Cytometers also cannot distinguish between single EVs and aggregates.</p>
<p>ELISA</p> <p>[175, 267, 273-275]</p>	<p>Specific molecules analysis (Biomarker characterisation)</p> <p>Protein analysis</p>	<p>EVs are seeded and bind to plates coated in the capture antibody. The addition of a second labelled antibody for the selected antigen of interest can be detected using a fluorescent plate reader.</p>	<p>Quantitative</p> <p>Accessible</p> <p>Well described</p> <p>Fast</p> <p>Requires small sample.</p>	<p>Multistep so can result in user error.</p> <p>Cannot detect heterogeneity in an EV sample.</p>

Bradford or micro-bicinchonic acid (BCA) [190]	Protein analysis (general protein quantification)	Biochemical reaction and colorimetric detection	Simple Fast Accessible Low cost	Samples lacking in purity and containing contaminants could have their protein concentration overestimated.
Western blotting [175, 190, 261]	Protein analysis (general and specific protein quantification)	Protein mixtures are separated based on molecular weight, which represents a specific protein type.	Well described Accessible	Work intensive Requires large sample lysate volumes Time consuming
Mass Spectrometry [190, 259]	Protein analysis (specific protein quantification)	Ionised molecules/atoms are separated by differences in their mass/charge; m/z ratio.	Analysis of thousands of proteins. Extremely high throughput. Highly sensitive	Complicated sample preparation Requires large amounts of sample.

5.1.2.2 Classical and Novel Characterisation Techniques

Reviewing the most universally accepted nanoparticle characterisation techniques, as summarised in table 8, reinforced the importance of employing multiple methods to build a valid and reliable EV profile. Specific methods were then chosen by their contrasting advantages and weaknesses, as well as the potential to access these technologies. Some of the methods adopted were innovative adaptations of the traditional methods previously listed. For example, several solutions have been trialled for heightening the sensitivity of the conventional flow cytometer, including; optimising and enhancing the current system, introducing algorithms which can differentiate individual EVs from aggregates or coupling EVs to micro scale latex beads via specific antibody-antigen interactions [261, 276].

As an alternative to traditional FCM systems, figure 17 includes the novel NanoFCM, which uses a very thin sample stream (1.4µm) and extended dwell time for greater detection by single-photon counting modules to create single nanoparticle analysis platform with enhanced precision and specificity (down to 40µm). In comparison to NTA, the NanoFCM has faster detection speeds, shows greater reproducibility and analysis of data using the built-in software is much simpler. However, the main advantage of NTA is the camera visualization, which both

reinforce the average particle count and heterogeneity measurements, as well as easing the cleaning process, to ensure there is no sample carry-over.

In order to characterise EVs surface biomarkers, we employed an EV specific ELISA (ExoLISA) and the ExoView platform. The ExoView merges both capture antibody immunofluorescent staining with single-particle interferometric reflectance imaging sensor-based analysis (SP-IRIS), as illustrated in figure 17. Each sample is incubated on a chip covered in an array of immobilised antibody probe spots, where the antibody of interest captures specific EV antigens. Following this, the captured EVs are co-localised with fluorochrome-conjugated antibodies and fluorescence detected by reflected intensity for each pixel. A customised algorithm then quantifies the isolated, bound EVs for number, size and surface markers, with no interference from free proteins. Although a highly informative technique, throughput is low and the process is time consuming. Additionally, the technique for drying the chips is fiddly, with high occurrence of user errors, making the chip no longer suitable for analysis and hence expensive (wasted chips).

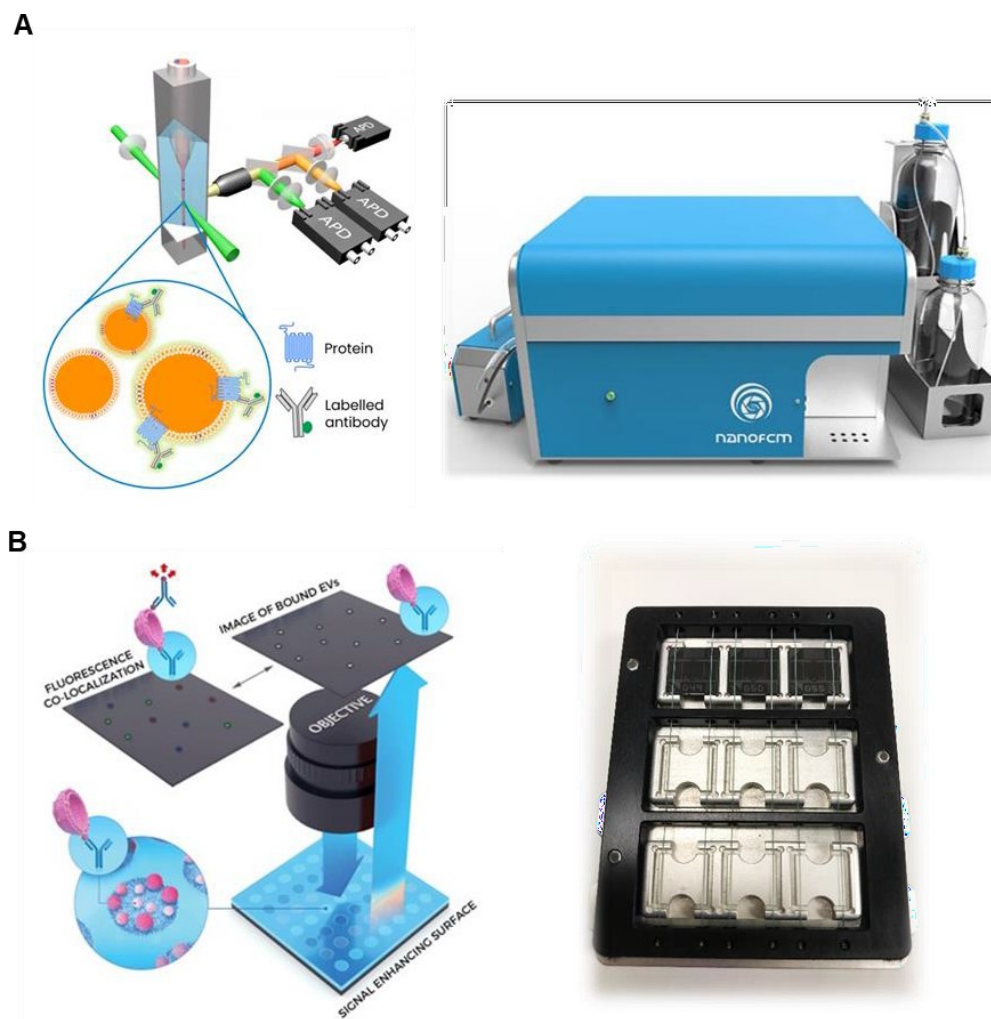


Figure 17: The principle and technologies used by advanced commercial EV characterisation techniques. Images of NanoFCM single particle detection mechanism as well as the instrument (A) and ExoView fluorescent co-localisation method on the chip surface (B).

To reinforce the size measurements and visually show the presence of sEVs, TEM was used as the gold standard method for nanoparticle imaging and to conclude the requirements for MISEV EV characterisation [267].

It was also important that the project investigate the effects of bioprocessing and 3D production of EVs on their proteomic profile, which hence gives a detailed description of their biological fingerprint. To achieve this, digested purified EVs were analysed via Mass Spectrometry against a proteome database to draw relationships between expressed proteins from SF samples and to deduce which functional categories, which they were associated with [261].

5.2 Aims

As well as comparing EV characterisation techniques, MISEV also stresses the importance of analysis standardisation. For instance, it was specified that preparations of EVs should be standardised quantitatively to their secreting parental cells by volume of collected biofluid or number of source cells etc. During this research, reproducibility of EVs from different batches and cell lines was assessed, to determine if variations in characterisation profiles came from bioprocessing and physical culture conditions or parental cells biology. In addition, the effects of isolation method on purified secretome and EV properties was evaluated to reinforce the reasoning behind the application of each process.

Therefore, the aims of this chapter were to:

Characterise EVs and isolated sEVs from optimised SFs across the culture timeline and compare:

1. Batches of EVs from the same cell line.
2. Differences between secreting cell line.
3. Selected methods and techniques for EV analysis.
4. Both isolation methods (TFF vs TFF + SEC).
5. Against EVs collected from planar conditions (2D).

5.3 Results

The consistent increase in cell count across the bioprocess timeline was not mirrored in the particle count.

Commercial rooster 263, 267 and 271 cells were expanded under optimised bioprocessing conditions (as concluded in chapter 4) and total cell counts were performed using the Nucleocounter software on day 3, 5, 7 and 10 of SF 3D culture. Alongside this, particle counts were also performed on TFF purified MSC-EVs which had been collected on timeline matched days. This provided us with a baseline understanding of the relationship between MSC expansion and nanoparticle secretion within agitated suspension culture.

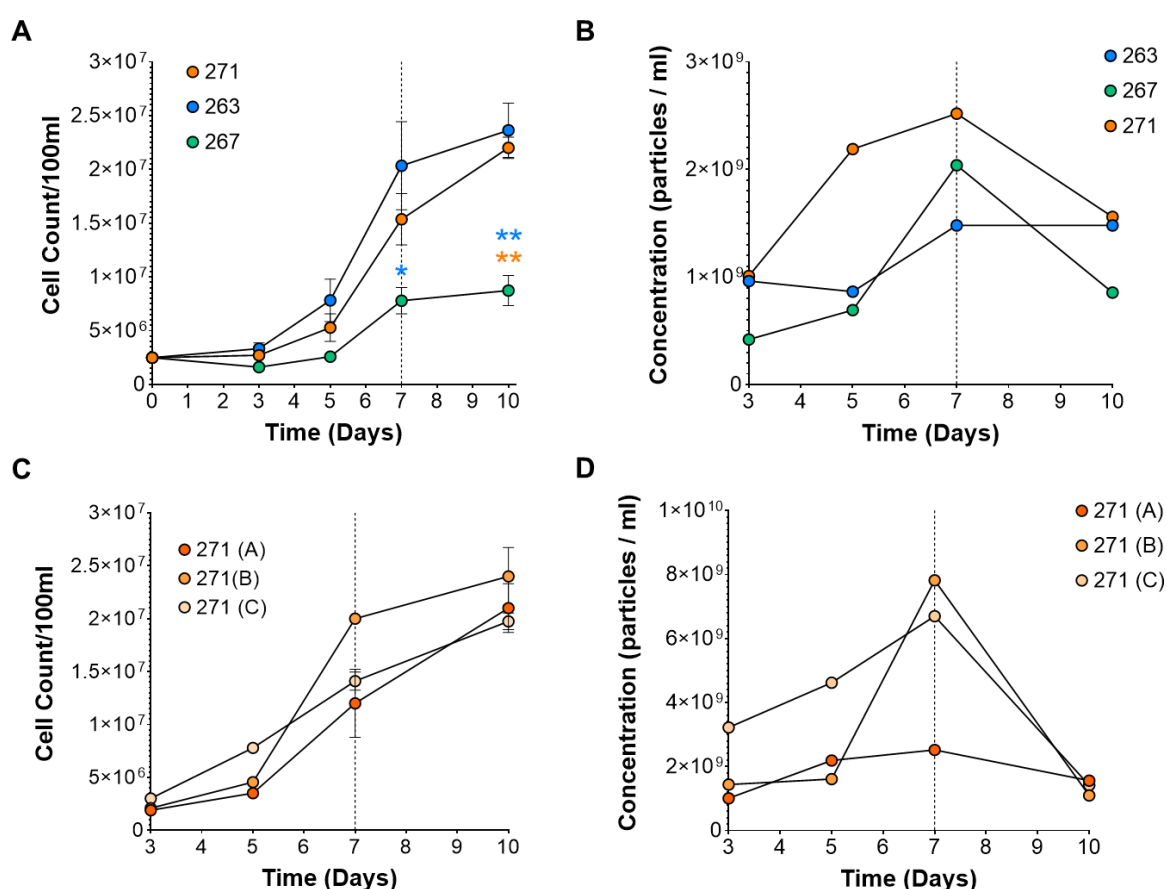


Figure 18: Cell counts and particle concentration across the culture timeline from an optimised SF protocol. Three batch repeats (independent SFs) of three rooster cell lines were expanded in SFs over 7 days in UC media and then RC media for the final 3 days. Graph A shows cell counts of both independent and MSC line repeats (n=3), where graph C illustrates the variability between three batch repeats (independent SFs) for cell line 271 (n=1). Thus, SEM bars in graph C represent three individual cell counts from 3 samples of 1 SF (technical replicates). Particles from these SFs were extracted and TFF purified for NanoFCM

measurements at day 3, 5, 7 and 10. Graph B represents the particle concentrations from 1 independent SF from 3 cell lines (n=1) and 3 independent SFs/batches from 1 cell line, 271 (n=1).

Comparing the growth kinetics, only on cell harvest day (day 10) was there a significant difference in cell number observed between cell line 267 and both 271 ($p < 0.01$) and 263 ($p < 0.01$), as depicted in fig18A. Whereas on day 7 there a significant difference in cell count between 263 and 267 alone ($p < 0.05$). As an example of batch consistency, fig18C shows how there is less variation between batches than cell lines (fig18A), especially at the latter time points of day 7 and 10.

The consistent increase in cell counts over the course of the bioprocessing timeline (fig18A and C) was not reflected in the particle counts. Samples were diluted to within the detectable range of the NanoFCM and the particle population size and concentration were assessed. Although particle concentration rose between day 3 and day 7, this increase fluctuated substantially between the cell lines (fig18B) and between 271 batches (fig18D). In addition to this, following the switch to RC collection media at day 7, by day 10 particle counts had either dropped or plateaued for each cell line and batch run (fig18B and fig18D). To further investigate the cause of this reduction in particles after day 7 when switching to Rooster Collect, we stained the same populations with Memglow 488 and measured particles a second time using the NanoFCM. This fluorogenic plasma membrane probe specifically identifies lipid encapsulated EVs from within the TFF purified secretome, selectively discounting for unstained particles e.g. protein aggregates, collagen fibrils, fibronectin etc.

Concentration of Memglow 488 stained vesicular particles rose across the bioprocess timeline, most rapidly after day 7.

As a strategy for clarifying the results of fig18 and determining if nanoparticles detected from MSC purified secretome were characteristic of EVs, Memglow 488 staining was performed on batch matched samples. This reagent specifically highlighted the presence of lipid rich nanoparticles from background particles within the 40-200nm detection window.

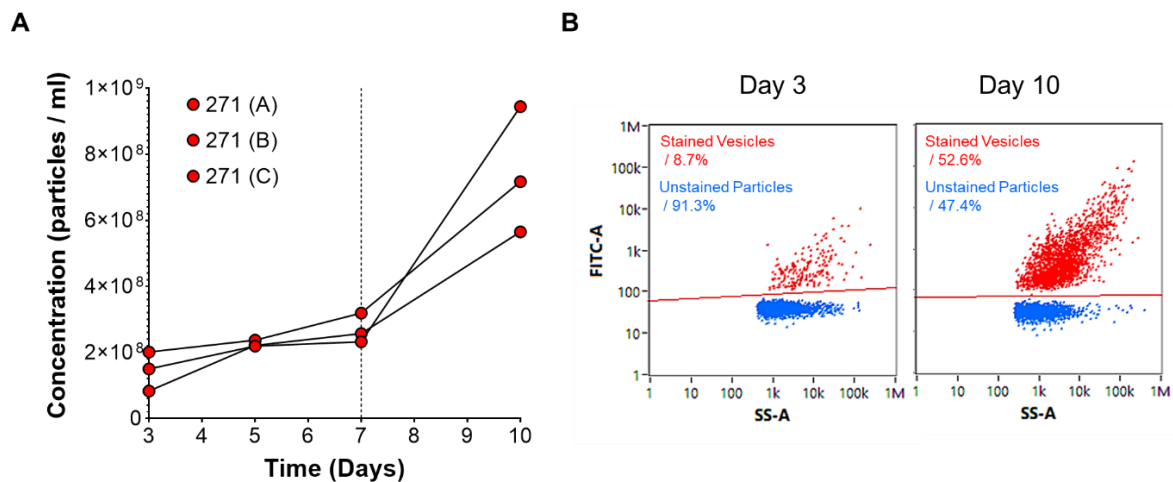


Figure 19: MemGlow 488 stained particle concentration across the SF culture timeline. TFF purified particles from the three 271 SF batches time points were stained with Memglow 488 and their concentration measured on the NanoFCM (A) (n=1). Day 3 and day 10 scatter plots (B) demonstrate the change in ratio of stained Vesicle to unstained Particle.

As portrayed in fig19A, there is a steady increase in stained lipid particle concentration across 271 batches between day 3 and 7, with an extensive jump in particle concentration by day 10. This data are also presented visually by the scatterplots in (fig19B) showing the increase in percentage-stained particles between day 3 and day 10 of culture. 91.3% of particles at day 3 were shown to be unstained and not representative of a vesicle population, whilst at day 10 this fell to 47.4%, suggesting an EV rich secretome at day 10.

There is no difference in median size between EVs which have been collected at time points across the culture period.

Using the NanoFCM particle size distribution datasets, particle median size data were calculated also within the software and plotted to depict particle size consistency over the bioprocess timeline.

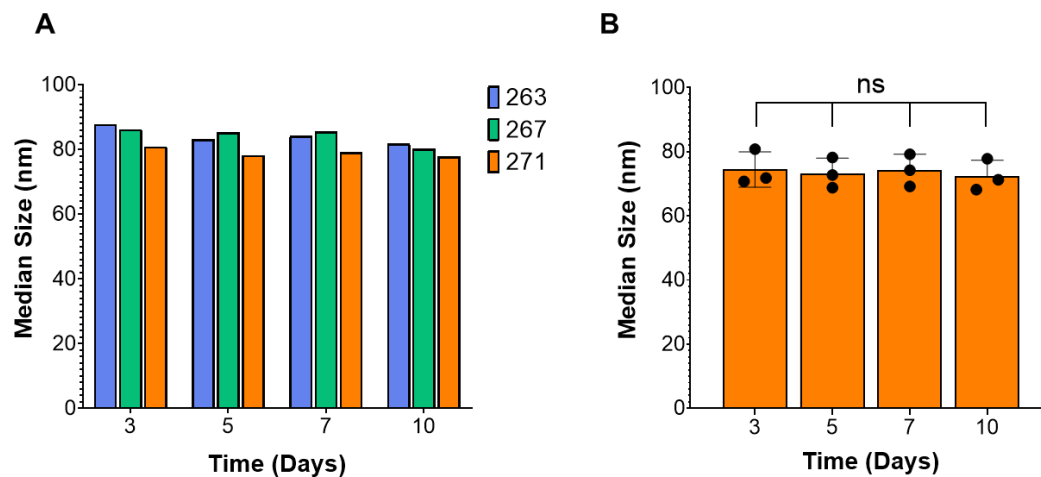


Figure 20: Median size of particles across the SF bioprocess timeline as measured using NanoFCM. Graph A demonstrates three MSC cell lines particle sizes (n=1) whilst B demonstrates the mean and SEM of three combined MSC-particle batches of the same cell line (271) (n=3).

Fig20A indicates that between cell lines 263, 267 and 271 there is very little difference in median size of nanoparticles. Fig20B confirms that within batch runs of cell line 271 there is no significant difference in measured median particle size.

There are some disparities in particle size distributions between EV batches which have been characterised using different methods.

Whilst there is consistency between lipid stained particle concentrations and median particle sizes when measuring using NanoFCM, we wanted to see if the same results could be shown using NTA. As mentioned previously, although both methods are capable of analysing EVs, they apply differing technologies and degrees of specificity towards biological populations. Hence it was critical to us to compare our SF EV rich secretome samples using both techniques, especially to greater understand previous data sets generated by NTA, prior to gaining access to the NanoFCM software.

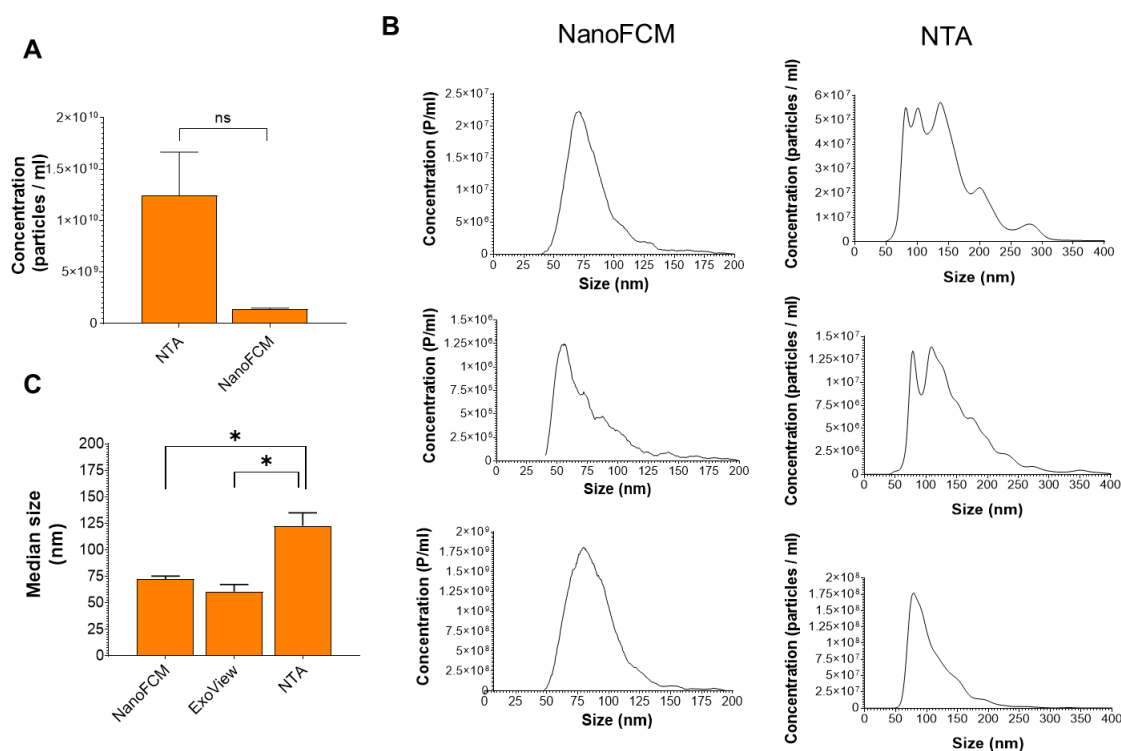


Figure 21: Method comparison for analysis of 271 TFF purified particles harvested from Day 10 of each individual SF batch runs. Graph A depicts the difference in concentration between 3 batches of particles measured by NTA and NanoFCM and statistically analysed using an unpaired T-test ($n=3$), whilst B illustrates the particle size distribution plots for these batches. The average median (D50) size values from these 3 batches were also compared using NTA, NanoFCM and ExoView systems (C) ($n=3$).

Figure 21 acknowledges the disparities between particle analysis of the same samples using either NanoFCM or NTA. Both detect nanoparticles in liquid suspension and plot nanoparticle size distributions, as demonstrated in histograms in fig21B. NanoFCM histograms appear to have a narrower size range (~ 40 - 125 nm) and are mainly single peak, whereas NTA can show as multiple particle population peaks and have wider size distribution (~ 50 - 270 nm). This is quantified in fig21C, where average median size across 3 271 batch repeats is significantly different between NTA and NanoFCM ($p < 0.05$), as well as ExoView software ($p < 0.05$). There is however no significant difference in particle concentration between NanoFCM and NTA (fig21A), where the mean concentration and SEM bar size is much greater using NTA than using NanoFCM.

TEM images show the size and morphology of SF EVs within samples collected at different time points.

MISEV guidelines suggested the production of a physical image of sEVs in order to visibly show the presence of spherical membrane encompassed vesicles alongside the positivity for sEV biomarkers/tetraspanins.

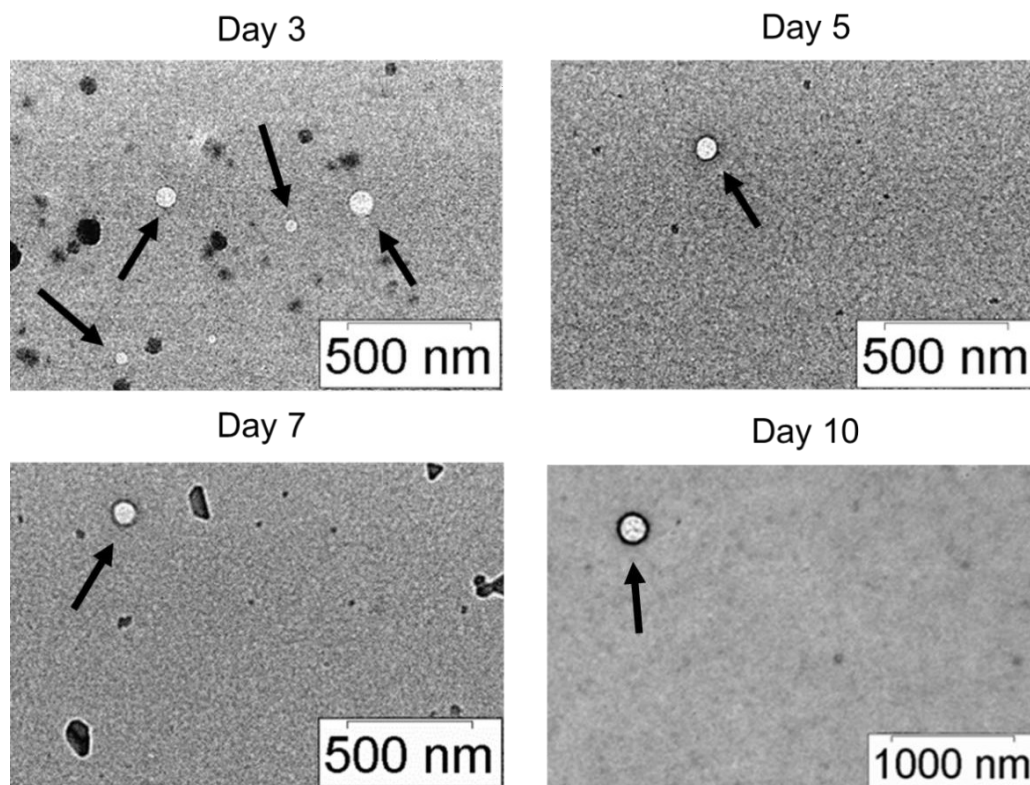


Figure 22: TEM images of 271 TFF secretome purified from SFs on day 3, 5, 7 and 10. Arrows point to vesicle like structures which are representative of the size of small EVs or Exosomes.

TEM snapshot images show that vesicular structures present in purified media samples resemble the size (30-200nm) and shape (spherical) of that expected from Extracellular Vesicles. These can be seen at all sample time points and hence reinforce the particle size data between figure 19-22.

Tetraspanins CD63, CD81 and CD9 are expressed by EVs across the bioprocess timeline, with Exoview data illustrating an increase in all markers over time.

Following the assessment of particles from MSC expansion in SFs, tetraspanin expression specific to sEV particles was performed in order to further characterise the structures. Levels of biomarkers CD9, CD63 and CD81 was determined by an immunofluorescent ELISA assay ExoELISA (fig23A and C) and the ExoView single particle interferometry chip analysis (fig23B and D).

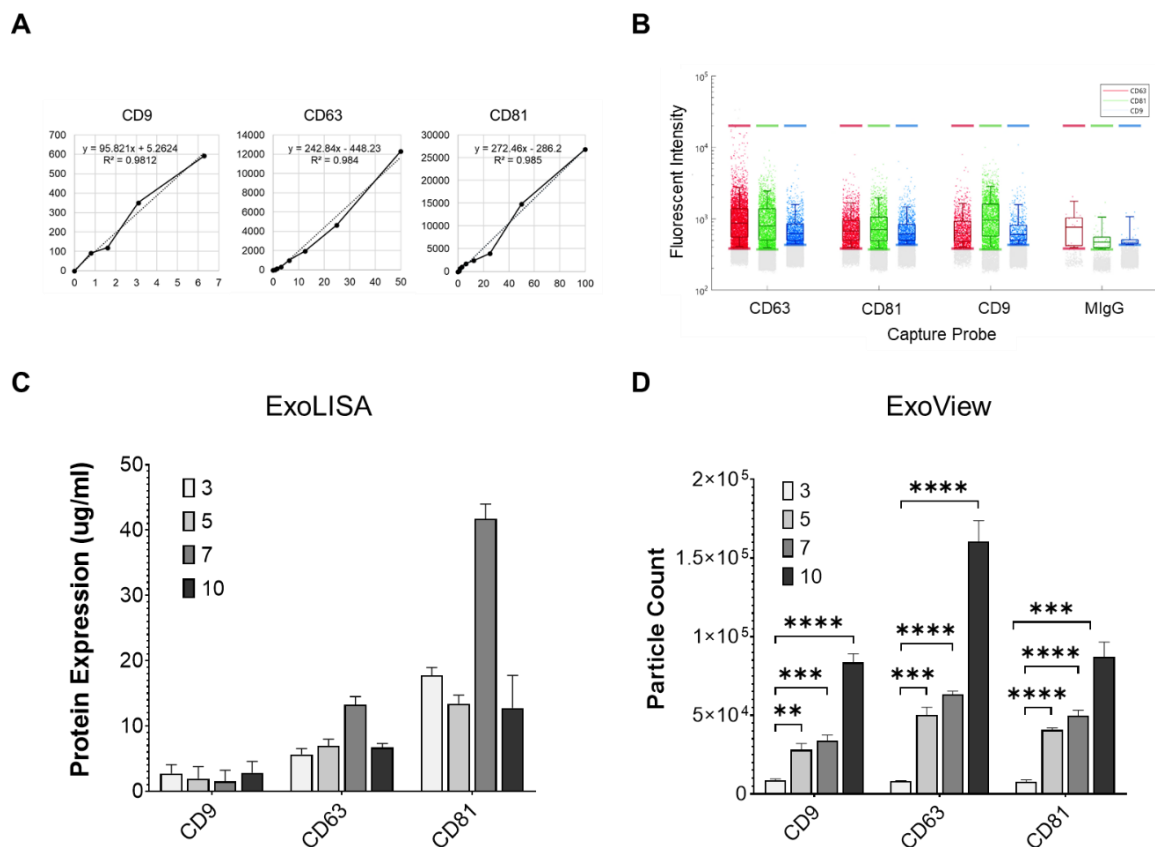


Figure 23: Extracellular Vesicle tetraspanin markers assessed across the 271 bioprocess timeline (Day 3, 5, 7 and 10). CD9, CD63 and CD81 expression was calculated using an ELISA assay (C), measuring tetraspanin positivity against standards (A); and also using the ExoView software (D), applying an IgG negative control (B). Graph B shows cutoffs, which were consistent across all experiments to control against non-specific binding to IgG. ELISAs were performed and both mean and SEM values plotted using 3 technical replicates ($n=3$), whilst ExoView mean and SEM data were derived from 3 independent grafting spots ($n=3$).

Primarily samples from the SF bioprocess timeline were analysed by single particle fluorescence Intensity detection and cut off values set against a known negative control (Mouse IgG) using the ExoView analysis software. Fig23B depicts an example chip scatter plot of individual particle surface positivity for CD9, CD63 and CD81. Particle count for each

marker increased significantly over time in respect to the initial SF sample at day 3, with particle count displaying a 10 fold increase by day 10 for CD9 and CD81 markers (fig23D). In addition to this CD63 appears to be the dominantly expressed biomarker across the EV time points, with a 6 fold increase in particle count between day 3 and 5 and a 20 fold increase by day 10. Nonetheless it should be noted from fig23D that increase in expression between day 5 and 7 appears to be less prominent for all tetraspanins.

As a secondary, more classical method, the ExoLISA technique was employed and expression established by plotting the purified sample fluorescence data against that of known technical biomarker positive control standard curve, measured in $\mu\text{g/ml}$. For this method expression was conveyed in protein concentration ($\mu\text{g/ml}$) due to measurement against standards. Data produced from this technique describes a contradicting expression profile to the ExoView, with CD81 being the most heavily expressed surface marker and CD9 showing minimal expression over all time points (fig23C). Moreover, concentration peaks at day 7 for CD63 and CD81 before dropping by day 10 to similar levels as seen on day 5 (fig23C).

Generally, tetraspanin expression is consistent between EV batches but significantly different between cell lines 263 and 271.

As well as understanding how concentration of EVs, which are tetraspanin positive, change over the bioprocess timeline, it was also essential for us to determine consistency between EV batches collected from SFs. Hence, Day 10 secretome from 3 independent SF runs using the 263 donor cells was analysed using the ExoView software.

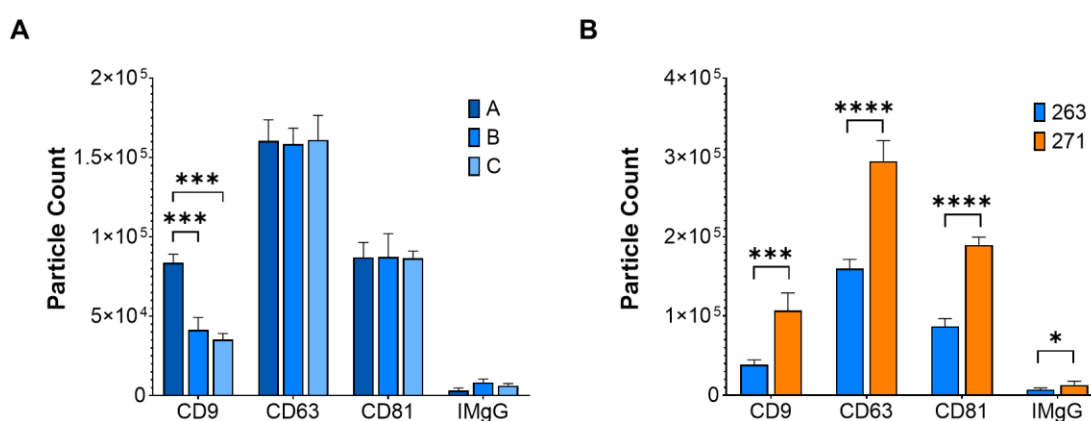


Figure 24: Assessment of TFF purified EVs tetraspanins, measured by ExoView software. Graph A depicts particle count across batches of 263 day 10 EVs and graph B differences between cell lines 263 and 271 EVs. Data and SEM from each batch was plotted from 3 independent grafting spot measurements ($n=3$), whilst cell line results (B) were obtained from

both 3 spot replicates and 2 independent batch chip measurements and data analysed using unpaired T-tests (n=3).

Fig 24A showed no significant difference in expression between batches of all markers (CD63 A, B and C – NS, CD81 A, B and C – NS, CD9 B and C – NS). However, CD9 positive particle count for batch A was significantly greater than that of B ($p < 0.001$) and C ($p < 0.001$). Of these three batch repeats, B and C were averaged and compared against cell line 271 secretome (fig24B). From this data it is apparent that particle count for each surface tetraspanin is significantly different between cell lines 263 and 271 (CD9 - $p < 0.001$, CD63 - $p < 0.0001$, CD81 - $p < 0.0001$) whilst order of expression, from CD63 as most abundant, followed by CD81 and CD9 as least, remains the same.

Mass spectrometry mapped 427 proteins mostly of Cytoplasmic, Exosomal and Nucleic origin which were heavily associated with the Extracellular Matrix, Transporter activity and Cellular communication, as well as Cell growth and/or Maintenance.

In order to reinforce and deepen understanding into the subtype and characteristics of sEVs identified by the ExoView software, Mass Spectrometry was performed on three batches of Day 10 271 TFF+SEC isolated sEVs. The purpose of this was to identify and group sEV attributed proteins to reveal their biogenesis mechanism, as well as specific biological process they had an affiliated with and possibly enhanced functionality towards.

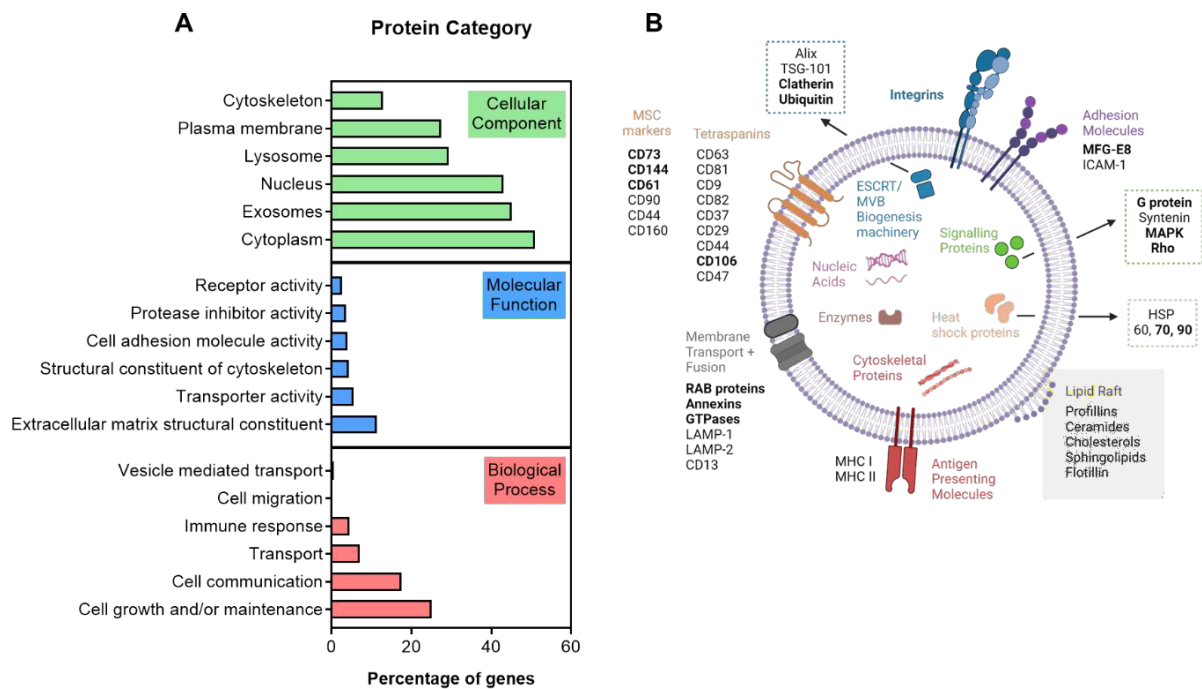


Figure 25: Mass Spectrometry data depicting gene % within each protein category (A) as well as highlighted (bold) specific genes associated with sEVs and MSCs (B). Data were retrieved from three batches of 271 TFF+SEC isolated sEVs (n=3).

Using Progenesis Q1 and FunRich software, 427 genes were mapped from three batches of Day 10 271 TFF+SEC isolated sEVs. Of these most were associated with Cytoplasmic, Exosomal and Nucleic cellular components, which was supported by these components sitting within the two highest Molecular function categories, Extracellular matrix structural constituents and Transporter activity (fig25A). Additionally, from the mapping of associated gene subsets, Biological process' with greatest percentage of detected genes were primarily Cell growth and/or maintenance, closely followed by Cell communication and finally both Transport and Immune response. Fig25B identifies, in bold, proteins detected by Mass Spectrometry and which subgroups of sEV allied surface/ cytoplasmic/ trafficking/ signalling component subgroups they fall within. Moreover, key MSC biomarkers CD73, CD144 and CD61 were also detected.

Mass spectrometry analysis shows depletion and enrichment of various proteins across the bioprocess timeline, including those associated with sEV biogenesis.

The presence of proteins associated with different categories between day 5 and 10 was also assessed using the FunRich software by analysing quantity fold value change. This provided us with a detailed picture of how to sEV protein profile changes over the culture timeline.

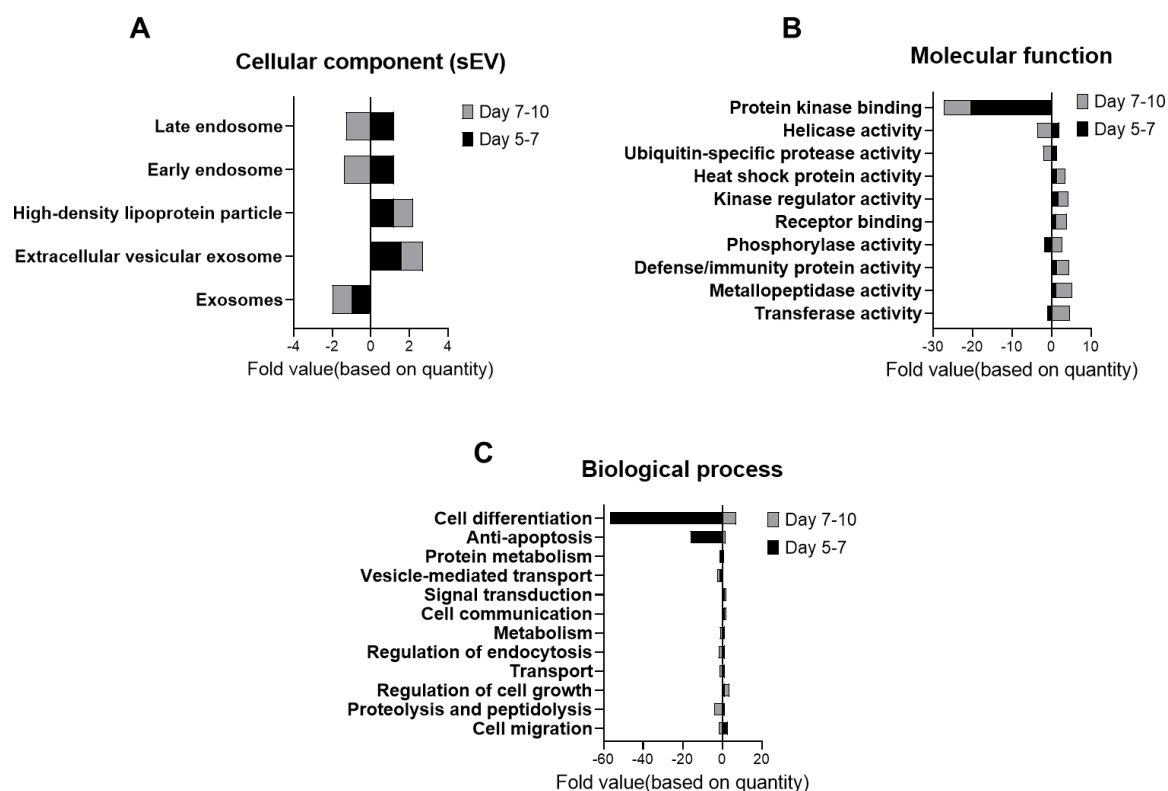


Figure 26: Mass Spectrometry data depicting gene fold value change between culture time points 5-7 and 7-10 within each protein category compiled from 3 batches of 271 TFF+SEC isolated sEVs (n=3). Graph A outlines protein fold change levels from cellular components which are sEV specific. Graph C illustrates fold change in categories associated with molecular function, whilst D illustrates greatest fold change for biological process'.

Mass spectrometry data showed there was a shift in many proteins between day 5 and 7 and 7 and 10. Fig26A highlights that where early and late endosomal proteins were upregulated between day 5 and 7, they were downregulated between day 7 and 10. High-density lipoprotein particle and Extracellular vesicular exosome continued to be upregulated between day 5 and 10, whereas Exosomes continued to be downregulated between day 5 and 10. Fig26B demonstrates increased upregulation of most of the molecular function associated proteins listed including heat shock proteins and metallopeptidase activity. Ubiquitin-specific protease activity linked to ESCRT machinery switched from being upregulated between day 5 and 7 to being downregulated between day 7 and 10. With the greatest levels of fold value, protein kinase binding proteins were downregulated by \sim -20 between day 5 and 7 and by a further \sim -7 between day 7 and 10. Finally, Fig26C illustrates the greatest fold value for proteins associated with biological process' was in the families of cell differentiation and anti-apoptosis where these switched from depleted by \sim -55 and \sim -15 between day 5 and 7 to enriched by to \sim 7 and \sim 2 between day 7 and 10 respectively.

3D SF culture produced significantly more tetraspanin positive sEVs than planar 2D culture.

It was important prior to moving onto functional assessment of sEVs to measure if 3D SF production of EV rich secretome was more effective than 2D planar production. This data would be key to reinforce why it is preferential to use suspension bioreactor systems when looking to work at scale, rather than culturing in multiple T flasks.

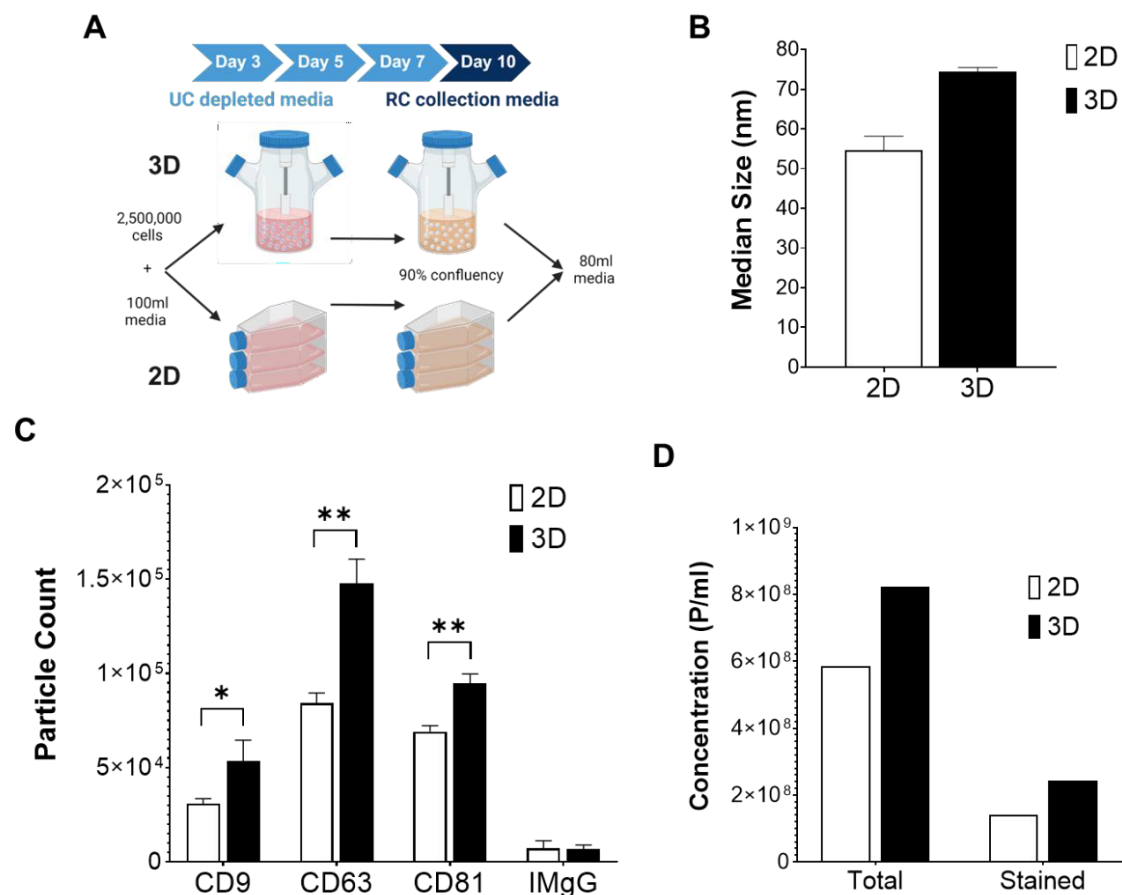


Figure 27: Characterisation summaries of TFF purified EVs produced from 3D and 2D culture conditions. Diagram A summarises both media collection protocols from SFs (3D) and Planar flasks (2D). Graph C summarises the difference in tetraspanin positivity using the unpaired T-test statistical test (n=3), whilst graph C identifies sEV median size (B) through the ExoView software. The overall concentration of particles/ml from samples of 2D and 3D TFF purified secretome was analysed by NanoFCM and is presented in graph D.

For the purpose of standardising EV rich secretome collection from both the 2D and 3D platform, Fig27A. illustrates how cultures were performed. Both methods matched the number of cells initially seeded into the platforms and volume of secretome collected at day 10 of culture, from MSCs which had achieved 90% confluency and undergone ~10 fold expansion.

Initial analysis of TFF purified particles from both the 2D and 3D platforms was performed using the ExoView system. The comparison of median size of tetraspanin positive EVs in graph B describes a reduction in sEV size when cell culture was performed under 2D conditions (fig27B). In addition, fig27C reveals sEVs collected from normalised 2D and 3D culture, exhibited a significant difference in expression of CD9 ($p < 0.05$), CD63 ($p < 0.01$) and CD81 ($p < 0.01$), where 3D culture consistently illustrated higher tetraspanin positive particle count. As a secondary measurement of change in particle concentration between 2D and 3D culture, Memglow staining was performed and batch matched samples run through the NanoFCM. Similarly, as shown on the ExoView, the total and lipid stained particle concentration was greater for TFF purified EVs from 3D conditions (fig27D).

Both protein concentration and Nanoparticle concentration is reduced following SEC isolation.

Following EV concentration and secretome purification using TFF, a secondary SEC isolation step was applied to further deplete protein and remove larger vesicular bodies, as both DLS and BCA data revealed it's presence in the samples. This step was especially key for *in vitro* healing and immunomodulatory studies to ensure that excess protein didn't mask the functional capacity of the sEVs alone.

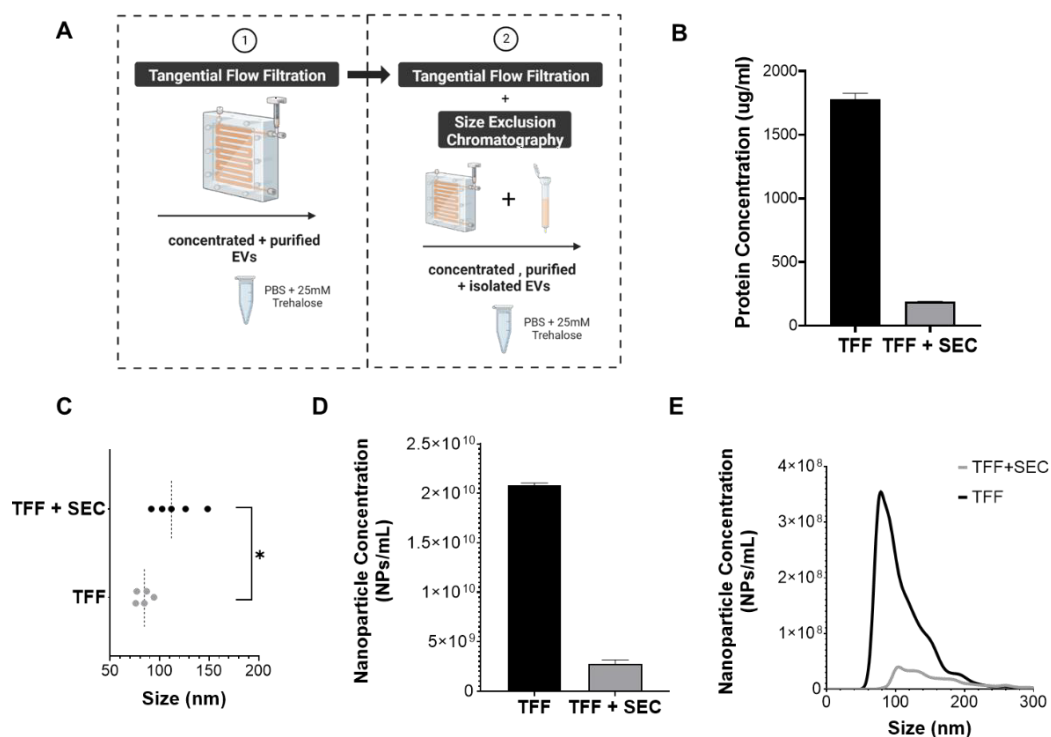


Figure 28: Differences in 271 EVs concentration and size when isolated by TFF + SEC compared to TFF alone. A visual representation of the two different isolation methods and the

resultant EV/secretome concentrate (1) and EV isolate (2) is illustrated in graphic A. Graph B portrays the difference in protein concentration between both isolation methods using a BCA assay, whilst graphs C, D and E employ NTA to initially assess both samples modal size and nanoparticle concentration. Graph B and D is plotted mean and SEM data from 3 technical repeats (n=3). Whilst graph C is plotted median of modal values for size distribution from 5 independent repeats analysed using an unpaired T-test (n=5).

Fig28B describes a considerable drop in protein concentration after SEC but additionally a substantial reduction in nanoparticle concentration (fig28D). Size distribution fig28E reinforces the lowered particle concentration but with a slight shift to larger particles, as shown to be significant (112nm compared to 84.5nm) when assessing median modal sizes in fig28C ($p < 0.05$).

There is a significant reduction in tetraspanin positive EVs following SEC isolation but total memglow stained vesicles appears to be largely unchanged.

As suggested in the chapter 4, where TFF is able to concentrate and purify EVs from SF media, it fails to deplete samples of extensive free background proteins and thus there is necessity for a second purification step to purify and concentrate sEVs. SEC was therefore employed prior to functional assessment of sEVs as we needed to ensure that pure populations of sEVs were affecting healing and immunomodulatory performance, and it was not the effects of secretome contaminants. Where SEC was employed, it was important to assess any impact it had on particle concentration, size and tetraspanin profile.

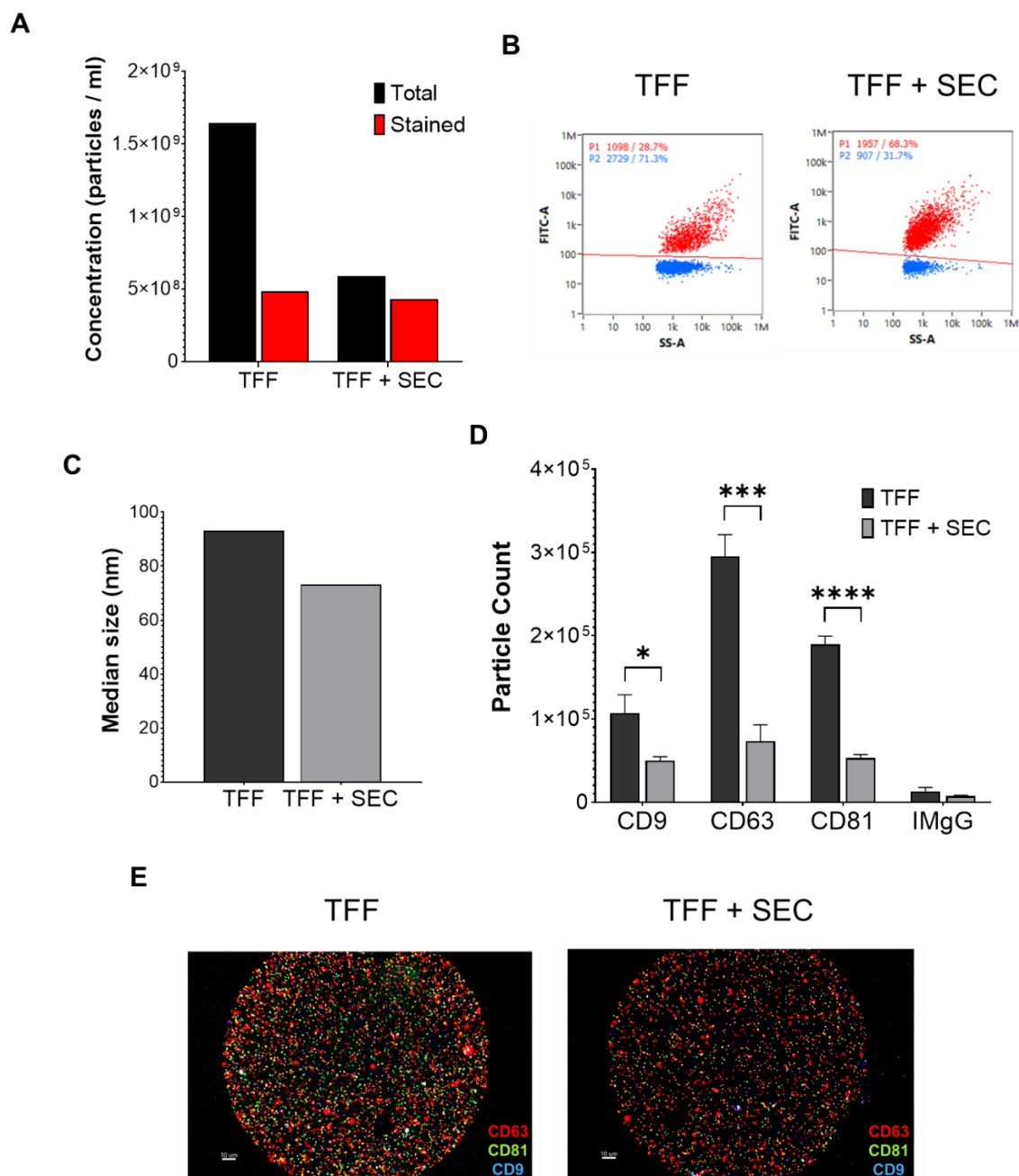


Figure 29: Comparison of particle characteristics between TFF purified and TFF+SEC isolated SF sEVs on Day 10 of collection. Lipid particles were labelled with Memglow 488 and three isolated batches analysed using the NanoFCM for concentration (A) and percentage staining (B). From this data, the average median particle size was also plotted (C). TFF vs TFF+SEC isolates were analysed through the ExoView software to fluorescently image (E) and quantify (D) this for tetraspanin positivity. Graph D represents data from 3 independent spot repeats (n=3) statistically analysed by unpaired T-test.

NanoFCM data in fig29A demonstrates how the addition of a SEC isolation step, reduces the overall particle concentration to approximately one third, but barely changes the concentration

of membrane stained vesicular structures. These findings are reinforced by the scatter plots (fig29B), which show that of the total particles purified by TFF alone, approximately 29% were membrane stained vesicular structures and that the performance of SEC increases the percentage of membrane stained particles to around 68%. There is also a noticeable difference in overall particle median size between the TFF purification (fig29C). Figures here suggest much larger stained particles following TFF purification but considerably smaller stained particles subsequent to TFF + SEC isolation. Applying the ExoView method, tetraspanin positivity between TFF purified and TFF + SEC isolated particles was determined. Generally, though to varying extents, there was a significant reduction in CD9 ($p < 0.05$), CD63 ($p < 0.001$) and CD81 ($p < 0.0001$) expression succeeding SEC isolation (fig29D). This decrease in tetraspanin staining is illustrated visually in fig29E with the fainter fluorescence intensity after TFF + SEC isolation.

SEC fraction analysis describes the benefits of collecting Fraction 2 and 3 to prevent unnecessary loss of lipid stained particles.

As there was revealed to be a loss in total, stained and tetraspanin positive EVs succeeding SEC isolation, assessment of different fractions were performed on the NanoFCM to ascertain if collection of other fractions would retain the sEV yield.

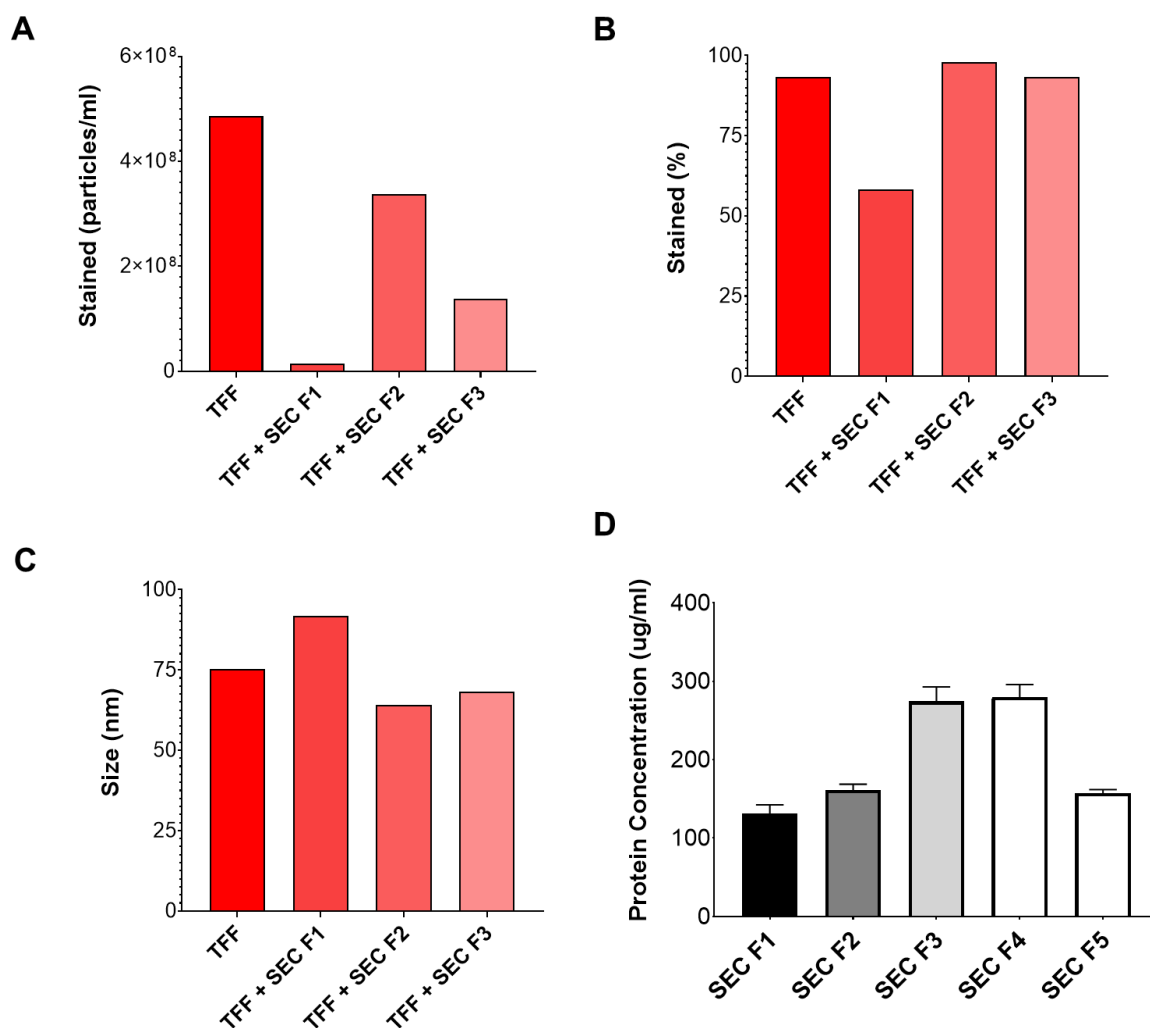


Figure 30: Comparing TFF and SEC fractions for lipid stained nanoparticle presence. Graph A outlines stained particle concentration, whilst B depicts what % fraction of all particles were lipid membrane bound and C compares the median size of stained particles in each sample. Graph D mean and SEM protein concentration data for each fraction was produced by 3 technical BCA repeats (n=1). Graphs A,B and C were plotted from means of a single TFF concentrated and SEC isolated batch (n=1).

A variation of stained particle concentrations were measured between the TFF purification step and SEC isolation fractions, with TFF containing the highest concentration of lipid particles, followed by SEC fraction 2, SEC fraction 3, then SEC fraction 1 (fig30A). Between these samples, TFF + SEC F1 also illustrated the greatest median size of 91.8nm whilst fraction 2 and 3 contained smaller particles (64.2 and 84.2nm) (fig30C). Whilst TFF, TFF + SEC 2 and 3 also all depicted similar lipid particle % staining, the value for fraction 1 was considerably lower at ~58% compared to ≥ 93% (fig30B). A BCA assay provided information into the concentration of protein collected from each fraction. This appeared to increase from fraction to fraction until fraction 5, which was the 2nd/4 wash steps.

5.4 Discussion

RoosterBio EV secreting bmMSC cell lines 263, 267 and 271 were seeded and expanded within SFs under an optimised cell culture protocol, tailored to maximise functional, stem cell growth. Under these conditions, 267 cell line depicted slower expansion and significantly fewer MSCs in comparison to 263 ($p < 0.01$) and 271 ($p < 0.01$) on harvest day 10 (fig18A). Regardless of these dissimilarities in expansion, this doesn't appear to be mimicked in each cell lines particle concentration where there is no correlation between cell counts and TFF purified particle count across the bioprocess timeline (fig18B). This relationship was also measured between bmMSC 271 batch SF runs, where more uniformity across the exponential phase of growth between batch A,B and C at day 7 (ns) and day 10 (ns), was not mirrored in their secreted particle concentration (fig18C and D). However, a similarity between both batches and cell lines NanoFCM measurements is that secreted particle concentration fall or plateau between day 7 and 10, following switching from UC depleted media to Rooster collection media (fig18B and D). Although there were inconsistencies in general particle concentrations across time points of batch runs, the same samples stained with lipid membrane dye, Memglow 488, depict much less variation. Additionally concentration of membrane encompassed vesicular structures demonstrated a steady rise from day 3-7, as did cell counts from those batch runs, but with a noticeable surge in stained particles between day 7 and 10 (fig19A and B). In regards to cell expansion, these results suggest that MSC cell line counts over time shown less consistency but the same pattern as batch repeats from an individual cell line. Combined with secretome particle concentration data, it is apparent that as MSCs proliferate over time, lipid particle count also increases. It appears that upon switching to Rooster Collect media at day 7, non-specific particle presence falls/plateaus whereas lipid vesicular structure release escalates. This suggests that Rooster collect media encourages the production of EVs by MSCs and supports results of chapter 4 which identified Rooster Collect media being clean of contaminants including protein and lipid associated particulates.

The upsurge in general and membrane stained nanoparticles over the course of the culture time line was supported by ExoView assessment of key EV tetraspanins. There was a significant difference in CD63, CD81 and CD9 positive EVs between each day and day 3 (fig23D), proposing that not only lipid particles, but specifically the concentration of sEVs increase over time in line with cell expansion. Again, this technique also acknowledges that the most prominent rise in quantity of tetraspanin positive EVs is between day 7 and 10 (~2 fold increase). Again reinforcing that this was a result of switching to rooster collect, which is commercialised as “*a bioprocess engine for rapid EV production*” “designed to increase total hMSC-EV yields” [277]. There is however no published evidence to back this statement

directly and the components of the collection media, including additives which have been suggested to escalate EV production (e.g. lipopolysaccharides), are undisclosed [161, 278]. Hence, we cannot discount that the surge in Vesicular lipid particles could be a result of alternative culture conditions. For example, the nature of Rooster Collect evidenced as being higher purity and XF links it to serum starvation, which has been frequently described by many authors to stimulate EV secretion [279, 280]. As well as the chemical composition of the collected media, it was also theorised that increased discharge of vesicles between day 7 and 10 could be a stress response to the bioreactor environment during this time period. It was considered that where there was exponential growth of bmMSCs, there was greater MC confluency, formation of aggregates and so indirectly related oxidative stress and physical pressure potentially acting on the MSCs [281]. According to cancer cell line literature, hypoxic or low oxygen conditions can cause the upregulation of Rab27a and respectively downregulation of Rab7, which are both associated with sEV secretion [278, 282, 283]. Although these concepts are all plausible, there is a lack of research into the effects of bioprocessing on MSC directed EV secretion, which could clarify the reason for particle concentration surge between day 7 and 10. As a result, further, more elaborate investigations are necessary before any conclusions can be drawn. In regards to our bioprocess we did nonetheless decide to maintain the employment of Rooster Collect as it was preferable to the collection of purer sEV populations of higher yield.

In contrast to particle number, the NanoFCM size data for particles across the MSC timeline is highly consistent with no significant difference between the three batches at each time point and similarly minimal variation between cell lines (fig20A and B). These NanoFCM size measurements appear to be comparable to that made using the Exoview software, with only a difference in SEM, which is most likely due to their mechanism for assessing particle size. Whereas readings from the NTA illustrate significantly larger particles than both NanoFCM ($p < 0.05$) and Exoview ($p < 0.05$) when assessing the same sample (fig21C). The large SEM for the NTA measurements are also depicted in the size distributions (fig21B), where NTA displays multiple peaks and a wide area under the curve. NanoFCM however has much smaller margins and displays mostly single peak size distributions (fig21B) as expected from purified EV rich secretome. The discrepancies between both methods have been often noted in studies, where the ranges in particle sizes were frequently wider in NTA [284-286]. This was shown in a paper by Dong et al. to be more substantial with NTA measurements ranging from 10–400 nm and nanoFCM from 40-150nm for multiple samples [285]. This occurs as a result of NTA overestimating the populations of larger vesicles due to the intensity of their light scattering obscuring smaller particles, as mentioned previously. Variations in measurements between both EV surface tetraspanin assessment techniques was demonstrated by the

difference in quantity of positivity between the ExoLISA and ExoView. The ExoLISA indicated a peak in fluorescent detection, normalised to protein concentration, for CD81 (~42µg/ml) and CD63 (~14µg/ml) at day 7 where the ExoView describes a different order in magnitude of tetraspanins (CD63>CD81>CD9), with their highest concentrations at day 10 (fig23C and D). As again there are many unavoidable disparities between how both platforms quantify EVs, including single-particle vs whole sample measurements, it is difficult to pinpoint exactly why the inconsistencies between results occur, but essential to recognise that they do [287-289]. Hence, more analytical methods need to be adopted in order to determine which tetraspanins most likely were genuinely more prevalent in our samples. Although it was difficult to determine which technique was more accurate, when analysing multiple samples on the ExoView, the data were highly consistent between batches analysed on individual chips. As shown in fig24A, the only significant difference in tetraspanin positivity was between A and B ($p < 0.001$) and A and C ($p < 0.001$) for CD9 particle count, which was regarded as an anomaly due to concentration the defect on the chip creating heavy background fluorescence (see appendix Fig1F). Across cell lines there was recurrent significant differences for all tetraspanin particle counts but no change in their expression ranking (fig24B), which suggests mainly only a different in sEV tetraspanin positive particle numbers for each cell line, as already depicted by nanoFCM data in fig18B.

As a final method for characterising MSC-sEV and assessing their protein profile across the culture timeline, Mass Spectrometry analysis was performed on 3 cell lines of MSCs cultured in SFs. Of the 427 genes mapped from the day 10 EVs, most were attributed to the Cytoplasmic, Exosomal and Nucleic domains with their molecular function being associated with Extracellular matrix structural constituents and Transporter activity (fig25A). As well as this, data from fig25A demonstrated that the greatest detected levels of proteins associated with biological process' were those which commonly define sEV function such as cell growth and/or maintenance, cell communication and transport. Reinforcing this, presence of genes for proteins linked to EV biogenesis mechanisms were indicated in fig25B. The functions of these proteins included; calcium dependent (Annexins) and MEK dependent (MAPK) release pathways [290], coordinated transport of MVBs to fuse with the cell plasma membrane (Rab GTPases) [147], actin cytoskeleton remodelling to facilitate sEV discharge (Rho) [147], sEV cargo sorting via ubiquitination of endosomal sorting complex required for transport (ESCRT) proteins (ubiquitin) [291], internalisation and endocytosis of sEVs via transmembrane receptors, ligands and triskelion scaffold (clathrin) [291]. The presence of such proteins further strengthened the presence of sEVs specifically characteristic of Exosomes within our SF isolated secretome.

A more detailed analysis into the regulatory shift in proteins between day 5 and 7 and 7 and 10 was also performed using Mass Spectrometry, with the results much harder to interpret. Combined they appear to show enrichment of endosomal proteins, Ubiquitin-specific protease activity and protein kinase binding proteins, linked to sEV trafficking, exocytosis and secretion were enriched between day 5 and 7 but depleted between day 7 and 10 (fig26). Nonetheless sEV and Exosomal proteins depicted the opposite expression profile. There was no literature to support or explain this finding and hence it is a result which needs additional research to be truly understood.

Easier to comprehend was fig26C data which depicted downregulated anti apoptosis proteins between day 5 and 7 but upregulated expression between day 7 and 10. This was expected to be a result of formation of MSC aggregates closer to day 7, where oxidative stress and depleted nutrients to some cells could cause an apoptotic stress response, which recovered upon Rooster Collect serum starvation and thus dissociation of aggregates between day 7 and 10 [292]. The enrichment of differentiation proteins as the SF culture progressed between day 5 and 10 did indicate that there was possibly a degree of potency loss over time in the agitated suspension culture but again this was something to be reassessed and tackled with additional investigations into the culture biochemistry and cellular physiology across the culture timeline. This would provide reassurance that 3D SF culture of MSCs and MSC-EVs maintains their stemness whilst encouraging sEV production and higher yields.

Therefore, it was also an aim of this chapter to evidence why 3D SF production of sEVs was more valuable than 2D planar flask expansion. In order to standardise the EV retrieval process from both methods we used harvesting confluency and final media volume, following applying the same initial seeding density (fig27A). This meant that sEVs from both bioprocesses were comparable. Using the ExoView software, 3D bioprocessing was shown to promote bigger particle median size of 75nm to 55nm from 2D bioprocessing (fig27B). In addition, the NanoFCM indicated both unstained and membrane stained particle concentration was higher following media collection and purification from 3D SFs (fig27D). Increased particle counts were reinforced by significantly greater tetraspanin positive vesicle counts for CD9 ($p < 0.05$) CD63 ($p < 0.01$) and CD81 ($p < 0.01$) using the ExoView platform (fig27C). The concept that bioreactors and agitated 3D cultures promote higher vesicle numbers has been heavily described in other research groups. For example when normalised to cell number, EV secretion from bioreactor based culture of MSCs on MCs was shown to be 2.5, 5.7 and 7.5 fold greater than 2D planar culture in a select few studies [249, 293, 294]. Thus, it was apparent that optimised and standardised 3D SF culture increases the secretion of MSC sEVs in comparison to 2D planar culture and so is the preferable method for MSC and EV scale up.

Following the full characterisation of TFF purified EVs, it was important to do so for SEC isolated sEVs, which were later applied within functional assays. Fig 28D primarily showed that there was extensive loss of nanoparticles following SEC isolation as well as a substantial decrease in general protein concentration. Fig 29A reinforced this by demonstrating a decrease in unstained particle concentration but fortunately not in memglow stained lipid vesicle concentration post SEC. There also appears to be a general shift in percentage stained vesicles following secondary SEC isolation from 28.7% to 68.3% (fig29B), signifying that the TFF + SEC isolated EVs are depleted of free proteins and other particles (fig28BandD), but not of membranous vesicle structures (fig29A). To complicate these findings, further assessment of EV tetraspanins between TFF and TFF + SEC isolates showed a significant decrease in CD9 ($p < 0.05$) CD63 ($p < 0.001$) and CD81 ($p < 0.0001$) positive sEVs (fig29D), visually emphasised by the intensity of the spot staining (fig29E). Interpreting this was complex, as most scientific literature recognises the main advantages of SEC is that it promotes a high and pure recovery, with emphasis on yielding particles characteristic of Exosomal/sEV biomarkers [180, 289, 295]. However, there is discussion into the impact of the vast available commercial SEC kits, which adopt mixed isolation methods and produce data which is not always representative of this statement [296, 297]. This was described statistically by Feng et al whom outlined published SEC recovery rates from various studies at between 40-80% [298]. As an example of the SEC isolation tool we chose to adopt, the commercial ExoSpin isolation kit applies high-speed centrifugation and a precipitation step, which are associated with mixed recovery of sEVs [299, 300]. A critical analysis by Konoshenko et al. provides an in depth breakdown of each classic isolation strategy and how papers described conflicting views into which method provides optimum recovery [295]. They specifically mention how the ExoQuick, a popular form of PEG precipitation outperformed both density gradient centrifugation and SEC in terms of particle quantity retained. This was challenged in Feng et al's critical analysis which researched polymer precipitation recovery to be 5-30% [298]. Konoshenko et al. outlined that this is not the case when assessing content of markers (including CD9 and CD63) where isolation using SEC and density gradient centrifugation showed heightened expression [295]. From our results it therefore appears that although membranous particles have been retained after SEC with high recovery, tetraspanin positive protein markers have been lost and this could be due to the multi-step techniques involved with Exo-Spin columns (e.g. EV damage through centrifugation steps, loss during column fractioning). Although theoretically, a second option for these inconsistencies could be that the techniques by which the sample was measured varied in their detection sensitivity and specificity (e.g. NanoFCM specificity to non EV related membranous particles). In addition to particle count and tetraspanin expression, the application of SEC isolation reduces the median size of EVs from 93nm after TFF to 73nm after SEC (fig29C). This shift to a population of

generally much smaller particles was expected due to the removal of larger vesicles (e.g. microvesicles), which would have overshadowed sEVs/Exosomes prior to SEC isolation.

Although the addition of a SEC isolation step appears to have depleted sEVs from the EV rich secretome, when considering performing functional assessments of sEVs in *in vitro* assays, it was necessary to employ a much purer population. This meant that their effects on regeneration and immunomodulation could be attributed directly to the sEVs themselves and not to contaminating protein particles also harboured within the secretome. Hence, regardless of the loss of sEV yield and scalability of the SEC technique, it was still applied for sEV functional assays. Nevertheless, it was critical to consider an alternative scalable technique/further optimisation of the technique for future secretome purification, as the Cell Guidance Systems SEC columns, utilised as directed in the user manual, were not efficient. Therefore, in a final attempt to avoid loss of sEVs through the SEC columns, a reassessment of the protocol was performed by measuring stained lipid particles in each SEC fraction (figure 31). This data exhibited that fraction 3 contained a similar fraction of abundant lipid structures within a sEV size range, as well as fraction 2, which was the only suggested collection fraction in the protocol (fig30A,B and C). Thus this could potentially indicate that fraction 3 was where tetraspanin positive sEVs had been lost. Nevertheless, the BCA protein assessment of each fraction did show that fraction 3 comprised a higher protein:lipid-vesicle ratio than fraction 2 (fig30D) so the addition of it to fraction 2 SEC isolated sEVs would slightly reduce the purity. Thus, the decision was made to only include TFF + SEC F2 in functional assays.

Chapter 6: Therapeutic and regenerative potential of MSC-EVs

6.1 Introduction

Prior to the application of potential EV therapeutics *in vivo* using animal models, measurement of their potency and reproducibility in cell culture assays *in vitro* is key to establishing their biological interactions. The assays performed in this chapter measured the effect of a specific dose of EVs on a range of cellular targets or disease models, suggestive of a mode of action *in vivo*. Additionally, the results were quantifiable and easily reproduced with minimal variation and uniformity, making them examples of functional assays [301].

To assess the bioreactor derived EVs endogenous regenerative potential, scratch wound and proliferation assays were used; due to their simplicity they allow the high throughput comparison of multiple EV preparations from different growth conditions or donors. Proliferation assays were performed to give an indication of EV effects on cellular growth and division. The scratch wound assay illustrated EV effects on migration, both single cell and collective [302-304]. The translocation of individual cells is characterised by cytoskeletal polarisation, focal adhesion assembly/disassembly and cell body retraction [303, 305]. The coordination of these events between collections of cells is critical to a successful wound healing process, driven by external cues/chemoattractants such as exosomes [305]. The application of a fibroblast scratch wound functional assay an initial functional investigation to demonstrate the ability of EVs isolated from selected upstream (3D and 2D produced) and downstream (TFF and SEC isolation) bioprocessing conditions to promote wound healing.

As an element of the control and resolution of inflammation, MSC EVs modulate both the adaptive and innate immune responses, promoting the secretion of chemokines and pro-inflammatory factors to enhance or direct the immune response [306, 307]. Alternatively, they have also been well documented to express an immunomodulatory phenotype towards inhibiting the activation and proliferation of immune cells, such as CD4⁺ T lymphocytes [308-310]. This prevents direct target of foreign cells, antibody production by B cells and secretion of lymphokines [310]. Additionally, as part of the innate Immune system, macrophages are another category of lymphocyte which are a primary responder to invasion [311].

Although these functional assays have been performed previously by other groups, they are required to assess the immunomodulatory potential of MSC-EVs from the optimised bioreactor bioprocessing protocols. EVs were applied to a T-cell proliferation assay. It was important for us to determine if EVs collected from 3D conditions demonstrated different potency than those

derived classically from 2D conditions, as well as the effects of EV isolation and hence sample purity.

6.2 Aims

The aims of this chapter were to:

Assess the capacity of EVs from different collection and isolation conditions to:

- 1 Promote 3T3 Fibroblast proliferation.**
- 2 Encourage 3T3 Fibroblast scratch wound closure.**
- 3 Activate T cells within a PBMC assay.**

6.3 Functional Methods

6.3.1 EV dosage preparation

Dosage for each functional assay was determined by protein concentration via BCA assay (Pierce), where isolated EVs were applied at concentrations of 100µg/ml (Scratch wound and Proliferation) or 50µg/ml (T cell proliferation). As TFF samples contained small protein contaminants, the BCA readings produced an invaluable reading for EV protein concentration. Therefore, we dosed from TFF samples according to EV particle concentration matched to SEC sample particle concentration at 50µg/ml and 100µg/ml respectfully.

6.3.2 Fibroblast Proliferation Assay

3T3 Fibroblasts were seeded at 5000cells/cm² or 1562cells/ 96 well plate well in complete media and allowed to attach overnight before being exposed to 10µg/100µl EV containing SF media or 100SF control media. Following initial exposure, the CCK-8 live cell proliferation measurements were made and absorbance readings performed at 450nm on the ThermoScientific Multiscan Pro plate reader (ThermoScientific). Once raw data had been collected, it was converted to cell count by plotting against the standard curve of Fibroblasts seeded at specific densities. This was repeated every 24 hrs for 3 days total.

6.3.3 Scratch Wound Assay

3T3 Mouse fibroblast cells were seeded in 96 well plates at a density of 10000cells/cm² in complete media until 90-100% confluency. Once achieved, the monolayers were scratched in the centre of the well using a 10µl pipette tip. After initial inspection of each well on the Incucyte software, those wells with the best placement and consistency of scratch were chosen. Wells were washed with PBS and incubated with 100µg/ml EVs in SF media in a final volume of 100µl. Each well was imaged every 2hrs for a total of 2 days when most of the scratches are closed. Selected time points were chosen and analysed dependent on image quality (the incucyte often experienced errors and would fail to image wells or focus onto the wells). Downloaded images were cleaned (sharpen, despeckle) and edited (contrast) in a standardised manner to enhance image quality using the imagej software to enhance the contrast before being run through the wound assay plugin [312]. Variance settings for this were suggested by the creator and set between 2 and 25, depended on image quality, standardised between each experiment to provided an accurate depiction of true scratch area. The area fraction data from the analyses was then taken and equated to percentage of 100. Summary graphs A, B and C represent these quantified values from 3 technical repeats from 3 biological repeats (n=3). Statistics were performed as mentioned previously between the experimental conditions and control at each time point.

6.3.4 EV-PBMC Assay

PBMC preparation was performed as mentioned in 3.2.4.4 but stimulating with EVs instead of MSCs. Additionally, staining of PBMCs involved 1:2000 dilution in CFSE violet (Cell Trace pb450) as the new optimal solution for measuring PBMC activation on the flow cytometer. After staining, separate PBMC stock solutions were created dependent on the experimental condition with 10µl/ml PHA and 4µl /10ml IL-2: Positive control (PBMCs + PHA + IL2 in CM), negative control (PBMCs + IL2 in CM) and EV experimental condition (PBMCs + IL2 + EVs in Serum Free media). The experimental stocks were then supplemented with EVs in a dosage of either 25µg/ml or 50µg/ml with 50,000 PBMCs/100µl . 100µl of each stock suspension was then transferred to 96 well plates and left for 4 days until flow cytometry was carried out.

6.4 Results

TFF isolated EVs significantly enhanced fibroblast proliferation.

Effects of EVs on 3T3 fibroblast proliferation was evaluated by performing 3 independent cell CCK8 viability measurements every 24 hours for 3 days post 100µg/ml EV exposure. The colour change reaction and following absorbance reading was converted to a cell count measurement by plotting against a standard curve.

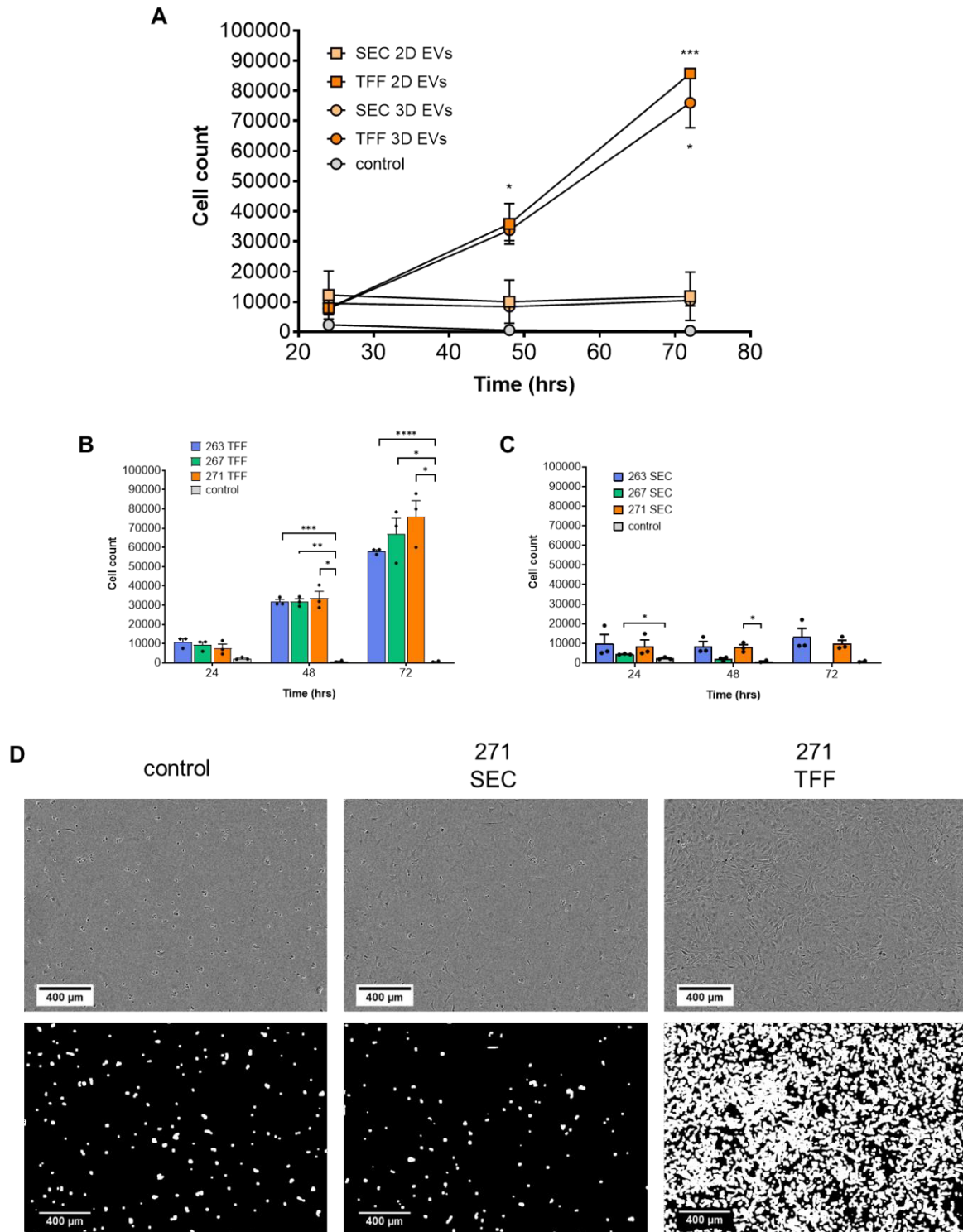


Figure 31: Effects of MSC-EVs on 3T3 Fibroblast proliferation. 100 μ g/ml MSC derived EVs were incubated with 5000 Fibroblasts/cm² for 72 hours to determine their effect on cell proliferation. (A) Graph highlights the CCK-8 live cell count readings between both 2D vs 3D derived and TFF vs SEC isolated EVs treated MSCs every 24 hours. In order to also assess the consistency in proliferation between these conditions, three independent MSC-EV cell lines were tested (B and C). (D) Representative enhanced (top) and ImageJ edited (below)

Incucyte images show differences in fibroblast confluency under SEC and TFF isolation conditions. All plotted data in A, B and C representative of 3 technical repeats within 3 independent experimental repeats (n=3).

From this count data, fig31A shows there is no difference between both 2D and 3D culture cell derived EVs in their ability to induce fibroblast proliferation and that the significant influencing factor is the isolation method used. TFF concentrated and purified EVs retrieved from 2D and 3D bioprocesses induce significant fibroblast cell expansion against the control at both the 48hr (2D TFF: $p < 0.05$, 3D TFF: $p < 0.05$) and 72 hrs time points (2D TFF: $p < 0.001$, 3D TFF: $p < 0.05$). Similarly fig31B and C reinforce that isolation method has a significantly greater contribution to cell proliferation, as shown by 3 cell lines at 48 hrs and 72 hrs post EV treatment (48hrs = 263 TFF: $p < 0.001$, 267 TFF: $p < 0.01$, 271 TFF: $p < 0.05$ and 72hrs = 263TFF: $p < 0.0001$, 267 TFF: $p < 0.05$, 271 TFF: $p < 0.05$). Conversely, the SEC isolated samples did not show significant cell count and levels of expansion compared to the EV free control media at 72hrs (fig31C). These quantitative readings are supported by the enhanced (top) and imageJ edited (below) incucyte microscope images (fig31D). 3T3 Fibroblasts appear to be attached, spreading and achieving confluency under TFF EV incubation, unlike treatment with SEC EV isolates and the SF control media (fig31D). These conditions have discouraged cell expansion, where cells would normally appear fibroblastic, they show an isolated, spherical morphology and are few in numbers.

SEC isolated EVs significantly enhanced fibroblast scratch wound closure in comparison to the control.

3T3 Mouse Fibroblast cells were seeded in 96 well plates at a density of 10000cells/cm² in complete media until 90-100% confluency. Once achieved, wells were scratched using a 10 μ l pipette tip and gently washed with serum free media in order to remove any scratch debris. After initial inspection of each well on the incucyte software, those with the best placement and consistency were chosen and scratches re incubated with 100 μ g/ml EVs to a final volume of 100 μ l. Each well was imaged every 2hrs for a total of 48 hrs when most of the scratches had closed. Selected time points were chosen and analysed dependent on image quality. Downloaded images were edited in imagej software before being run through the wound assay plugin as outlined in 6.3.3 Area fraction data from the analyses was then equated to % of 100.

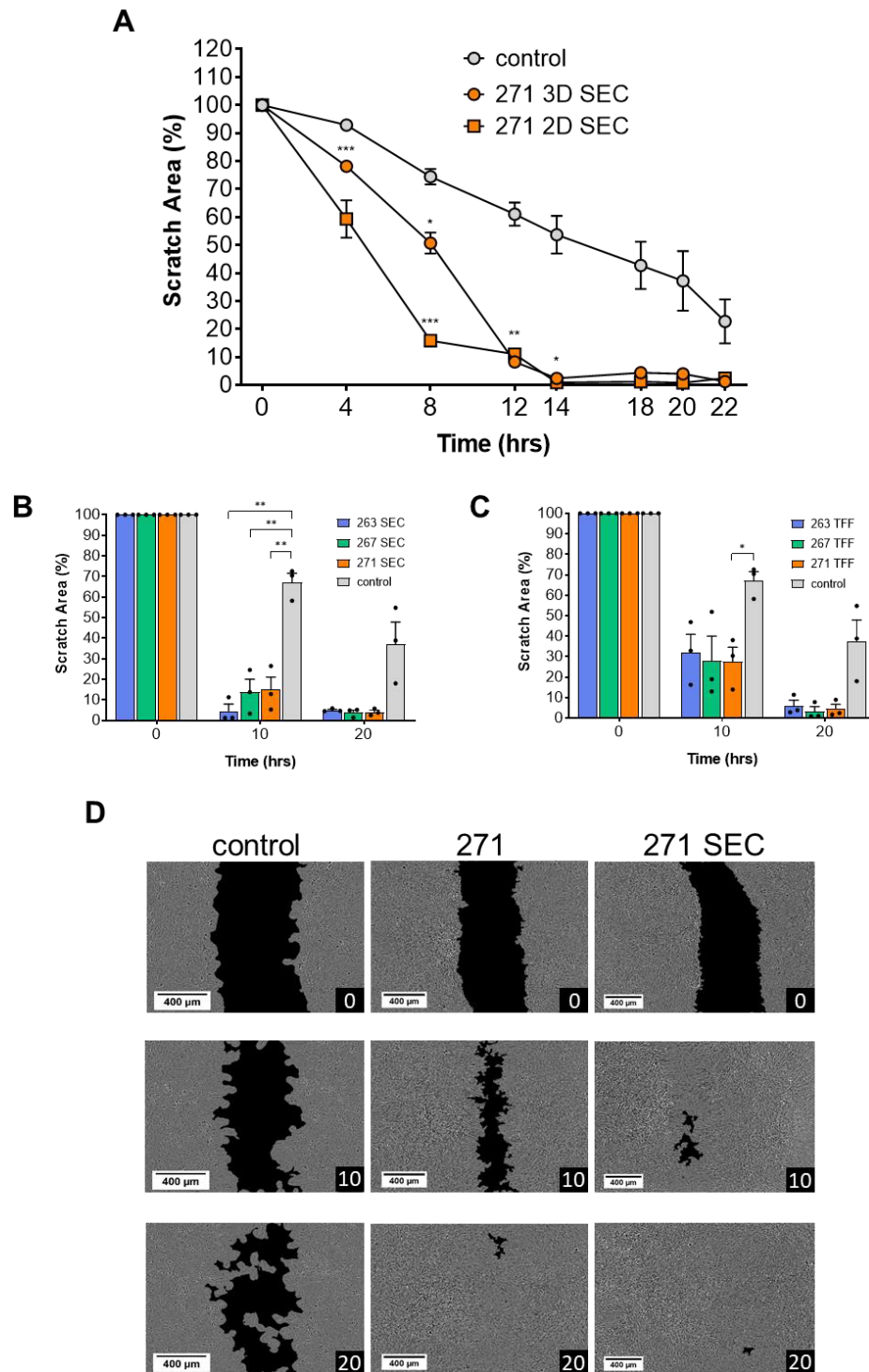


Figure 32: Effects of 100 μ g/ml MSC derived EVs exposed to a fibroblast scratch wound for 24 hours. (A) Graph shows the scratch area percentage change over time in the presence of either the 2D and 3D culture derived EVs, as well as the SF media control. Additionally scratches were treated with EVs from 3 MSC cell lines isolated by SEC in (B) and TFF in (C) scratch area (%) was measured at both 10 and 20 hrs to give an indication of the rate of closure. (D) Representative examples a selection of scratch closure images from which the

quantified percentage area values were derived. Summary graphs A, B and C represent 3 technical repeats within 3 independent experimental repeats (n=3).

Fig32A depicts scratch area with a visible difference in scratch % between 271 3D SEC and 271 2D SEC against the control at all time points. In addition, these were statistically different between day 8 and 14 for both 3D and 2D SEC EVs. This trend was the same in all 3D SEC isolated EV cell lines on day 10 in fig32B (263, 267 and 271 SEC sEVs - $p < 0.01$) and scratches appeared to have closed by day 20 when exposed to both SEC and TFF sEVs in comparison to the control which remained open. However, interestingly TFF EVs from the same cell lines do not show the same level of closure at day 10 and significance was only observed in 271 TFF EVs against the serum free control ($p < 0.05$) in fig32C. Fig32D illustrates % closure by highlighting scratch area in black. Again, it is obvious from these images that scratches were completely closed with TFF and SEC EVs by day 20 but not with serum free media.

SEC isolated EVs conduces a low proliferation index in PBMCs similar to that of an unstimulated control

MSC-EVs effects on T cell proliferation was assessed using a PBMC assay and comparing against a stimulated and unstimulated T cell population. This would indicate if SF MSC-EVs were immunoprivileged.

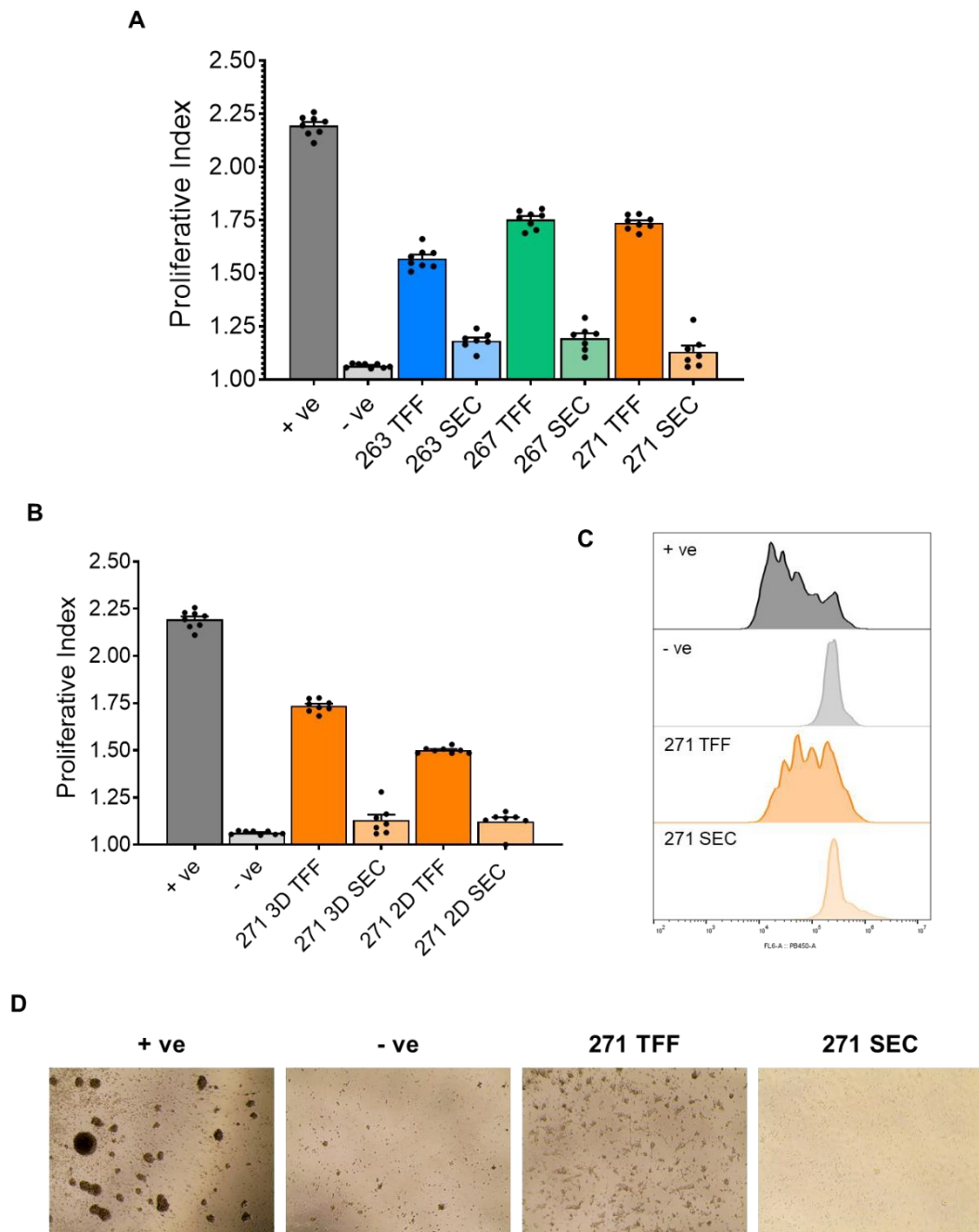


Figure 33: Effects of EVs on T cell proliferation. Proliferation dye labelled PBMCs were incubated in the presence or absence of PHA and IL-2, and effects on proliferation assessed by flow cytometry. Histograms from the gated control, illustrated in C, shows distinct peaks for each population for divided and undivided cells. Calculated proliferation index from each condition were plotted in B and C, assessing the differences between different MSC cell line EVs (A), EV isolation method and EV 3D vs 2D bioproduction (B) on PBMC proliferation. Images in D demonstrate the visual change between aggregated stimulated PBMCs and unstimulated PBMCs after four days of treatment. All plotted data in A and B represent seven

technical repeats within one biological repeats ($n=1$), hence no statistical tests were performed for this data set.

In order to assess the effects of EVs on fluorescently stained PBMCs proliferation, a 5 day PHA stimulated positive control was initially run through the flow cytometer once it had exhibited the clonal expansion morphology shown in fig33D. Following this, each control and experimental condition was measured and later analysed. Changes in proliferation were assessed against the positive control (stimulated PBMCs in the absence of EVs). As all conditions (including the negative control) had been primed also with T cell survival cytokine signalling molecule IL-2 we know all PBMCs were viable and able to be stimulated. Nonetheless, it is obvious from fig33C that the negative control shows a completely unstimulated profile, with most cells grouped within the D0 division subset, nearly identical to that of the SEC isolated EV group with 1 single negative peak. Although the TFF concentrated and purified EVs also produced a large negative PBMC peak, there are multiple subsets of cells that appear to have proliferated, with a notifiable difference in PBMC morphology as indicated in the microscope image (fig33D). There is consistency also between the proliferation index readings between MSC-EV cell lines for both the TFF and SEC isolated EVs (fig33A). When assessing the effects of 3D vs 2D bioprocessed EVs (fig33B), it also seems that this is not a key factor when it comes to PBMC proliferative index and that the key outcome of this assay is how SEC isolation promotes prominently reduced PBMC proliferation and stimulation.

6.5 Discussion

Upon assessing the ability of small EVs derived from 3D culture (SFs) and 2D culture (planar flasks) to promote fibroblast proliferation and scratch wound closure, there is no clear significant difference (figure 32). There is little published research specifically related to stirred tank bioreactors that can reinforce this data, however a July 2023 paper described how EVs from hMSCs cultured in a vertical wheel bioreactor promoted superior scratch closure to 2D MSC-EVs [249]. However the significance of this result is not obvious, with data showing large error bars and an unclear conclusion [249]. The majority of research looking at the wound healing capacity of EVs produced in 3D conditions or Bioreactors come from spheroid based culture in which findings suggest enhanced functionality of 3D EVs over 2D EVs [313, 314]. For example Kim et al used both *in vitro* and *in vivo* mouse models to show how MSC-EVs from micro-patterned well spheroid culture were able to increase proliferation and migration of both keratinocytes and fibroblasts [315]. However this paper did not directly compare their

results to 2D bioprocess derived EVs, stating as many other studies that 3D culture augments secretion of EVs with advanced therapeutic phenotypes and contents (miRNAs and cytokines) [316]. Directly measuring this in functional and potency assays is a requirement nonetheless and hence should be investigated further.

It was established that our Bioreactor MSC secretome which had been concentrated and purified by centrifugation and TFF (TFF EVs) could accelerate both fibroblast proliferation and migration in 2 separate functional assays (Figures 31 and 32). Although, we were aware from our protein concentration and particle measurements that these EVs were contaminated by excess protein and thus EVs needed to be purified and isolated by SEC before we could definitely conclude that the wound healing capacity of EV samples was due to isolated small EVs/Exosomes and not a result of sample contaminants (e.g. cytokines) [317]. Once further isolated using SEC, MSC-EVs of all three patient samples significantly lowered percentage scratch area after ten hours of treatment in comparison to the TFF EVs (fig32B). Therefore the purer EV/Exosome population exhibited consistently better migratory and healing potential (figure 32). This is unsurprising, as isolated small EV populations have repeatedly shown their potential to mediate and enhance wound healing in fibroblast, keratinocyte and corneal wound models [318-320]. The inability though of the SEC-EVs to induce fibroblast proliferation was difficult to interpret (figure 31). As little negative data were found in the literature, it was presumed to be a result of the lack of free soluble proteins available to support the proliferation phase of wound healing. During proliferation and remodelling, soluble substances can enhance fibroblast migration and importantly the deposition of ECM components, including collagens I and III, which consequently accelerate cell expansion and wound contraction [321]. Therefore, this suggested that the complex closure process of fibroblast scratch wounds in fig32 may rely more heavily on migration than proliferation as scratch wound closure could be supported by purified sEVs alone. The ability of purified sEVs to have a superior effect on wound healing process' has been shown by both ameliorating and balancing the inflammatory response in some studies [322]. Additionally a systematic review by Prasai et al exposed MSC-exosomes as the major source of miRNA in secretome, with evidence pointing towards MSC-exosomes being enriched with thirteen unique miRNAs, which were also shown to be mainly responsible for mediating the wound healing process in those studies [161, 323]. Although it is difficult to directly measure the effects of free, soluble factors on wound healing, in comparison to exosomes alone, due to the inability to prove 100% isolation at such small scales [324, 325].

In addition to the wound healing functionality of 3D MSC-EVs, the preliminary data into the lack of T cell activation by SEC isolated EVs appears highly promising, with a profile similar to that of a completely unstimulated negative control (figure 33). Additionally, the TFF-EVs also

revealed a proliferative index lower to that of the positive control in both the 3D-EV and 2D-EV groups. These findings have been made by other research groups working in similar fields and thus shows bioreactor MSC-EVs display great potential for further research into their immunomodulatory capacity [326-328]. Interestingly, there appears to be a change in T cell morphology after the addition of 271 TFF EVs which could suggest T cells scanning for Antigen Presenting Cells or polarising macrophages (fig33D). This is something we wish to investigate further in the future by performing macrophage polarisation assays or staining for T cell CD4 and CD8 markers.

Chapter 7: General Discussion

7.1 General summary

7.1.1 MSC and MSC-EV downstream bioprocessing in SFs

The initial priority of SF optimisation studies was to design a benchtop suspension culture platform which facilitated MSC expansion on MCs and permitted MSC-EV collection across the culture timeline. In addition to this, it was a necessity that MSCs retained both their potency and functionality whilst maximising proliferation and final harvest yields as it was predicted that this would correlate with MSC-EV concentrations.

From all the factors documented as influential to cell expansion we primarily found that increasing the length of the initial static hold period to 24hrs generated significantly higher MSC final yields ($p < 0.0001$ at day 10) (figure 8). In addition to this, application of an EV collection media (UC media), which was high in protein but depleted in lipid particles, conferred levels of expansion that were comparable to that observed to CM in the optimised protocol (figure 9). Thus combined, these design adaptations were conducive of significant MSC expansion on MCs with mostly retained viability, stemness, trilineage differentiation and immunoprivilege post-harvest.

In regards to higher cell counts conducting higher EV concentrations, this was demonstrated in terms of stained lipid vesicles (figure 19), measured using NanoFCM, and traditional sEV tetraspanins (fig23D), assessed by ExoView software. In particular, SP-IRIS ExoView analysis depicted an increasing difference in CD9, CD63 and CD81 expression across the culture timeline with significant differences between all day 5, 7 and 10 measurements and day 3. There was also batch consistency between SF runs in relation to both MSC cell counts (fig18C) and lipid particle concentrations (fig19A) across the expansion time course and on harvest day 10 (fig24A). Illustrating SF culture batch consistency was essential for delivering a regulated process with reproducibility and matched sEV production outputs (so predictability). This level of standardisation heightens expert's confidence in EV manufacture from stirred suspension culture and bioreactors, proving in addition its scalability and thus benefit when aiming to affordably and easily produce large quantities of sEVs. Though well evidenced by other academic groups, it was decided to verify that, in comparison to 2D planar culture, through 3D agitated culture greater scale MSC-sEV secretion was constituted [241, 285, 286]. Figure 27 supported this concept, depicting 3D culture endorsed higher stained lipid nanoparticle concentration (by around 2x) and significantly increased positivity for sEV classic

tetraspanins. This further elevated preference for bioreactor manufacture of sEVs, especially as a feasible platform when aiming to yield therapeutic volumes.

Nevertheless, unless these yields of sEVs were maintained in the downstream bioprocessing of secretome, the ability to scale up the bio production MSC sEVs upstream was irrelevant. Therefore, it was imperative that the processing (concentration, purification and isolation) of heterogeneous nanoparticles within the secretome was evaluated and loss of sEVs quantified.

7.1.2 MSC-EV upstream bioprocessing in SFs

The decision on which isolation method to adopt was reached by initially reviewing a vast array of literature and prioritising techniques with high throughput and scalability, able to achieve high retention and purity of product. Hence, as TFF conveyed most of these features it was implemented initially in a single stage technique [183, 184]. Upon validation, TFF demonstrated it's ability to filter out protein (fig16D), whilst being impermeable to nanoparticles within the sEV size range (40-200nm) (fig16B and C). Nonetheless, TFF retentate conveyed continuing high protein concentrations post secretome concentration (fig28B), suggesting the application of a second isolation step, for which SEC was selected as it had become well accepted in the research community [177-181]. Although fig28D and E described nanoparticle concentration decreased considerably following it's use, additional assessment of stained lipid vesicles and sEV tetraspanins indicated that fewer sEV particles had been lost than previously believed (figure 29). Moreover, where there was reduced sEVs in the SEC sEV isolate fraction (fraction 2), assessment of lipid stained nanoparticles (NanoFCM) suggested the presence of sEVs also in fraction 3 (fig30A) and thus the possibility of regaining yield there.

The ability of this selected downstream bioprocessing platform to retain a high sEV yield reinforces the abundant evidence that TFF combined with SEC is a superior 2-step isolation model. Nonetheless, there is room to improve the platform to enhance it's scalability and specificity by considering the replacement of SEC with for instance an innovative microfluidic device. By adapting the TFF and a flow through capture antibody impregnated device, the downstream bioprocessing of sEVs could be streamlined in an integrated, single, enclosed scalable system. A bioreactor connectable isolation platform such as this could be an invaluable tool for groups aiming to minimise manual handling when it comes to sEV manufacture so that they can focus on *in vitro* application studies for instance. For the purposes of our investigations into sEV characterisation and functionality from SF culture, our current isolation procedure was satisfactory and hence there was no need to investigate downstream bioprocessing of sEVs further.

7.1.3 sEV characterisation

An unplanned objective within the project was to assess the differences in characterisation profiles and consistency between multiple traditional and contemporary analysis techniques. From these investigations, evident was the usefulness of NanoFCM, which provided a simple, efficient way of assessing particle counts in both unstained and stained samples, additionally allowing for the assessment of sEV surface biomarkers. Unlike NTA and DLS, which use brownian motion and light scattering when analysing samples, NanoFCM uses single-photon counting modules, which show higher efficiency analysing sEVs at higher precision in a heterogeneous samples. The repeatability of the NanoFCM results also made it the preferable technique for all concentration and size measurements.

Assessing the biological profile of MSC-EVs across the culture timeline suggests from day 3-7 there is a more gradual increase in quantities of stained lipid nanoparticles and tetraspanin positive MSC-sEVs, whereas by between day 7 and 10, the volume of secreted EVs appears to soar (fig19A and fig 23 D). As the only factor modified between these time points was collection media, it was assumed that commercial RC media stimulated sEV manufacture or discharge from MSCs. It had already been determined that RC medium was XF (as described by the manufacturer) and high glucose (fig9C) due to it's minimal levels of proteins and lipids and serum free nature (fig19B, fig10, fig 11, provoking MSCs to detach from MCs (fig9A). It was therefore predicted that this behaviour was indicative of an MSC stress response, provoked by the shock of moving from the low glucose proteinacious UC depleted media to high glucose XF RC media. Although this response achieved a higher MSC-sEV yield, without triggering a loss in MSC potency, and so was constructive to attaining or scale up goal, it did confer changes in sEV protein profile. As referenced in 4.1.2.3, this response had been evidenced previously by other authors. For instance, most obviously, cell differentiation proteins fold value reverse from being noticeably downregulated to becoming upregulated (fig26C). A similar reaction also occurred with anti-apoptotic proteins (fig26C). Specifically in relation to sEV biogenesis, where late endosome and early endosome packaging bodies became downregulated after day 7 (fig26A), sEV shedding continued to increase, thus suggesting elevated internal packaging of sEVs but not necessarily greater trafficking for surface expulsion. Alternatively, this may propose that the high turnover of this trafficking and shedding process could not be measured by mass spectrometry.

Nonetheless, this conveyed the influence of the SF biochemical microenvironment, mainly directed by the growth media, when sustaining MSC expansion and both sEV release profile and sEV phenotype. Thus, future research will involve focusing on defining an in house MSC

expansion and sEV collection media similar to RC, but which can provoke optimal levels of stress to sustain MSC adhesion to and proliferation on MCs, whilst encouraging production of bioactive sEV.

7.1.4 SF MSC-EV functionality

Although MSC-sEVs are documented as possessing healing and regenerative properties, it was key that we assessed this in those derived from the project's optimised SF suspension culture. Primarily, these features were exposed upon proteomic analysis of MSC sEVs in fig25A, where the highest percentage of biological process categorised genes were those which fell under cell growth and/or maintenance, cell communication, transport and immune response. Hence the revelation of their closely matched ability to close a fibroblast scratch wound in the same timeframe as planar culture collected sEVs, and significantly faster to that of the serum free control, reinforced that sEVs have measureable capacity to enhance cell migration.

Additionally, a functional advantage of sEVs is frequently referred to as their inability to evoke an immune response and navigate the immune system without detection. The ability of MSCs to do this was already emphasised in fig13, thus it was hoped that sEVs would illustrate a similar effect. However, the ability of different cell lines of MSC-EVs in secretome (TFF) and isolated MSC sEVs (SEC) to suppress T cell proliferation more obviously than MSCs was an exciting finding.

Chapter 8: Final conclusions

8.1 Novelty

Prior to the performance of the project, there was a lack of documented literature and research papers investigating MSC-sEV production from both SFs and bioreactors. Specifically, there was no clear data relating to sEV characterisation (particle number, size, surface biomarkers, protein profile etc.) across the course of the bioprocessing timeline and thus the ExoView, NanoFCM and proteomic assessment of the sEV population between day 3, 5, 7 and 10 of culture is truly novel. These results indicate the impact bioprocess parameters have on sEVs as well as the consistency of sEV population characteristics across a standardised agitated suspension culture process. The bioprocess itself is also unique in its optimisation and provides a simple, affordable platform dedicated to MSC-EV collection that can be employed by other research groups when looking to produce sEVs at scale. The batch reproducibility we have illustrated in regards to sEV tetraspanin profile and lipid nanoparticle numbers from independent SF runs is something that other research groups have not evidenced and thus should reinforce interest in our optimised bioprocess.

8.2 Future work

This project has achieved its aims and objectives of establishing a scalable bioprocessing platform for the manufacture of MSC-sEVs whilst producing reproducible results in terms of MSC expansion and EV yields. In addition, the sEVs describe consistent tetraspanin biomarker, concentration, size and functionality profiles. As a future aim of this project, it would be desirable to analyse the data we have collected into the proteomic profile of sEVs from different cell line and SF batch runs in order to establish further depth of consistency of MSC-sEV cargos. This level of standardisation could help in generating more homogenous populations of biologicals, with predictability in terms of functional and therapeutic outcome, making them suitable for application *in vivo*.

Although the optimised SF protocol permits sufficient support for MSC growth, sEV secretion and secretome collection, alterations including modifying the cell culture media and microenvironment to promote EV biogenesis and discharge would lead to greater yields of sEV product. For example, employing a chemically defined XF medium has been evidenced to evoke a stress response in MSCs, leading to greater sEV secretion, without inhibiting their

growth and retaining their stemness [225, 229]. As mentioned previously, coating MC surfaces to promote adhesion alongside the application of XF medium was a method for sustaining MSC attachment (section 4.4). For example, in a study by Krutty et al, they applied a synthetic polymer (P(PEGMEMA-r-VDM-r-GMA), PVG) and RGD peptide coating to their MC surfaces and described how MSCs grown in RoosterBio collect media illustrated integrin-mediated adhesion and improved expansion across the culture period [329].

In addition, the next obstacle on the path towards scaling up the SF platform would be moving into large stirred tank bioreactors (litre scale), which was automated (allowing for oxygen, key nutrient and metabolic monitoring), featuring perfusion media exchange capabilities. Being able to replicate the results from our optimised bioprocess at this magnitude would add a new dimension to the research, hopefully evoking interest from companies looking to produce sEVs at more of an industrial scale, rather than just for academic research purposes.

It would therefore be preferable that further testing in relation to sEV regenerative, healing and immunomodulatory potential was undertaken. For example, as well as demonstrating MSC-sEVs can inhibit the activation and proliferation of T lymphocytes, their interaction with Macrophages which form part of the innate immune system, would provide greater evidence of their immunoprivileged nature [311]. Macrophages are categorised into two subtypes: M1 classically activated macrophages, involved with pro-inflammatory activity such as inducing tissue damage and impeding cellular proliferation; and M2 alternatively activated macrophages commonly associated with tissue repair [311, 330]. Polarisation to each functional subset tends to be in response to environmental stimuli, where *in vitro* MSC-EVs have been illustrated to promote conversion to M2 Macrophages prompting regeneration at the injury site [310]. A macrophage polarisation assay would hence be an place to begin further testing the SF derived MSC-sEVs functionality. Following this, it would be interesting to perform some imaging studies, labelling sEVs and observing their uptake, possibly aiming to apply them in an *in vitro* disease model and observe how their effects differ from those demonstrated by MSCs. Most importantly, the choice of functional assays will depend on any future disease models the laboratory group wishes to investigate and determines clinical application the SF derived sEVs would show superior outcomes in.

Chapter 9: List of References

1. Wang, M., Q. Yuan, and L. Xie, *Mesenchymal Stem Cell-Based Immunomodulation: Properties and Clinical Application*. Stem Cells Int, 2018. **2018**: p. 3057624.
2. Volarevic, V., et al., *Mesenchymal stem cell-derived factors: Immuno-modulatory effects and therapeutic potential*. Biofactors, 2017. **43**(5): p. 633-644.
3. Filant, J., et al., *Isolation of Extracellular RNA from Serum/Plasma*. 2018. p. 43-57.
4. Gandhi Torizal, F., I. Horiguchi, and Y. Sakai, *Physiological Microenvironmental Conditions in Different Scalable Culture Systems for Pluripotent Stem Cell Expansion and Differentiation*. The Open Biomedical Engineering Journal, 2019. **13**: p. 41-54.
5. Cherian, D.S., et al., *Biological Considerations in Scaling Up Therapeutic Cell Manufacturing*. Frontiers in Pharmacology, 2020. **11**: p. 654.
6. Coumans, F.A.W., et al., *Methodological Guidelines to Study Extracellular Vesicles*. Circ Res, 2017. **120**(10): p. 1632-1648.
7. Koh, B., et al., *Three dimensional microcarrier system in mesenchymal stem cell culture: a systematic review*. Cell & Bioscience, 2020. **10**(1): p. 75.
8. Yamamoto, T., N. Kosaka, and T. Ochiya, *Latest advances in extracellular vesicles: from bench to bedside*. Science and Technology of Advanced Materials, 2019. **20**(1): p. 746-757.
9. Chen, J., et al., *Review on Strategies and Technologies for Exosome Isolation and Purification*. Frontiers in Bioengineering and Biotechnology, 2022. **9**.
10. Xu, K., et al., *Recent Progress of Exosome Isolation and Peptide Recognition-Guided Strategies for Exosome Research*. Frontiers in Chemistry, 2022. **10**.
11. Liangsupree, T., E. Multia, and M.-L. Riekkola, *Modern isolation and separation techniques for extracellular vesicles*. Journal of Chromatography A, 2021. **1636**: p. 461773.
12. Karnas, E., P. Dudek, and E.K. Zuba-Surma, *Stem cell- derived extracellular vesicles as new tools in regenerative medicine - Immunomodulatory role and future perspectives*. Front Immunol, 2023. **14**: p. 1120175.
13. Cieri, N., K. Maurer, and C.J. Wu, *60 Years Young: The Evolving Role of Allogeneic Hematopoietic Stem Cell Transplantation in Cancer Immunotherapy*. Cancer Research, 2021. **81**(17): p. 4373-4384.
14. Juric, M.K., et al., *Milestones of Hematopoietic Stem Cell Transplantation – From First Human Studies to Current Developments*. Frontiers in Immunology, 2016. **7**.
15. Margiana, R., et al., *Clinical application of mesenchymal stem cell in regenerative medicine: a narrative review*. Stem Cell Research & Therapy, 2022. **13**(1): p. 366.
16. Zakrzewski, W., et al., *Stem cells: past, present, and future*. Stem Cell Research & Therapy, 2019. **10**(1): p. 68.
17. Raynaud, C.M., et al., *Reprogramming for cardiac regeneration*. Global Cardiology Science and Practice, 2014. **2014**(3).
18. Casado-Díaz, A., *Stem Cells in Regenerative Medicine*. J Clin Med, 2022. **11**(18).
19. Kim, H.J. and J.-S. Park, *Usage of Human Mesenchymal Stem Cells in Cell-based Therapy: Advantages and Disadvantages*. Development & reproduction, 2017. **21**(1): p. 1-10.
20. Jang, S., K. Lee, and J. Ju, *Recent Updates of Diagnosis, Pathophysiology, and Treatment on Osteoarthritis of the Knee*. International Journal of Molecular Sciences, 2021. **22**: p. 2619.
21. Francis, S.L., et al., *Cartilage Tissue Engineering Using Stem Cells and Bioprinting Technology—Barriers to Clinical Translation*. Frontiers in Surgery, 2018. **5**.
22. Shi, Y., et al., *How mesenchymal stem cells interact with tissue immune responses*. Trends in immunology, 2012. **33**(3): p. 136-143.
23. Samara, A. and B.D. Belle, *Nanomaterials Upscaling Cell Production and Advancing Exosome-Based Stem Cell Therapies*. Frontiers in Nanotechnology, 2021. **3**.

24. Huang, P., et al., *Mechanism of mesenchymal stem cell–induced neuron recovery and anti-inflammation*. *Cytotherapy*, 2014. **16**(10): p. 1336-1344.
25. Dominici, M., et al., *Minimal criteria for defining multipotent mesenchymal stromal cells. The International Society for Cellular Therapy position statement*. *Cytotherapy*, 2006. **8**(4): p. 315-7.
26. Racchetti, G. and J. Meldolesi, *Extracellular Vesicles of Mesenchymal Stem Cells: Therapeutic Properties Discovered with Extraordinary Success*. *Biomedicines*, 2021. **9**(6).
27. T, L.R., et al., *MSC surface markers (CD44, CD73, and CD90) can identify human MSC-derived extracellular vesicles by conventional flow cytometry*. *Cell Commun Signal*, 2016. **14**: p. 2.
28. Musiał-Wysocka, A., M. Kot, and M. Majka, *The Pros and Cons of Mesenchymal Stem Cell-Based Therapies*. *Cell transplantation*, 2019. **28**(7): p. 801-812.
29. Semon, J.A., et al., *Comparison of human adult stem cells from adipose tissue and bone marrow in the treatment of experimental autoimmune encephalomyelitis*. *Stem cell research & therapy*, 2014. **5**(1): p. 2-2.
30. Lv, F., et al., *Intrinsic properties of mesenchymal stem cells from human bone marrow, umbilical cord and umbilical cord blood comparing the different sources of MSC*. *Current stem cell research & therapy*, 2012. **7** **6**: p. 389-99.
31. Pittenger, M.F., et al., *Multilineage potential of adult human mesenchymal stem cells*. *Science*, 1999. **284**(5411): p. 143-7.
32. D'Andrea, F., et al., *Large-scale production of human adipose tissue from stem cells: a new tool for regenerative medicine and tissue banking*. *Tissue Eng Part C Methods*, 2008. **14**(3): p. 233-42.
33. Casteilla, L. and C. Dani, *Adipose tissue-derived cells: from physiology to regenerative medicine*. *Diabetes Metab*, 2006. **32**(5 Pt 1): p. 393-401.
34. Sharma, S., et al., *Translational products of adipose tissue-derived mesenchymal stem cells: Bench to bedside applications*. *World J Stem Cells*, 2021. **13**(10): p. 1360-1381.
35. Li, C.-y., et al., *Comparative analysis of human mesenchymal stem cells from bone marrow and adipose tissue under xeno-free conditions for cell therapy*. *Stem Cell Research & Therapy*, 2015. **6**(1): p. 55.
36. Yusop, N., et al., *Isolation and Characterisation of Mesenchymal Stem Cells from Rat Bone Marrow and the Endosteal Niche: A Comparative Study*. *Stem Cells Int*, 2018. **2018**: p. 6869128.
37. Matsiko, A., T. Levingstone, and F. O'Brien, *Advanced Strategies for Articular Cartilage Defect Repair*. *Materials*, 2013. **6**: p. 637-668.
38. Liu, S., et al., *Mesenchymal stem cells as a potential therapy for COVID-19*. *Stem Cell Research & Therapy*, 2020. **11**(1): p. 169.
39. Caplan, A.I., *Mesenchymal Stem Cells: Time to Change the Name!* *Stem Cells Translational Medicine*, 2017. **6**(6): p. 1445-1451.
40. Wilson, A., A. Webster, and P. Genever, *Nomenclature and heterogeneity: consequences for the use of mesenchymal stem cells in regenerative medicine*. *Regenerative Medicine*, 2019. **14**(6): p. 595-611.
41. Viswanathan, S., et al., *Mesenchymal stem versus stromal cells: International Society for Cell & Gene Therapy (ISCT®) Mesenchymal Stromal Cell committee position statement on nomenclature*. *Cytotherapy*, 2019. **21**(10): p. 1019-1024.
42. Spencer, N.D., J.M. Gimble, and M.J. Lopez, *Mesenchymal Stromal Cells: Past, Present, and Future*. *Veterinary Surgery*, 2011. **40**(2): p. 129-139.
43. Wilson, A.J., et al., *Characterisation of mesenchymal stromal cells in clinical trial reports: analysis of published descriptors*. *Stem Cell Research & Therapy*, 2021. **12**(1): p. 360.
44. Caplan, A.I., *What's in a name?* *Tissue Eng Part A*, 2010. **16**(8): p. 2415-7.
45. Meirelles Lda, S., et al., *Mechanisms involved in the therapeutic properties of mesenchymal stem cells*. *Cytokine Growth Factor Rev*, 2009. **20**(5-6): p. 419-27.

46. Kabat, M., et al., *Trends in mesenchymal stem cell clinical trials 2004-2018: Is efficacy optimal in a narrow dose range?* STEM CELLS Translational Medicine, 2020. **9**(1): p. 17-27.
47. Pittenger, M.F., et al., *Mesenchymal stem cell perspective: cell biology to clinical progress.* npj Regenerative Medicine, 2019. **4**(1): p. 22.
48. Hassan, M.N.F.B., et al., *Large-Scale Expansion of Human Mesenchymal Stem Cells.* Stem Cells International, 2020. **2020**: p. 9529465.
49. Keshtkar, S., N. Azarpira, and M.H. Ghahremani, *Mesenchymal stem cell-derived extracellular vesicles: novel frontiers in regenerative medicine.* Stem Cell Res Ther, 2018. **9**(1): p. 63.
50. Rowland, A.L., et al., *Cross-matching of allogeneic mesenchymal stromal cells eliminates recipient immune targeting.* Stem Cells Transl Med, 2021. **10**(5): p. 694-710.
51. Leyendecker, A., Jr., et al., *The Use of Human Mesenchymal Stem Cells as Therapeutic Agents for the in vivo Treatment of Immune-Related Diseases: A Systematic Review.* Frontiers in immunology, 2018. **9**: p. 2056-2056.
52. Rohban, R. and T.R. Pieber, *Mesenchymal Stem and Progenitor Cells in Regeneration: Tissue Specificity and Regenerative Potential.* Stem cells international, 2017. **2017**: p. 5173732-5173732.
53. Chen, W., et al., *Immunomodulatory effects of mesenchymal stromal cells-derived exosome.* Immunol Res, 2016. **64**(4): p. 831-40.
54. Li, X., et al., *Exosome Derived From Human Umbilical Cord Mesenchymal Stem Cell Mediates MiR-181c Attenuating Burn-induced Excessive Inflammation.* EBioMedicine, 2016. **8**: p. 72-82.
55. Ti, D., et al., *LPS-preconditioned mesenchymal stromal cells modify macrophage polarization for resolution of chronic inflammation via exosome-shuttled let-7b.* J Transl Med, 2015. **13**: p. 308.
56. trials.gov, c. 2000, National Library of Medicine and National institute of health.
57. Fung, M., et al., *Responsible Translation of Stem Cell Research: An Assessment of Clinical Trial Registration and Publications.* Stem Cell Reports, 2017. **8**(5): p. 1190-1201.
58. Jossen, V., et al., *Manufacturing human mesenchymal stem cells at clinical scale: process and regulatory challenges.* Applied Microbiology and Biotechnology, 2018. **102**(9): p. 3981-3994.
59. Daneshmandi, L., et al., *Emergence of the Stem Cell Secretome in Regenerative Engineering.* Trends Biotechnol, 2020. **38**(12): p. 1373-1384.
60. Kalra, H., G.P. Drummen, and S. Mathivanan, *Focus on Extracellular Vesicles: Introducing the Next Small Big Thing.* Int J Mol Sci, 2016. **17**(2): p. 170.
61. Latifkar, A., et al., *New insights into extracellular vesicle biogenesis and function.* J Cell Sci, 2019. **132**(13).
62. Burrello, J., et al., *Stem Cell-Derived Extracellular Vesicles and Immune-Modulation.* Frontiers in Cell and Developmental Biology, 2016. **4**.
63. Bellani, C.F., et al., *Scale-Up Technologies for the Manufacture of Adherent Cells.* Frontiers in nutrition, 2020. **7**: p. 575146-575146.
64. Titus, K., et al., *Closed system cell culture protocol using HYPERStack vessels with gas permeable material technology.* J Vis Exp, 2010(45).
65. Cherian, D.S., et al., *Biological Considerations in Scaling Up Therapeutic Cell Manufacturing.* Frontiers in pharmacology, 2020. **11**: p. 654-654.
66. Tsai, A.-C., et al., *Influence of Microenvironment on Mesenchymal Stem Cell Therapeutic Potency: From Planar Culture to Microcarriers.* Frontiers in Bioengineering and Biotechnology, 2020. **8**.
67. Rafiq, Q.A., et al., *Culture of human mesenchymal stem cells on microcarriers in a 5 l stirred-tank bioreactor.* Biotechnol Lett, 2013. **35**(8): p. 1233-45.
68. Goh, T.K.-P., et al., *Microcarrier culture for efficient expansion and osteogenic differentiation of human fetal mesenchymal stem cells.* BioResearch open access, 2013. **2**(2): p. 84-97.

69. Godara, P., C.D. McFarland, and R.E. Nordon, *Design of bioreactors for mesenchymal stem cell tissue engineering*. Journal of Chemical Technology & Biotechnology, 2008. **83**(4): p. 408-420.
70. Lawson, T., et al., *Process development for expansion of human mesenchymal stromal cells in a 50L single-use stirred tank bioreactor*. Biochemical Engineering Journal, 2017. **120**: p. 49-62.
71. Kumar, A. and B. Starly, *Large scale industrialized cell expansion: producing the critical raw material for biofabrication processes*. Biofabrication, 2015. **7**(4): p. 044103.
72. Schirmer, C., et al., *An overview of drive systems and sealing types in stirred bioreactors used in biotechnological processes*. Applied Microbiology and Biotechnology, 2021. **105**(6): p. 2225-2242.
73. Martin, Y. and P. Vermette, *Bioreactors for tissue mass culture: design, characterization, and recent advances*. Biomaterials, 2005. **26**(35): p. 7481-503.
74. Rubin, D.M., et al., *Oxygen transfer characteristics of a hollow fiber dialyser: toward possible repurposing of dialysers as blood oxygenators in the context of constrained availability of respiratory support*. medRxiv, 2020: p. 2020.04.06.20055236.
75. Bettahalli, N.M., et al., *Integration of hollow fiber membranes improves nutrient supply in three-dimensional tissue constructs*. Acta Biomater, 2011. **7**(9): p. 3312-24.
76. Rafiq, Q.A., K. Coopman, and C.J. Hewitt, *Scale-up of human mesenchymal stem cell culture: current technologies and future challenges*. Current Opinion in Chemical Engineering, 2013. **2**(1): p. 8-16.
77. Singh, V., *Disposable bioreactor for cell culture using wave-induced agitation*. Cytotechnology, 1999. **30**(1-3): p. 149-58.
78. Eibl, R., S. Werner, and D. Eibl, *Bag bioreactor based on wave-induced motion: characteristics and applications*. Adv Biochem Eng Biotechnol, 2009. **115**: p. 55-87.
79. Wang, S.-J. and J.-J. Zhong, *Chapter 6 - Bioreactor Engineering*, in *Bioprocessing for Value-Added Products from Renewable Resources*, S.-T. Yang, Editor. 2007, Elsevier: Amsterdam. p. 131-161.
80. Ibrahim, S. and A.W. Nienow, *Suspension of Microcarriers for Cell Culture with Axial Flow Impellers*. Chemical Engineering Research and Design, 2004. **82**(9): p. 1082-1088.
81. Nienow, A.W., et al., *A potentially scalable method for the harvesting of hMSCs from microcarriers*. Biochemical Engineering Journal, 2014. **85**: p. 79-88.
82. Sousa, M.F., et al., *Production of oncolytic adenovirus and human mesenchymal stem cells in a single-use, Vertical-Wheel bioreactor system: Impact of bioreactor design on performance of microcarrier-based cell culture processes*. Biotechnol Prog, 2015. **31**(6): p. 1600-12.
83. Teixeira, G.Q., et al., *A multicompartiment holder for spinner flasks improves expansion and osteogenic differentiation of mesenchymal stem cells in three-dimensional scaffolds*. Tissue Eng Part C Methods, 2014. **20**(12): p. 984-93.
84. Van Wezel, A.L., *Growth of Cell-strains and Primary Cells on Micro-carriers in Homogeneous Culture*. Nature, 1967. **216**(5110): p. 64-65.
85. Jossen, V., et al., *Theoretical and Practical Issues That Are Relevant When Scaling Up hMSC Microcarrier Production Processes*. Stem Cells Int, 2016. **2016**: p. 4760414.
86. Alfred, R., et al., *Efficient suspension bioreactor expansion of murine embryonic stem cells on microcarriers in serum-free medium*. Biotechnol Prog, 2011. **27**(3): p. 811-23.
87. Simón, M., *Bioreactor design for adherent cell culture*. BioProcess International, 2015. **13**: p. 1.
88. de Soure, A.M., et al., *Scalable microcarrier-based manufacturing of mesenchymal stem/stromal cells*. J Biotechnol, 2016. **236**: p. 88-109.
89. Yang, J., et al., *Fabrication and surface modification of macroporous poly(L-lactic acid) and poly(L-lactic-co-glycolic acid) (70/30) cell scaffolds for human skin fibroblast cell culture*. J Biomed Mater Res, 2002. **62**(3): p. 438-46.

90. Li, B., et al., *Past, present, and future of microcarrier-based tissue engineering*. Journal of Orthopaedic Translation, 2015. **3**(2): p. 51-57.
91. Wu, C.-Y., et al., *Shaped 3D microcarriers for adherent cell culture and analysis*. Microsystems & Nanoengineering, 2018. **4**(1): p. 21.
92. Chen, X.-Y., et al., *Recent advances in the use of microcarriers for cell cultures and their ex vivo and in vivo applications*. Biotechnology Letters, 2020. **42**(1): p. 1-10.
93. Chen, C.S., et al., *Cell shape provides global control of focal adhesion assembly*. Biochemical and Biophysical Research Communications, 2003. **307**(2): p. 355-361.
94. Yu, C., et al., *Decellularized adipose tissue microcarriers as a dynamic culture platform for human adipose-derived stem/stromal cell expansion*. Biomaterials, 2017. **120**: p. 66-80.
95. Rodrigues, C.A.V., et al., *Stem cell cultivation in bioreactors*. Biotechnology Advances, 2011. **29**(6): p. 815-829.
96. Nisisako, T., *Recent advances in microfluidic production of Janus droplets and particles*. Current Opinion in Colloid & Interface Science, 2016. **25**.
97. Derakhti, S., et al., *Attachment and detachment strategies in microcarrier-based cell culture technology: A comprehensive review*. Materials Science and Engineering: C, 2019. **103**: p. 109782.
98. Preissmann, A., et al., *Investigations on oxygen limitations of adherent cells growing on macroporous micro-carriers*. Cytotechnology, 1997. **24**(2): p. 121-134.
99. Zwietering, T.N., *Suspending of solid particles in liquid by agitators*. Chemical Engineering Science, 1958. **8**(3): p. 244-253.
100. Luo, W., et al., *Laminar shear stress delivers cell cycle arrest and anti-apoptosis to mesenchymal stem cells*. Acta Biochimica et Biophysica Sinica, 2011. **43**(3): p. 210-216.
101. Yu, L., et al., *Fluid shear stress induces osteoblast differentiation and arrests the cell cycle at the G0 phase via the ERK1/2 pathway*. Mol Med Rep, 2017. **16**(6): p. 8699-8708.
102. Li, P., et al., *Cyclic fluid shear stress promotes osteoblastic cells proliferation through ERK5 signaling pathway*. Molecular and Cellular Biochemistry, 2012. **364**(1): p. 321-327.
103. Ji, Q., et al., *High shear stress suppresses proliferation and migration but promotes apoptosis of endothelial cells co-cultured with vascular smooth muscle cells via down-regulating MAPK pathway*. Journal of Cardiothoracic Surgery, 2019. **14**(1): p. 216.
104. Park, J.Y., et al., *Cell morphological response to low shear stress in a two-dimensional culture microsystem with magnitudes comparable to interstitial shear stress*. Biorheology, 2010. **47**: p. 165-178.
105. Ismadi, M.Z., et al., *Flow characterization of a spinner flask for induced pluripotent stem cell culture application*. PLoS One, 2014. **9**(10): p. e106493.
106. Ferrari, C., et al., *Limiting cell aggregation during mesenchymal stem cell expansion on microcarriers*. Biotechnology Progress, 2012. **28**(3): p. 780-787.
107. Berry, J.D., et al., *Characterisation of stresses on microcarriers in a stirred bioreactor*. Applied Mathematical Modelling, 2016. **40**(15): p. 6787-6804.
108. Cui, Y., et al., *Determination of glucose deficiency-induced cell death by mitochondrial ATP generation-driven proton homeostasis*. Journal of Molecular Cell Biology, 2017. **9**(5): p. 395-408.
109. Potier, E., et al., *Prolonged hypoxia concomitant with serum deprivation induces massive human mesenchymal stem cell death*. Tissue Eng, 2007. **13**(6): p. 1325-31.
110. Krampe, B. and M. Al-Rubeai, *Cell death in mammalian cell culture: molecular mechanisms and cell line engineering strategies*. Cytotechnology, 2010. **62**(3): p. 175-188.
111. Sun, C.N., *Lattice structures and osmiophilic bodies in the developing respiratory tissue of rats*. J Ultrastruct Res, 1966. **15**(3): p. 380-8.
112. Anderson, H.C., *Vesicles associated with calcification in the matrix of epiphyseal cartilage*. J Cell Biol, 1969. **41**(1): p. 59-72.

113. Bonucci, E., *Fine structure of early cartilage calcification*. J Ultrastruct Res, 1967. **20**(1): p. 33-50.
114. Nunez, E.A., J. Wallis, and M.D. Gershon, *Secretory processes in follicular cells of the bat thyroid. 3. The occurrence of extracellular vesicles and colloid droplets during arousal from hibernation*. Am J Anat, 1974. **141**(2): p. 179-201.
115. Harding, C., J. Heuser, and P. Stahl, *Receptor-mediated endocytosis of transferrin and recycling of the transferrin receptor in rat reticulocytes*. J Cell Biol, 1983. **97**(2): p. 329-39.
116. Pan, B.T. and R.M. Johnstone, *Fate of the transferrin receptor during maturation of sheep reticulocytes in vitro: selective externalization of the receptor*. Cell, 1983. **33**(3): p. 967-78.
117. Trams, E.G., et al., *Exfoliation of membrane ecto-enzymes in the form of micro-vesicles*. Biochim Biophys Acta, 1981. **645**(1): p. 63-70.
118. Johnstone, R.M., et al., *Vesicle formation during reticulocyte maturation. Association of plasma membrane activities with released vesicles (exosomes)*. J Biol Chem, 1987. **262**(19): p. 9412-20.
119. Witwer, K.W. and C. Théry, *Extracellular vesicles or exosomes? On primacy, precision, and popularity influencing a choice of nomenclature*. J Extracell Vesicles, 2019. **8**(1): p. 1648167.
120. Cocucci, E., G. Racchetti, and J. Meldolesi, *Shedding microvesicles: artefacts no more*. Trends in Cell Biology, 2009. **19**(2): p. 43-51.
121. Chuo, S.T., J.C. Chien, and C.P. Lai, *Imaging extracellular vesicles: current and emerging methods*. J Biomed Sci, 2018. **25**(1): p. 91.
122. Raposo, G., et al., *B lymphocytes secrete antigen-presenting vesicles*. J Exp Med, 1996. **183**(3): p. 1161-72.
123. Zitvogel, L., et al., *Eradication of established murine tumors using a novel cell-free vaccine: dendritic cell-derived exosomes*. Nat Med, 1998. **4**(5): p. 594-600.
124. Willms, E., et al., *Extracellular Vesicle Heterogeneity: Subpopulations, Isolation Techniques, and Diverse Functions in Cancer Progression*. Front Immunol, 2018. **9**: p. 738.
125. Agrahari, V., et al., *Extracellular Microvesicles as New Industrial Therapeutic Frontiers*. Trends in Biotechnology, 2019. **37**(7): p. 707-729.
126. Desrochers, Laura M., Marc A. Antonyak, and Richard A. Cerione, *Extracellular Vesicles: Satellites of Information Transfer in Cancer and Stem Cell Biology*. Developmental Cell, 2016. **37**(4): p. 301-309.
127. Kamerkar, S., et al., *Exosomes facilitate therapeutic targeting of oncogenic KRAS in pancreatic cancer*. Nature, 2017. **546**(7659): p. 498-503.
128. Wen, J., et al., *Comparison of immunotherapy mediated by apoptotic bodies, microvesicles and exosomes: apoptotic bodies' unique anti-inflammatory potential*. Journal of Translational Medicine, 2023. **21**(1): p. 478.
129. Tricarico, C., J. Clancy, and C. D'Souza-Schorey, *Biology and biogenesis of shed microvesicles*. Small GTPases, 2017. **8**(4): p. 220-232.
130. Yamamoto, S., et al., *Inflammation-induced endothelial cell-derived extracellular vesicles modulate the cellular status of pericytes*. Scientific Reports, 2015. **5**(1): p. 8505.
131. Samanta, S., et al., *Exosomes: new molecular targets of diseases*. Acta Pharmacol Sin, 2018. **39**(4): p. 501-513.
132. Zhang, Y., et al., *Exosomes: biogenesis, biologic function and clinical potential*. Cell & Bioscience, 2019. **9**(1): p. 19.
133. Savva, C.G., et al., *Selective activation of TNFR1 and NF-κB inhibition by a novel biyouyanagin analogue promotes apoptosis in acute leukemia cells*. BMC Cancer, 2016. **16**(1): p. 279.
134. Akers, J.C., et al., *Biogenesis of extracellular vesicles (EV): exosomes, microvesicles, retrovirus-like vesicles, and apoptotic bodies*. J Neurooncol, 2013. **113**(1): p. 1-11.
135. Xu, X., Y. Lai, and Z.-C. Hua, *Apoptosis and apoptotic body: disease message and therapeutic target potentials*. Bioscience reports, 2019. **39**(1): p. BSR20180992.

136. Stachowiak, J.C., et al., *Membrane bending by protein–protein crowding*. Nature Cell Biology, 2012. **14**(9): p. 944-949.
137. Raiborg, C. and H. Stenmark, *The ESCRT machinery in endosomal sorting of ubiquitylated membrane proteins*. Nature, 2009. **458**(7237): p. 445-452.
138. Hurley, J.H., *The ESCRT complexes*. Critical Reviews in Biochemistry and Molecular Biology, 2010. **45**(6): p. 463-487.
139. Baietti, M.F., et al., *Syndecan–syntenin–ALIX regulates the biogenesis of exosomes*. Nature Cell Biology, 2012. **14**(7): p. 677-685.
140. Nabhan, J.F., et al., *Formation and release of arrestin domain-containing protein 1-mediated microvesicles (ARMMs) at plasma membrane by recruitment of TSG101 protein*. Proc Natl Acad Sci U S A, 2012. **109**(11): p. 4146-51.
141. Camussi, G., et al., *Exosomes/microvesicles as a mechanism of cell-to-cell communication*. Kidney Int, 2010. **78**(9): p. 838-48.
142. Al-Nedawi, K., et al., *Intercellular transfer of the oncogenic receptor EGFRvIII by microvesicles derived from tumour cells*. Nature Cell Biology, 2008. **10**(5): p. 619-624.
143. Munster, M., et al., *Anti-VEGF-A affects the angiogenic properties of tumor-derived microparticles*. PLoS One, 2014. **9**(4): p. e95983.
144. Sedgwick, A., et al., *Extracellular microvesicles and invadopodia mediate non-overlapping modes of tumor cell invasion*. Scientific Reports, 2015. **5**.
145. Schlienger, S., S. Campbell, and A. Claing, *ARF1 regulates the Rho/MLC pathway to control EGF-dependent breast cancer cell invasion*. Mol Biol Cell, 2014. **25**(1): p. 17-29.
146. Blanc, L. and M. Vidal, *New insights into the function of Rab GTPases in the context of exosomal secretion*. Small GTPases, 2018. **9**(1-2): p. 95-106.
147. Xu, M., et al., *The biogenesis and secretion of exosomes and multivesicular bodies (MVBs): Intercellular shuttles and implications in human diseases*. Genes & Diseases, 2023. **10**(5): p. 1894-1907.
148. Bunggulawa, E.J., et al., *Recent advancements in the use of exosomes as drug delivery systems*. J Nanobiotechnology, 2018. **16**(1): p. 81.
149. Han, Q.-F., et al., *Exosome biogenesis: machinery, regulation, and therapeutic implications in cancer*. Molecular Cancer, 2022. **21**(1): p. 207.
150. Henne, W.M., N.J. Buchkovich, and S.D. Emr, *The ESCRT pathway*. Dev Cell, 2011. **21**(1): p. 77-91.
151. Horbay, R., et al., *Role of Ceramides and Lysosomes in Extracellular Vesicle Biogenesis, Cargo Sorting and Release*. Int J Mol Sci, 2022. **23**(23).
152. Tang, T.-T., et al., *Extracellular Vesicles: Opportunities and Challenges for the Treatment of Renal Diseases*. Frontiers in Physiology, 2019. **10**(226).
153. Lv, L.-L., et al., *Therapeutic application of extracellular vesicles in kidney disease: promises and challenges*. Journal of Cellular and Molecular Medicine, 2018. **22**(2): p. 728-737.
154. Ha, D., N. Yang, and V. Nadithe, *Exosomes as therapeutic drug carriers and delivery vehicles across biological membranes: current perspectives and future challenges*. Acta Pharmaceutica Sinica B, 2016. **6**(4): p. 287-296.
155. Yang, B., Y. Chen, and J. Shi, *Exosome Biochemistry and Advanced Nanotechnology for Next-Generation Theranostic Platforms*. Advanced Materials, 2019. **31**(2): p. 1802896.
156. van den Boorn, J.G., et al., *SiRNA delivery with exosome nanoparticles*. Nature Biotechnology, 2011. **29**(4): p. 325-326.
157. van Dommelen, S.M., et al., *Microvesicles and exosomes: Opportunities for cell-derived membrane vesicles in drug delivery*. Journal of Controlled Release, 2012. **161**(2): p. 635-644.
158. Lai, C.P., et al., *Dynamic Biodistribution of Extracellular Vesicles in Vivo Using a Multimodal Imaging Reporter*. ACS Nano, 2014. **8**(1): p. 483-494.

159. Wiklander, O.P.B., et al., *Extracellular vesicle in vivo biodistribution is determined by cell source, route of administration and targeting*. Journal of Extracellular Vesicles, 2015. **4**(1): p. 26316.
160. Cabral, J., et al., *Extracellular vesicles as modulators of wound healing*. Adv Drug Deliv Rev, 2018. **129**: p. 394-406.
161. Ti, D., et al., *LPS-preconditioned mesenchymal stromal cells modify macrophage polarization for resolution of chronic inflammation via exosome-shuttled let-7b*. Journal of Translational Medicine, 2015. **13**(1): p. 308.
162. Caruso, S. and I.K.H. Poon, *Apoptotic Cell-Derived Extracellular Vesicles: More Than Just Debris*. Frontiers in Immunology, 2018. **9**(1486).
163. Desdín-Micó, G. and M. Mittelbrunn, *Role of exosomes in the protection of cellular homeostasis*. 2017, Taylor and Francis Inc. p. 127-134.
164. Fattore, A.D., et al., *Immunoregulatory effects of mesenchymal stem cell-derived extracellular vesicles on T lymphocytes*. Cell Transplantation, 2015. **24**(12): p. 2615-2627.
165. Zeng, F. and A.E. Morelli, *Extracellular vesicle-mediated MHC cross-dressing in immune homeostasis, transplantation, infectious diseases, and cancer*. 2018, Springer Verlag. p. 477-490.
166. Mardpour, S., et al., *Interaction between mesenchymal stromal cell-derived extracellular vesicles and immune cells by distinct protein content*. 2019, Wiley-Liss Inc. p. 8249-8258.
167. Mendt, M., et al., *Generation and testing of clinical-grade exosomes for pancreatic cancer*. JCI Insight, 2018. **3**(8).
168. Li, J., et al., *Serum-free culture alters the quantity and protein composition of neuroblastoma-derived extracellular vesicles*. Journal of extracellular vesicles, 2015. **4**: p. 26883-26883.
169. Brindley, D., et al., *Bioprocess forces and their impact on cell behavior: implications for bone regeneration therapy*. J Tissue Eng, 2011. **2011**: p. 620247.
170. Bollini, S., et al., *The Regenerative Role of the Fetal and Adult Stem Cell Secretome*. Journal of clinical medicine, 2013. **2**(4): p. 302-327.
171. Crescitelli, R., et al., *Distinct RNA profiles in subpopulations of extracellular vesicles: apoptotic bodies, microvesicles and exosomes*. Journal of extracellular vesicles, 2013. **2**: p. 10.3402/jev.v2i0.20677.
172. Colao, I.L., et al., *Manufacturing Exosomes: A Promising Therapeutic Platform*. Trends Mol Med, 2018. **24**(3): p. 242-256.
173. Wen, Y.T., et al., *Collection of in vivo-like liver cell secretome with alternative sample enrichment method using a hollow fiber bioreactor culture system combined with tangential flow filtration for secretomics analysis*. Anal Chim Acta, 2011. **684**(1-2): p. 72-9.
174. Gimona, M., et al., *Manufacturing of Human Extracellular Vesicle-Based Therapeutics for Clinical Use*. Int J Mol Sci, 2017. **18**(6).
175. Chiriaco, M., et al., *Lab-on-Chip for Exosomes and Microvesicles Detection and Characterization*. Sensors, 2018. **18**: p. 3175.
176. An, Y., et al., *An ultrasensitive electrochemical aptasensor for the determination of tumor exosomes based on click chemistry*. Biosensors and Bioelectronics, 2019. **142**: p. 111503.
177. Théry, C., *Minimal information for studies of extracellular vesicles 2018 (MISEV2018): a position statement of the International Society for Extracellular Vesicles and update of the MISEV2014 guidelines*. Journal of Extracellular Vesicles, 2018. **7**(1): p. 1535750.
178. Benjamin-Davalos, S., et al., *Co-Isolation of Cytokines and Exosomes: Implications for Immunomodulation Studies*. Frontiers in Immunology, 2021. **12**.
179. Clos-Sansalvador, M., et al., *Commonly used methods for extracellular vesicles' enrichment: Implications in downstream analyses and use*. European Journal of Cell Biology, 2022. **101**: p. 151227.

180. Nordin, J.Z., et al., *Ultrafiltration with size-exclusion liquid chromatography for high yield isolation of extracellular vesicles preserving intact biophysical and functional properties*. *Nanomedicine: Nanotechnology, Biology and Medicine*, 2015. **11**(4): p. 879-883.
181. Oeyen, E., et al., *Ultrafiltration and size exclusion chromatography combined with asymmetrical-flow field-flow fractionation for the isolation and characterisation of extracellular vesicles from urine*. *Journal of Extracellular Vesicles*, 2018. **7**(1): p. 1490143.
182. Guan, S., et al., *Characterization of Urinary Exosomes Purified with Size Exclusion Chromatography and Ultracentrifugation*. *Journal of Proteome Research*, 2020. **19**(6): p. 2217-2225.
183. Heinemann, M.L., et al., *Benchtop isolation and characterization of functional exosomes by sequential filtration*. *Journal of Chromatography A*, 2014. **1371**: p. 125-135.
184. Gámez-Valero, A., et al., *Size-Exclusion Chromatography-based isolation minimally alters Extracellular Vesicles' characteristics compared to precipitating agents*. *Scientific Reports*, 2016. **6**(1): p. 33641.
185. Samsonraj, R.M., et al., *Establishing criteria for human mesenchymal stem cell potency*. *Stem Cells*, 2015. **33**(6): p. 1878-91.
186. Jeyaram, A. and S.M. Jay, *Preservation and Storage Stability of Extracellular Vesicles for Therapeutic Applications*. *Aaps j*, 2017. **20**(1): p. 1.
187. Welch, J.L., et al., *Effect of prolonged freezing of semen on exosome recovery and biologic activity*. *Sci Rep*, 2017. **7**: p. 45034.
188. Gelibter, S., et al., *The impact of storage on extracellular vesicles: A systematic study*. *J Extracell Vesicles*, 2022. **11**(2): p. e12162.
189. Witwer, K.W., et al., *Standardization of sample collection, isolation and analysis methods in extracellular vesicle research*. *Journal of Extracellular Vesicles*, 2013. **2**(1): p. 20360.
190. Théry, C., et al., *Minimal information for studies of extracellular vesicles 2018 (MISEV2018): a position statement of the International Society for Extracellular Vesicles and update of the MISEV2014 guidelines*. *J Extracell Vesicles*, 2018. **7**(1): p. 1535750.
191. Görgens, A., et al., *Identification of storage conditions stabilizing extracellular vesicles preparations*. *J Extracell Vesicles*, 2022. **11**(6): p. e12238.
192. Budgude, P., V. Kale, and A. Vaidya, *Cryopreservation of mesenchymal stromal cell-derived extracellular vesicles using trehalose maintains their ability to expand hematopoietic stem cells in vitro*. *Cryobiology*, 2021. **98**: p. 152-163.
193. Sivanantham, A. and Y. Jin, *Impact of Storage Conditions on EV Integrity/Surface Markers and Cargos*. *Life*, 2022. **12**(5): p. 697.
194. El Baradie, K.B.Y., et al., *Freeze-Dried Extracellular Vesicles From Adipose-Derived Stem Cells Prevent Hypoxia-Induced Muscle Cell Injury*. *Front Cell Dev Biol*, 2020. **8**: p. 181.
195. de Almeida Fuzeta, M., et al., *Scalable Production of Human Mesenchymal Stromal Cell-Derived Extracellular Vesicles Under Serum-/Xeno-Free Conditions in a Microcarrier-Based Bioreactor Culture System*. *Frontiers in Cell and Developmental Biology*, 2020. **8**.
196. Haraszti, R.A., et al., *Exosomes Produced from 3D Cultures of MSCs by Tangential Flow Filtration Show Higher Yield and Improved Activity*. *Molecular Therapy*, 2018. **26**(12): p. 2838-2847.
197. Cao, J., et al., *Three-dimensional culture of MSCs produces exosomes with improved yield and enhanced therapeutic efficacy for cisplatin-induced acute kidney injury*. *Stem Cell Res Ther*, 2020. **11**(1): p. 206.
198. Watson, D.C., et al., *Efficient production and enhanced tumor delivery of engineered extracellular vesicles*. *Biomaterials*, 2016. **105**: p. 195-205.
199. Jeske, R., et al., *Bioreactor Expansion Reconfigures Metabolism and Extracellular Vesicle Biogenesis of Human Adipose-derived Stem Cells In Vitro*. *Biochemical Engineering Journal*, 2022. **188**: p. 108711.

200. Rafiq, Q.A., et al., *Systematic microcarrier screening and agitated culture conditions improves human mesenchymal stem cell yield in bioreactors*. Biotechnol J, 2016. **11**(4): p. 473-86.
201. Navaei, A., et al., *Important considerations for cell therapy manufacturing of mesenchymal stem cell*. Cytotherapy, 2020. **22**(5, Supplement): p. S92.
202. Van Beylen, K., I. Papantoniou, and J.-M. Aerts, *Microcarrier Screening and Evaluation for Dynamic Expansion of Human Periosteum-Derived Progenitor Cells in a Xenogeneic Free Medium*. Frontiers in Bioengineering and Biotechnology, 2021. **9**.
203. Loubière, C., et al., *Impact of the type of microcarrier and agitation modes on the expansion performances of mesenchymal stem cells derived from umbilical cord*. Biotechnology Progress, 2019. **35**(6): p. e2887.
204. Tsai, A.C. and T. Ma, *Expansion of Human Mesenchymal Stem Cells in a Microcarrier Bioreactor*. Methods Mol Biol, 2016. **1502**: p. 77-86.
205. Kaiser, S., et al., *Fluid flow and cell proliferation of mesenchymal adipose-derived stem cells in small-scale, stirred, single-use bioreactors*. Chemie Ingenieur Technik, 2013. **85**(1-2): p. 95-102.
206. Jossen, V., et al., *Theoretical and Practical Issues That Are Relevant When Scaling Up hMSC Microcarrier Production Processes*. Stem Cells International, 2016. **2016**: p. 4760414.
207. Yuan, Y., et al., *Improved expansion of human bone marrow-derived mesenchymal stem cells in microcarrier-based suspension culture*. Journal of Tissue Engineering and Regenerative Medicine, 2014. **8**(3): p. 210-225.
208. Hanga, M.P., et al., *Bioprocess development for scalable production of cultivated meat*. Biotechnology and Bioengineering, 2020. **117**(10): p. 3029-3039.
209. Zhang, J., et al., *Hydrodynamics and mass transfer in spinner flasks: Implications for large scale cultured meat production*. Biochemical Engineering Journal, 2021. **167**: p. 107864.
210. Tsai, H.H., et al., *The Effects of Different Dynamic Culture Systems on Cell Proliferation and Osteogenic Differentiation in Human Mesenchymal Stem Cells*. Int J Mol Sci, 2019. **20**(16).
211. Verbruggen, S., et al., *Bovine myoblast cell production in a microcarriers-based system*. Cytotechnology, 2018. **70**(2): p. 503-512.
212. Takahashi, I., et al., *Effects of agitation rate on aggregation during beads-to-beads subcultivation of microcarrier culture of human mesenchymal stem cells*. Cytotechnology, 2017. **69**(3): p. 503-509.
213. Valentin, J., et al., *Mass Production of Mesenchymal Stem Cells — Impact of Bioreactor Design and Flow Conditions on Proliferation and Differentiation*, in *Cells and Biomaterials in Regenerative Medicine*, E. Daniel, Editor. 2014, IntechOpen: Rijeka. p. Ch. 5.
214. Hervy, M., et al., *Long term expansion of bone marrow-derived hMSCs on novel synthetic microcarriers in xeno-free, defined conditions*. PLoS One, 2014. **9**(3): p. e92120.
215. Carmelo, J.G., et al., *A xeno-free microcarrier-based stirred culture system for the scalable expansion of human mesenchymal stem/stromal cells isolated from bone marrow and adipose tissue*. Biotechnol J, 2015. **10**(8): p. 1235-47.
216. Petry, F., et al., *Manufacturing of Human Umbilical Cord Mesenchymal Stromal Cells on Microcarriers in a Dynamic System for Clinical Use*. Stem Cells Int, 2016. **2016**: p. 4834616.
217. Tan, K.Y., et al., *Serum-free media formulations are cell line-specific and require optimization for microcarrier culture*. Cytotherapy, 2015. **17**(8): p. 1152-65.
218. Lembong, J., et al., *Bioreactor Parameters for Microcarrier-Based Human MSC Expansion under Xeno-Free Conditions in a Vertical-Wheel System*. Bioengineering, 2020. **7**(3): p. 73.
219. Rogers, R.E., et al., *A scalable system for generation of mesenchymal stem cells derived from induced pluripotent cells employing bioreactors and degradable microcarriers*. STEM CELLS Translational Medicine, 2021. **10**(12): p. 1650-1665.

220. Rafiq, Q.A., et al., *Process development of human multipotent stromal cell microcarrier culture using an automated high-throughput microbioreactor*. *Biotechnol Bioeng*, 2017. **114**(10): p. 2253-2266.
221. Rafiq, Q.A., et al., *Process development of human multipotent stromal cell microcarrier culture using an automated high-throughput microbioreactor*. *Biotechnology and Bioengineering*, 2017. **114**(10): p. 2253-2266.
222. Lässer, C., et al., *Human saliva, plasma and breast milk exosomes contain RNA: uptake by macrophages*. *Journal of Translational Medicine*, 2011. **9**(1): p. 9.
223. Caby, M.P., et al., *Exosomal-like vesicles are present in human blood plasma*. *Int Immunol*, 2005. **17**(7): p. 879-87.
224. Almeria, C., et al., *Heterogeneity of mesenchymal stem cell-derived extracellular vesicles is highly impacted by the tissue/cell source and culture conditions*. *Cell Biosci*, 2022. **12**(1): p. 51.
225. Bost, J.P., et al., *Growth Media Conditions Influence the Secretion Route and Release Levels of Engineered Extracellular Vesicles*. *Advanced Healthcare Materials*, 2022. **11**(5): p. 2101658.
226. Witwer, K.W., et al., *Defining mesenchymal stromal cell (MSC)-derived small extracellular vesicles for therapeutic applications*. *J Extracell Vesicles*, 2019. **8**(1): p. 1609206.
227. Haraszti, R.A., et al., *Serum Deprivation of Mesenchymal Stem Cells Improves Exosome Activity and Alters Lipid and Protein Composition*. *iScience*, 2019. **16**: p. 230-241.
228. Li, G., et al., *Reversible Anion Exchange Reaction in Solid Halide Perovskites and Its Implication in Photovoltaics*. *The Journal of Physical Chemistry C*, 2015. **119**(48): p. 26883-26888.
229. Scheiber, A.L., et al. *Culture Condition of Bone Marrow Stromal Cells Affects Quantity and Quality of the Extracellular Vesicles*. *International Journal of Molecular Sciences*, 2022. **23**, DOI: 10.3390/ijms23031017.
230. Davies, R., et al., *Extracellular Vesicle Depletion Protocols of Foetal Bovine Serum Influence Umbilical Cord Mesenchymal Stromal Cell Phenotype, Immunomodulation, and Particle Release*. *Int J Mol Sci*, 2023. **24**(11).
231. Eitan, E., et al., *Extracellular vesicle-depleted fetal bovine and human sera have reduced capacity to support cell growth*. *J Extracell Vesicles*, 2015. **4**: p. 26373.
232. Forteza-Genestra, M.A., et al., *Purity Determines the Effect of Extracellular Vesicles Derived from Mesenchymal Stromal Cells*. *Cells*, 2020. **9**(2): p. 422.
233. Pilgrim, C.R., et al., *A Review of Fetal Bovine Serum in the Culture of Mesenchymal Stromal Cells and Potential Alternatives for Veterinary Medicine*. *Front Vet Sci*, 2022. **9**: p. 859025.
234. Martin, W., et al., *A functional corona around extracellular vesicles enhances angiogenesis during skin regeneration and signals in immune cells*. *bioRxiv*, 2021: p. 808808.
235. Silva Couto, P., et al., *Expansion of human mesenchymal stem/stromal cells (hMSCs) in bioreactors using microcarriers: lessons learnt and what the future holds*. *Biotechnology Advances*, 2020. **45**: p. 107636.
236. Chen, A.K.-L., et al., *Increasing efficiency of human mesenchymal stromal cell culture by optimization of microcarrier concentration and design of medium feed*. *Cytotherapy*, 2015. **17**(2): p. 163-173.
237. Tsai, A.-C. and C.A. Pacak, *Bioprocessing of Human Mesenchymal Stem Cells: From Planar Culture to Microcarrier-Based Bioreactors*. *Bioengineering*, 2021. **8**(7): p. 96.
238. Cunha, B., et al., *Exploring continuous and integrated strategies for the up- and downstream processing of human mesenchymal stem cells*. *Journal of Biotechnology*, 2015. **213**: p. 97-108.
239. dos Santos, F., et al., *A xenogeneic-free bioreactor system for the clinical-scale expansion of human mesenchymal stem/stromal cells*. *Biotechnology and Bioengineering*, 2014. **111**(6): p. 1116-1127.

240. Busatto, S., et al., *Tangential Flow Filtration for Highly Efficient Concentration of Extracellular Vesicles from Large Volumes of Fluid*. Cells, 2018. **7**(12).
241. Heath, N., et al., *Rapid isolation and enrichment of extracellular vesicle preparations using anion exchange chromatography*. Scientific Reports, 2018. **8**(1): p. 5730.
242. Costa, M.H.G., et al., *Enhanced bioprocess control to advance the manufacture of mesenchymal stromal cell-derived extracellular vesicles in stirred-tank bioreactors*. Biotechnology and Bioengineering, 2023. **120**(9): p. 2725-2741.
243. Heath, N., et al., *Rapid isolation and enrichment of extracellular vesicle preparations using anion exchange chromatography*. Sci Rep, 2018. **8**(1): p. 5730.
244. Dimov, N., et al., *Formation and purification of tailored liposomes for drug delivery using a module-based micro continuous-flow system*. Scientific Reports, 2017. **7**(1): p. 12045.
245. Tengattini, S., *Chromatographic Approaches for Purification and Analytical Characterization of Extracellular Vesicles: Recent Advancements*. Chromatographia, 2019. **82**(1): p. 415-424.
246. Hassan, M., et al., *Large-Scale Expansion of Human Mesenchymal Stem Cells*. Stem Cells Int, 2020. **2020**: p. 9529465.
247. de Soure, A.M., et al., *Scalable microcarrier-based manufacturing of mesenchymal stem/stromal cells*. Journal of Biotechnology, 2016. **236**: p. 88-109.
248. Tsai, A.C. and C.A. Pacak, *Bioprocessing of Human Mesenchymal Stem Cells: From Planar Culture to Microcarrier-Based Bioreactors*. Bioengineering (Basel), 2021. **8**(7).
249. Jeske, R., et al., *Upscaling human mesenchymal stromal cell production in a novel vertical-wheel bioreactor enhances extracellular vesicle secretion and cargo profile*. Bioact Mater, 2023. **25**: p. 732-747.
250. Gobin, J., et al., *Hollow-fiber bioreactor production of extracellular vesicles from human bone marrow mesenchymal stromal cells yields nanovesicles that mirrors the immuno-modulatory antigenic signature of the producer cell*. Stem Cell Research & Therapy, 2021. **12**(1): p. 127.
251. Devashree, V., et al., *Stem Cell-Derived Exosomes as New Horizon for Cell-Free Therapeutic Development: Current Status and Prospects*, in *Possibilities and Limitations in Current Translational Stem Cell Research*, K. Diana, Editor. 2023, IntechOpen: Rijeka. p. Ch. 3.
252. Lee, J.H., et al., *Reproducible Large-Scale Isolation of Exosomes from Adipose Tissue-Derived Mesenchymal Stem/Stromal Cells and Their Application in Acute Kidney Injury*. International Journal of Molecular Sciences, 2020. **21**(13): p. 4774.
253. Yang, M., et al., *An efficient method to isolate lemon derived extracellular vesicles for gastric cancer therapy*. Journal of nanobiotechnology, 2020. **18**(1): p. 1-12.
254. Li, P., et al., *Progress in Exosome Isolation Techniques*. Theranostics, 2017. **7**(3): p. 789-804.
255. Tieu, A., et al., *An Analysis of Mesenchymal Stem Cell-Derived Extracellular Vesicles for Preclinical Use*. ACS Nano, 2020. **14**(8): p. 9728-9743.
256. Ludwig, N., et al., *Optimization of cell culture conditions for exosome isolation using mini-size exclusion chromatography (mini-SEC)*. Experimental Cell Research, 2019. **378**(2): p. 149-157.
257. Heinemann, M.L., et al., *Benchtop isolation and characterization of functional exosomes by sequential filtration*. J Chromatogr A, 2014. **1371**: p. 125-35.
258. Monguió-Tortajada, M., et al., *Extracellular vesicle isolation methods: rising impact of size-exclusion chromatography*. Cellular and Molecular Life Sciences, 2019. **76**(12): p. 2369-2382.
259. Aretz, I. and D. Meierhofer, *Advantages and Pitfalls of Mass Spectrometry Based Metabolome Profiling in Systems Biology*. Int J Mol Sci, 2016. **17**(5).
260. Skoczylas, Ł., et al., *Immune capture and protein profiling of small extracellular vesicles from human plasma*. PROTEOMICS. n/a(n/a): p. 2300180.
261. Shao, H., et al., *New Technologies for Analysis of Extracellular Vesicles*. Chem Rev, 2018. **118**(4): p. 1917-1950.
262. Bagrov, D.V., et al., *Application of AFM, TEM, and NTA for characterization of exosomes produced by placenta-derived mesenchymal cells*. Journal of Physics: Conference Series, 2021. **1942**(1): p. 012013.

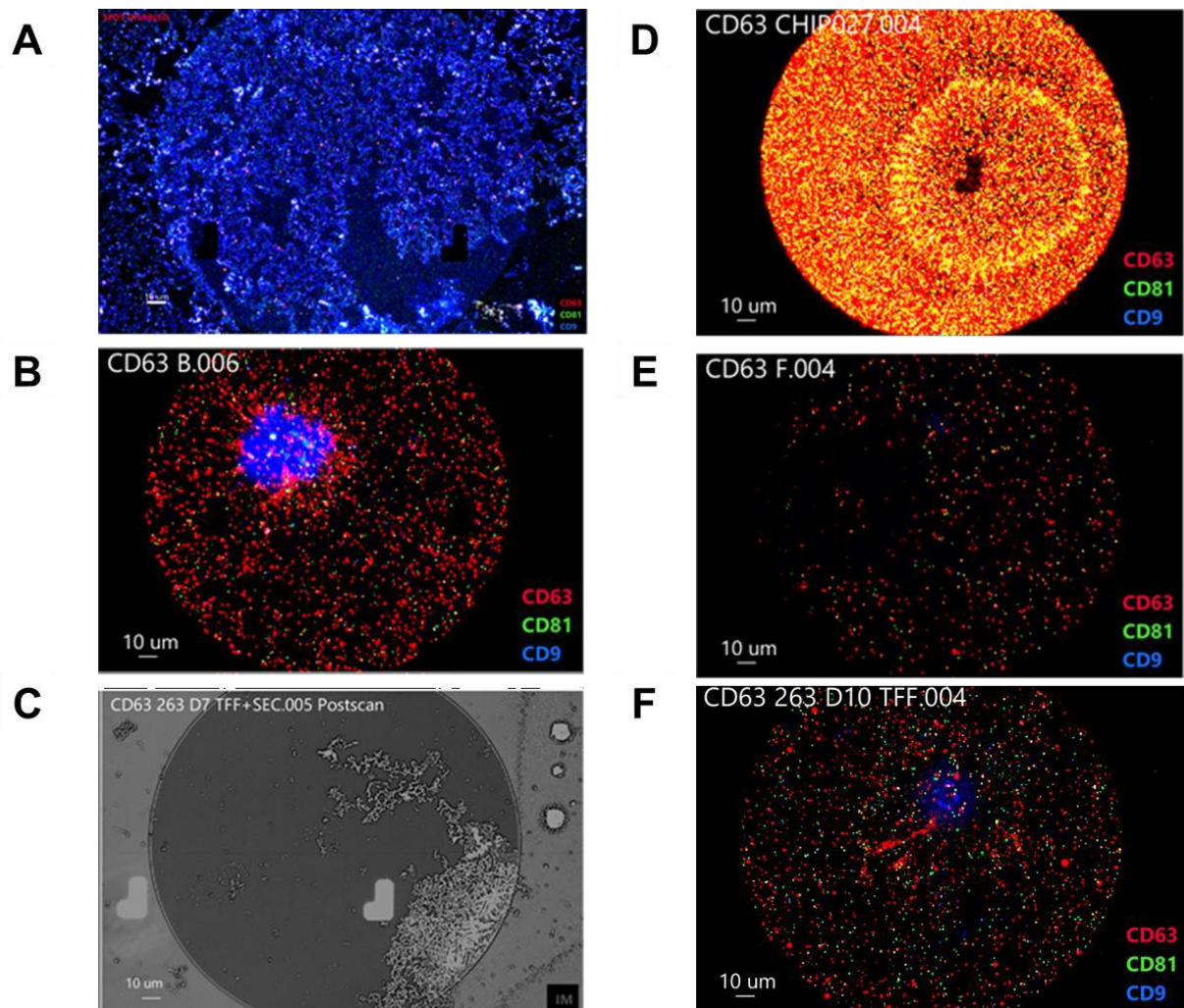
263. Li, M.I., et al., *Multiparametric atomic force microscopy imaging of single native exosomes*. *Acta Biochim Biophys Sin (Shanghai)*, 2021. **53**(3): p. 385-388.
264. van der Pol, E., et al., *Optical and non-optical methods for detection and characterization of microparticles and exosomes*. *J Thromb Haemost*, 2010. **8**(12): p. 2596-607.
265. Akers, J.C., et al., *Comparative Analysis of Technologies for Quantifying Extracellular Vesicles (EVs) in Clinical Cerebrospinal Fluids (CSF)*. *PLOS ONE*, 2016. **11**(2): p. e0149866.
266. Chiriaco, M.S., et al., *Lab-on-Chip for Exosomes and Microvesicles Detection and Characterization*. *Sensors (Basel)*, 2018. **18**(10).
267. Bağcı, C., et al., *Overview of extracellular vesicle characterization techniques and introduction to combined reflectance and fluorescence confocal microscopy to distinguish extracellular vesicle subpopulations*. *Neurophotonics*, 2022. **9**(2): p. 021903.
268. Maas, S.L.N., M.L.D. Broekman, and J. de Vrij, *Tunable Resistive Pulse Sensing for the Characterization of Extracellular Vesicles*, in *Exosomes and Microvesicles: Methods and Protocols*, A.F. Hill, Editor. 2017, Springer New York: New York, NY. p. 21-33.
269. Gardiner, C., et al., *Extracellular vesicle sizing and enumeration by nanoparticle tracking analysis*. *Journal of Extracellular Vesicles*, 2013. **2**(1): p. 19671.
270. Shao, H., et al., *New Technologies for Analysis of Extracellular Vesicles*. *Chemical Reviews*, 2018. **118**(4): p. 1917-1950.
271. van der Pol, E., et al., *Single vs. swarm detection of microparticles and exosomes by flow cytometry*. *J Thromb Haemost*, 2012. **10**(5): p. 919-30.
272. Arraud, N., et al., *A simple flow cytometry method improves the detection of phosphatidylserine-exposing extracellular vesicles*. *Journal of Thrombosis and Haemostasis*, 2015. **13**(2): p. 237-247.
273. Ueda, K., et al., *Antibody-coupled monolithic silica microtips for highthroughput molecular profiling of circulating exosomes*. *Sci Rep*, 2014. **4**: p. 6232.
274. Duijvesz, D., et al., *Immuno-based detection of extracellular vesicles in urine as diagnostic marker for prostate cancer*. *International Journal of Cancer*, 2015. **137**(12): p. 2869-2878.
275. Serrano-Pertierra, E., et al., *Extracellular Vesicles: Current Analytical Techniques for Detection and Quantification*. *Biomolecules*, 2020. **10**(6).
276. Gomes, J., et al., *Analytical Considerations in Nanoscale Flow Cytometry of Extracellular Vesicles to Achieve Data Linearity*. *Thromb Haemost*, 2018. **118**(9): p. 1612-1624.
277. RoosterBio. *RoosterCollect EV Pro*. 2023 [cited 2023 2023]; Available from: <https://www.roosterbio.com/products/roostercollect-ev-pro-k41001/>.
278. Syromiatnikova, V., A. Prokopeva, and M. Gomzikova, *Methods of the Large-Scale Production of Extracellular Vesicles*. *Int J Mol Sci*, 2022. **23**(18).
279. Haraszti, R.A., et al., *Serum Deprivation of Mesenchymal Stem Cells Improves Exosome Activity and Alters Lipid and Protein Composition*. *iScience*, 2019. **16**: p. 230-241.
280. Giannasi, C., et al., *Serum starvation affects mitochondrial metabolism of adipose-derived stem/stromal cells*. *Cytotherapy*, 2023. **25**(7): p. 704-711.
281. Esmaeili, A., et al., *Co-aggregation of MSC/chondrocyte in a dynamic 3D culture elevates the therapeutic effect of secreted extracellular vesicles on osteoarthritis in a rat model*. *Sci Rep*, 2022. **12**(1): p. 19827.
282. Bister, N., et al., *Hypoxia and extracellular vesicles: A review on methods, vesicular cargo and functions*. *J Extracell Vesicles*, 2020. **10**(1): p. e12002.
283. Hahm, J., J. Kim, and J. Park, *Strategies to Enhance Extracellular Vesicle Production*. *Tissue Eng Regen Med*, 2021. **18**(4): p. 513-524.
284. Arab, T., et al., *Characterization of extracellular vesicles and synthetic nanoparticles with four orthogonal single-particle analysis platforms*. *J Extracell Vesicles*, 2021. **10**(6): p. e12079.
285. Dong, L., et al., *Comprehensive evaluation of methods for small extracellular vesicles separation from human plasma, urine and cell culture medium*. *J Extracell Vesicles*, 2020. **10**(2): p. e12044.

286. Phan, T.H., et al., *New Multiscale Characterization Methodology for Effective Determination of Isolation–Structure–Function Relationship of Extracellular Vesicles*. *Frontiers in Bioengineering and Biotechnology*, 2021. **9**.
287. Kurian, T.K., et al., *Elucidating Methods for Isolation and Quantification of Exosomes: A Review*. *Mol Biotechnol*, 2021. **63**(4): p. 249-266.
288. Seymour, E., M.S. Ünlü, and J.H. Connor, *A high-throughput single-particle imaging platform for antibody characterization and a novel competition assay for therapeutic antibodies*. *Sci Rep*, 2023. **13**(1): p. 306.
289. Silva, A.M., et al., *Quantification of protein cargo loading into engineered extracellular vesicles at single-vesicle and single-molecule resolution*. *J Extracell Vesicles*, 2021. **10**(10): p. e12130.
290. Agarwal, K., et al., *Analysis of exosome release as a cellular response to MAPK pathway inhibition*. *Langmuir*, 2015. **31**(19): p. 5440-8.
291. Gurung, S., et al., *The exosome journey: from biogenesis to uptake and intracellular signalling*. *Cell Communication and Signaling*, 2021. **19**(1): p. 47.
292. McKee, C. and G.R. Chaudhry, *Advances and challenges in stem cell culture*. *Colloids and Surfaces B: Biointerfaces*, 2017. **159**: p. 62-77.
293. Adlerz, K., et al., *Comparison of msc-evs manufactured in 2D versus scalable 3D bioreactor systems*. *Cytotherapy*, 2019. **21**(5): p. S58.
294. Man, K., et al., *Bioengineering extracellular vesicles: smart nanomaterials for bone regeneration*. *Journal of Nanobiotechnology*, 2023. **21**(1): p. 137.
295. Konoshenko, M.Y., et al., *Isolation of Extracellular Vesicles: General Methodologies and Latest Trends*. *Biomed Res Int*, 2018. **2018**: p. 8545347.
296. Baranyai, T., et al., *Isolation of Exosomes from Blood Plasma: Qualitative and Quantitative Comparison of Ultracentrifugation and Size Exclusion Chromatography Methods*. *PLoS One*, 2015. **10**(12): p. e0145686.
297. Shu, S., et al., *A Rapid Exosome Isolation Using Ultrafiltration and Size Exclusion Chromatography (REIUS) Method for Exosome Isolation from Melanoma Cell Lines*. *Methods Mol Biol*, 2021. **2265**: p. 289-304.
298. Feng, Z.Y., et al., *Techniques for increasing the yield of stem cell-derived exosomes: what factors may be involved?* *Sci China Life Sci*, 2022. **65**(7): p. 1325-1341.
299. Van Deun, J., et al., *The impact of disparate isolation methods for extracellular vesicles on downstream RNA profiling*. *Journal of Extracellular Vesicles*, 2014. **3**(1): p. 24858.
300. Lobb, R.J., et al., *Optimized exosome isolation protocol for cell culture supernatant and human plasma*. *J Extracell Vesicles*, 2015. **4**: p. 27031.
301. Nguyen, V.V.T., et al., *Functional assays to assess the therapeutic potential of extracellular vesicles*. *J Extracell Vesicles*, 2020. **10**(1): p. e12033.
302. Norden, C. and V. Lecaudey, *Collective cell migration: general themes and new paradigms*. *Curr Opin Genet Dev*, 2019. **57**: p. 54-60.
303. Jain, S., et al., *The role of single-cell mechanical behaviour and polarity in driving collective cell migration*. *Nature Physics*, 2020. **16**(7): p. 802-809.
304. Sung, B.H., C.A. Parent, and A.M. Weaver, *Extracellular vesicles: Critical players during cell migration*. *Dev Cell*, 2021. **56**(13): p. 1861-1874.
305. Sung, B.H. and A.M. Weaver, *Directed migration: Cells navigate by extracellular vesicles*. *J Cell Biol*, 2018. **217**(8): p. 2613-2614.
306. Wu, R., et al., *Mesenchymal Stem Cell-Derived Extracellular Vesicles in Liver Immunity and Therapy*. *Front Immunol*, 2022. **13**: p. 833878.
307. Jiang, W. and J. Xu, *Immune modulation by mesenchymal stem cells*. *Cell Prolif*, 2020. **53**(1): p. e12712.

308. Álvarez, V., et al., *The immunomodulatory activity of extracellular vesicles derived from endometrial mesenchymal stem cells on CD4+ T cells is partially mediated by TGFβ*. *J Tissue Eng Regen Med*, 2018. **12**(10): p. 2088-2098.
309. Kim, H., et al., *Comprehensive Molecular Profiles of Functionally Effective MSC-Derived Extracellular Vesicles in Immunomodulation*. *Mol Ther*, 2020. **28**(7): p. 1628-1644.
310. Liu, X., et al., *Immunomodulatory potential of mesenchymal stem cell-derived extracellular vesicles: Targeting immune cells*. *Frontiers in Immunology*, 2023. **14**.
311. Tang, D., et al., *Extracellular Vesicle/Macrophage Axis: Potential Targets for Inflammatory Disease Intervention*. *Front Immunol*, 2022. **13**: p. 705472.
312. Suarez-Arnedo, A., et al., *An image J plugin for the high throughput image analysis of in vitro scratch wound healing assays*. *PLoS One*, 2020. **15**(7): p. e0232565.
313. Yuan, X., et al., *Engineering extracellular vesicles by three-dimensional dynamic culture of human mesenchymal stem cells*. *J Extracell Vesicles*, 2022. **11**(6): p. e12235.
314. Kouroupis, D. and D. Correa, *Increased Mesenchymal Stem Cell Functionalization in Three-Dimensional Manufacturing Settings for Enhanced Therapeutic Applications*. *Frontiers in Bioengineering and Biotechnology*, 2021. **9**.
315. Kim, J., et al., *Clinical-Scale Mesenchymal Stem Cell-Derived Extracellular Vesicle Therapy for Wound Healing*. *Int J Mol Sci*, 2023. **24**(5).
316. Cha, J.M., et al., *Efficient scalable production of therapeutic microvesicles derived from human mesenchymal stem cells*. *Sci Rep*, 2018. **8**(1): p. 1171.
317. Riedl, J., et al., *Mesenchymal stromal cells in wound healing applications: role of the secretome, targeted delivery and impact on recessive dystrophic epidermolysis bullosa treatment*. *Cytotherapy*, 2021. **23**(11): p. 961-973.
318. Hoang, D.H., et al., *Differential Wound Healing Capacity of Mesenchymal Stem Cell-Derived Exosomes Originated From Bone Marrow, Adipose Tissue and Umbilical Cord Under Serum- and Xeno-Free Condition*. *Frontiers in Molecular Biosciences*, 2020. **7**.
319. An, S., et al., *Wound-Healing Effects of Mesenchymal Stromal Cell Secretome in the Cornea and the Role of Exosomes*. *Pharmaceutics*, 2023. **15**(5): p. 1486.
320. Tutuianu, R., et al., *Human Mesenchymal Stromal Cell-Derived Exosomes Promote In Vitro Wound Healing by Modulating the Biological Properties of Skin Keratinocytes and Fibroblasts and Stimulating Angiogenesis*. *Int J Mol Sci*, 2021. **22**(12).
321. Ahangar, P., et al., *Human gingival fibroblast secretome accelerates wound healing through anti-inflammatory and pro-angiogenic mechanisms*. *npj Regenerative Medicine*, 2020. **5**(1): p. 24.
322. Marofi, F., et al., *MSCs and their exosomes: a rapidly evolving approach in the context of cutaneous wounds therapy*. *Stem Cell Res Ther*, 2021. **12**(1): p. 597.
323. Prasai, A., et al., *Role of Exosomes in Dermal Wound Healing: A Systematic Review*. *J Invest Dermatol*, 2022. **142**(3 Pt A): p. 662-678.e8.
324. He, C., et al., *Comparison of two cell-free therapeutics derived from adipose tissue: small extracellular vesicles versus conditioned medium*. *Stem Cell Research & Therapy*, 2022. **13**(1): p. 86.
325. Tokhanbigli, S., et al., *Immunoregulatory impact of human mesenchymal-conditioned media and mesenchymal derived exosomes on monocytes*. *Mol Biol Res Commun*, 2019. **8**(2): p. 79-89.
326. Cheng, A., et al., *Human multipotent mesenchymal stromal cells cytokine priming promotes RAB27B-regulated secretion of small extracellular vesicles with immunomodulatory cargo*. *Stem Cell Research & Therapy*, 2020. **11**(1): p. 539.
327. Lai, P., et al., *A potent immunomodulatory role of exosomes derived from mesenchymal stromal cells in preventing cGVHD*. *Journal of Hematology & Oncology*, 2018. **11**(1): p. 135.
328. Pachler, K., et al., *An In Vitro Potency Assay for Monitoring the Immunomodulatory Potential of Stromal Cell-Derived Extracellular Vesicles*. *Int J Mol Sci*, 2017. **18**(7).

329. Krutty, J.D., et al., *Xeno-Free Bioreactor Culture of Human Mesenchymal Stromal Cells on Chemically Defined Microcarriers*. ACS Biomaterials Science & Engineering, 2021. **7**(2): p. 617-625.
330. Wang, J., et al., *Mesenchymal stem cell-derived extracellular vesicles alter disease outcomes via endorsement of macrophage polarization*. Stem Cell Res Ther, 2020. **11**(1): p. 424.

Appendices



Appendix figure 1: ExoView errors when performing EV tetraspanin analysis. Image A illustrates the effect of poor drying on chip appearance under a fluorescent microscope. Image B demonstrates background fluorescence from an unknown source, most likely drying effect from a droplet which remained on the chip after drying. Image C reveals how drying effect appears on a postscan of the chip, prior to fluorescent imaging for EVs. Image D shows a saturated chip, on which the sEVs are too concentrated and need diluting. Image E

highlights the possibility of patchy sEV attachment to chip spots during the incubation stage. Finally F shows autofluorescence from a dust fragment bound to the chip surface.